



## 저작자표시-비영리-변경금지 2.0 대한민국

이용자는 아래의 조건을 따르는 경우에 한하여 자유롭게

- 이 저작물을 복제, 배포, 전송, 전시, 공연 및 방송할 수 있습니다.

다음과 같은 조건을 따라야 합니다:



저작자표시. 귀하는 원저작자를 표시하여야 합니다.



비영리. 귀하는 이 저작물을 영리 목적으로 이용할 수 없습니다.



변경금지. 귀하는 이 저작물을 개작, 변형 또는 가공할 수 없습니다.

- 귀하는, 이 저작물의 재이용이나 배포의 경우, 이 저작물에 적용된 이용허락조건을 명확하게 나타내어야 합니다.
- 저작권자로부터 별도의 허가를 받으면 이러한 조건들은 적용되지 않습니다.

저작권법에 따른 이용자의 권리는 위의 내용에 의하여 영향을 받지 않습니다.

이것은 [이용허락규약\(Legal Code\)](#)을 이해하기 쉽게 요약한 것입니다.

[Disclaimer](#)

공학박사학위논문

Welding Deformation Analysis  
based on Improved Equivalent  
Strain Method to cover External  
Constraint during cooling Stage

냉각 시 외적 구속 조건을 고려한 개선된  
등가변형도법 기반 용접 해석에 관한 연구

2014년 2월

서울대학교 대학원

조선해양공학과

김 태 준

Welding Deformation Analysis  
based on Improved Equivalent Strain Method  
to cover External Constraint during cooling Stage

냉각 시 외적 구속 조건을 고려한 개선된  
등가변형도법 기반 용접 해석에 관한 연구

지도 교수 장범선

이 논문을 공학박사학위논문으로 제출함.  
2014년 2월

서울대학교 대학원  
조선해양공학과  
김 태 준

김태준의 박사학위논문을 인준함.  
2014년 1월

위 원 장 \_\_\_\_\_ (印)

부위원장 \_\_\_\_\_ (印)

위 원 \_\_\_\_\_ (印)

위 원 \_\_\_\_\_ (印)

위 원 \_\_\_\_\_ (印)

## Abstract

# Welding Deformation Analysis based on Improved Equivalent Strain Method to cover External Constraint during cooling Stage

Kim, Tae Jun

Dept. of Naval Architecture and Ocean Engineering

The Graduate School

Seoul National University

The prediction and control of welding deformation at design stage has been an essential task in shipbuilding industry to ensure high fabrication quality as well as high productivity.

The most widely used method is the thermal elasto-plastic analysis method due to its high accuracy in the simulation results. However, it has a disadvantage in computational time due to the consideration of non-linearity of material and temperature-dependent material properties. In order to overcome the difficulties, a few efficient approaches which are applicable to complicated welding process of ship hull blocks have been developed.

In the present study, the existing equivalent strain method is

improved to make up for its weaknesses. The improved inherent strain model is built considering more sophisticated three dimensional constraints which are embodied by six cubic elements attached on three sides of a core cubic element.

From a few case studies, it is found that the inherent strain is mainly affected by the changes in restraints induced by changes of temperature-dependent material properties of the restraining elements. On the other hand, the degree of restraints is identified to be little influential to the inherent strain. Thus, the effect of temperature gradients over plate thickness and plate transverse direction normal to welding is reflected in the calculation of the inherent strain chart.

A 3D contour of inherent strain is plotted versus temperature gradients of thickness direction and transverse direction for a maximum welding temperature value. A series of inherent strain charts are obtained varying the maximum welding temperature value. The welding deformation can be calculated by an elastic FE analysis using the inherent strain values taken from the inherent strain chart.

The proposed method is verified by comparing the calculated welding deformation analysis results with the existing method, thermal elasto-plastic FE analysis, and experimental results.

External restraints imposed normal to plate during cooling stage is identified to be effective to the reduction of angular

distortion of butt-welded or fillet-welded plate. The external restraint is represented by vertical force on work piece at both sides and bending stress forms in transverse direction. The additional bending stress distribution across plate thickness is reflected into the improved inherent strain model and a set of inherent strain charts with different levels of bending stress are newly calculated. Welding deformation can be calculated from an elastic linear FE analysis using the inherent strain values taken from the chart and compared with those from a 3D thermal elastoplastic FE analysis.

**Keywords:** Welding deformation, Inherent strain, Equivalent strain, External Constraint

**Student Number:** 2004-20999

# LIST OF CONTENTS

1. Introduction.....	1
1.1. Background of this study .....	1
1.2. Research Status .....	2
1.3. Objectives .....	7
1.4. Organization .....	7
2. Equivalent strain method based on inherent strain.....	9
2.1. Definition of the inherent strain.....	9
2.2. Welding analysis based on inherent strain .....	1 1
2.3. Calculation of the inherent strain in a previous equivalent strain method.....	1 4
2.3.1. Simplified inherent strain model for equivalent strain method .....	1 4
2.3.2. Inherent strain chart for equivalent strain method	1 7
2.3.3. Distribution of the highest temperature.....	1 8
2.3.4. Calculation of degree of restraint .....	1 9
3. Limitation of equivalent strain method in previous study	2 0
3.1. Absence of consideration of the temperature distribution .....	2 0
3.2. Repetitive calculation of degree of restraint.....	2 7
3.3. Strain input .....	2 9
4. Improved equivalent strain method considering the temperature distribution .....	3 3
4.1. Improved solid–spring model.....	3 3
4.1.1. Restraint positions of solid–spring model .....	3 4

4.1.2. Boundary condition of solid–spring model.....	3 7
4.1.3. Calculation of elastic modulus of the periphery elements .....	4 0
4.2. Degree of restraint determination .....	4 6
4.2.1. Inherent strain of the elements subjected to tri– axial stress. ....	4 6
4.2.2. Degree of restraint in room temperature .....	5 2
4.2.3. Changes in degree of restraint due to temperature	5 5
4.3. Inherent strain chart considering temperature gradient .....	5 8
4.3.1. Definition of thermal gradient TG .....	5 8
4.3.2. Application of TG to welding model .....	6 0
4.3.3. Inherent strain chart.....	6 2
4.4. Strain input .....	6 7
4.5. Welding analysis procedure based on improved equivalent strain method.....	6 9
4.6. Summary of comparison with the previous study .....	7 0
5. Welding analysis using improved equivalent strain method .....	7 2
5.1. Butt welding.....	7 2
5.1.1. Comparison of 6mm plate .....	7 6
5.1.2. Comparison of 10mm plate .....	7 9
5.1.3. Comparison of 15mm plate .....	8 2
5.1.4. Comparison of 20mm plate .....	8 5
5.1.5. Summary and discussion.....	8 8
5.2. Fillet welding .....	9 2

5.2.1. Comparison of 8mm plate .....	9	5
5.2.2. Comparison of 15mm plate .....	9	8
5.2.3. Comparison of 18mm plate .....	1	0 1
5.2.4. Summary and discussion .....	1	0 4
6. Welding analysis considering external constraint during cooling .....	1	0 8
6.1. The effect of external constraint in welding .....	1	0 8
6.2. Simplifying of welding analysis considering external constraint during cooling.....	1	1 0
6.3. Identification of assumption.....	1	1 7
6.4. Inherent strain model considering external constraint during cooling.....	1	1 8
7. Comparison of the welding analysis considering external constraint during cooling stage .....	1	2 3
7.1. Analysis considering various external force .....	1	2 3
7.2. Analysis of model related to external force inducing equal bending moment.....	1	2 9
8. Comparison of analysis time .....	1	3 8
9. Conclusion .....	1	4 0

# LIST OF FIGURES

Fig.1 Definition of the inherent strain .....	9
Fig.2 Procedure for prediction of deformation using equivalent loading method.....	1 3
Fig.3 Procedure for prediction of deformation and residual stress using equivalent strain method .....	1 3
Fig. 4 Simplified thermal elasto-plastic analysis model .....	1 5
Fig. 5 Simplified thermal elasto-plastic FE analysis model .....	1 6
Fig. 6 Inherent strain chart of butt welding.....	1 7
Fig. 7 Inherent strain chart of fillet welding (Vertical direction of weld line) .....	1 8
Fig. 8 Inherent strain chart of fillet welding (Weld line direction).....	1 8
Fig. 9 Calculation of equivalent strain .....	1 9
Fig. 10 Inherent strain chart (0.4-0.7 degree of restraint).....	2 1
Fig. 11 Thermal history of plastic strain.....	2 3
Fig. 12 Temperature and residual plastic strain distributions of same FE model with different heat input.....	2 4
Fig. 13 Temperature and residual plastic strain distributions of same point with same degree of restraint and highest temperature.....	2 5
Fig. 14 Concept of welding model in equivalent loading method.....	2 7
Fig. 15 Actual temperature distributions .....	2 7

Fig. 16 Heat affected region and the periphery.....	2 8
Fig. 17 Complex welding analyses .....	2 9
Fig. 18 Strain input .....	3 0
Fig. 19 Temperature distributions between spot input model and actual model .....	3 1
Fig. 20 Residual stress distribution (x-direction).....	3 2
Fig. 21 Working surface of the restraint .....	3 3
Fig. 22 The extreme cases of working surface of restraint.....	3 4
Fig. 23 Uniaxial restraints model .....	3 5
Fig. 24 Biaxial restraints model .....	3 5
Fig. 25 Tri-axial restraints model .....	3 6
Fig. 26 Disassembled view of tri-axial restraints model.....	3 6
Fig. 27 Restraining elements for the each load direction.....	3 7
Fig. 28 Boundary condition on the core element .....	3 8
Fig. 29 Expansion of core element .....	3 9
Fig. 30 Shrinkage of core element .....	3 9
Fig. 31 Definition of stress .....	4 1
Fig. 32 Restraint element for the each load direction .....	4 1
Fig. 33 Unit load method of welding model.....	4 6
Fig. 34 Thermal history of strain, CASE I .....	4 7
Fig. 35 Thermal history of strain, CASE II.....	4 8
Fig. 36 Thermal history of strain, CASE III (x,y-direction).....	4 9
Fig. 37 Thermal history of strain, CASE III (z-direction).....	4 9
Fig. 38 Thermal history of strain, CASE IV (x,y-direction).....	5 0
Fig. 39 Thermal history of strain, CASE IV (z-direction).....	5 0

Fig. 40 Thermal history of strain, CASE V (x,y-direction) .....	5 1
Fig. 41 Thermal history of strain, CASE V (z-direction) .....	5 1
Fig. 42 Degree of restraint calculate location (Planar type) .....	5 3
Fig. 43 Degree of restraint calculate location (Fillet type) .....	5 4
Fig. 44 Temperature-degree of restraint relation .....	5 6
Fig. 45 Temperature gradient at TG=1.....	5 9
Fig. 46 Temperature gradient at TG=0.7.....	5 9
Fig. 47 Temperature gradient at TG <sub>x</sub> =0.8, TG <sub>y</sub> =0.5 .....	6 0
Fig. 48 Definition of TG in the thermal analysis model .....	6 1
Fig. 49 Example model of finding TG.....	6 2
Fig. 50 Inherent strain chart(at highest temperature 600-1000°C of the core element) .....	6 4
Fig. 51 Inherent strain chart(at highest temperature 1100- 1500°C of the core element) .....	6 5
Fig. 52 Inherent strain chart .....	6 6
Fig. 53 Inherent strain curve at TG <sub>z</sub> = 0.4.....	6 7
Fig. 54 Inherent strain curve at TG <sub>x</sub> = 0.4.....	6 7
Fig. 55 Strain input point .....	6 8
Fig. 56 Heat transfer direction .....	6 9
Fig. 57 Heat transfer results .....	6 9
Fig. 58 Welding analysis procedure using improved inherent strain method .....	7 0
Fig. 59 Comparison with experiment (Satoh and Terasaki[2])..	7 3
Fig. 60 Displacement in z direction (t=6mm).....	7 6

Fig. 61 Displacement in z direction (t=6mm).....	7 6
Fig. 62 Residual stress in x direction (t=6mm).....	7 7
Fig. 63 Residual stress in x direction (t=6mm).....	7 7
Fig. 64 Residual stress in y direction (t=6mm) .....	7 8
Fig. 65 Residual stress in y direction (t=6mm) .....	7 8
Fig. 66 Displacement in z direction (t=10mm).....	7 9
Fig. 67 Displacement in z direction (t=10mm).....	7 9
Fig. 68 Residual stress in x direction (t=10mm).....	8 0
Fig. 69 Residual stress in x direction (t=10 mm).....	8 0
Fig. 70 Residual stress in y direction (t=10mm) .....	8 1
Fig. 71 Residual stress in y direction (t=10mm) .....	8 1
Fig. 72 Displacement in z direction (t=15mm).....	8 2
Fig. 73 Displacement in z direction (t=15mm).....	8 2
Fig. 74 Residual stress in x direction (t=15mm).....	8 3
Fig. 75 Residual stress in x direction (t=15mm).....	8 3
Fig. 76 Residual stress in y direction (t=15mm) .....	8 4
Fig. 77 Residual stress in y direction (t=15mm) .....	8 4
Fig. 78 Displacement in z direction (t=20mm).....	8 5
Fig. 79 Displacement in z direction (t=20mm).....	8 5
Fig. 80 Residual stress in x direction (t=20mm).....	8 6
Fig. 81 Residual stress in x direction (t=20mm).....	8 6
Fig. 82 Residual stress in y direction (t=20mm) .....	8 7
Fig. 83 Residual stress in x direction (t=20mm).....	8 7
Fig. 84 Angular distortion .....	8 8
Fig. 85 Comparison with experiment (Kim) .....	9 3

Fig. 86 Displacement in z direction (t=8mm).....	9 5
Fig. 87 Displacement in z direction (t=8mm).....	9 5
Fig. 88 Residual stress in x direction (t=8mm).....	9 6
Fig. 89 Residual stress in x direction (t=8mm).....	9 6
Fig. 90 Residual stress in y direction (t=8mm) .....	9 7
Fig. 91 Residual stress in y direction (t=8mm) .....	9 7
Fig. 92 Displacement in z direction (t=15mm).....	9 8
Fig. 93 Displacement in z direction (t=15mm).....	9 8
Fig. 94 Residual stress in x direction (t=15mm).....	9 9
Fig. 95 Residual stress in x direction (t=15mm).....	9 9
Fig. 96 Residual stress in y direction (t=15mm) .....	1 0 0
Fig. 97 Residual stress in y direction (t=15mm) .....	1 0 0
Fig. 98 Displacement in z direction (t=18mm).....	1 0 1
Fig. 99 Displacement in z direction (t=18mm).....	1 0 1
Fig. 100 Residual stress in x direction (t=18mm).....	1 0 2
Fig. 101 Residual stress in x direction (t=18mm).....	1 0 2
Fig. 102 Residual stress in y direction (t=18mm) .....	1 0 3
Fig. 103 Residual stress in y direction (t=18mm) .....	1 0 3
Fig. 104 Angular distortion .....	1 0 4
Fig. 105 Constraint condition .....	1 0 8
Fig. 106 Deformation in z direction.....	1 0 9
Fig. 107 Welding deformation algorithm .....	1 1 1
Fig. 108 Analysis model subjected to external load .....	1 1 2
Fig. 109 A cross sectional view of simplified concept model	1 1 3
Fig. 110 Analysis results of the model that external force is	

acting during cooling .....	1	1	7
<b>Fig. 111 Inherent strain model considering external constraint</b>			
during cooling.....	1	1	9
<b>Fig. 112 Inherent strain chart considering external constraint</b>			
during cooling (900°C) .....	1	2	0
<b>Fig. 113 Inherent strain chart considering external constraint</b>			
during cooling (1200°C) .....	1	2	0
<b>Fig. 114 Inherent strain chart considering external constraint</b>			
during cooling (1500°C) .....	1	2	1
<b>Fig. 115 Mechanism of restraint degree regarding external force</b>			
during cooling.....	1	2	2
<b>Fig. 116 Analysis cased that force is applied on both ends,</b>			
perpendicular to the weld line .....	1	2	4
<b>Fig. 117 Displacement in z direction (0 MPa).....</b>	1	2	5
<b>Fig. 118 Displacement in z direction (0 MPa).....</b>	1	2	5
<b>Fig. 119 Displacement in z direction (30 MPa).....</b>	1	2	5
<b>Fig. 120 Displacement in z direction (30 MPa).....</b>	1	2	5
<b>Fig. 121 Displacement in z direction (60 MPa).....</b>	1	2	6
<b>Fig. 122 Displacement in z direction (60 MPa).....</b>	1	2	6
<b>Fig. 123 Displacement in z direction (90 MPa).....</b>	1	2	6
<b>Fig. 124 Displacement in z direction (90 MPa).....</b>	1	2	6
<b>Fig. 125 Displacement in z direction (120 MPa).....</b>	1	2	7
<b>Fig. 126 Displacement in z direction (120 MPa).....</b>	1	2	7
<b>Fig. 127 Displacement in z direction (150 MPa).....</b>	1	2	7

Fig. 128 Displacement in z direction (150 MPa).....	1 2 7
Fig. 129 Maximum displacement in z direction (0 to 150 MPa)	1 2 8
Fig. 130 Three analysis cases that the external force is applied	1 3 0
Fig. 131 Improved equivalent strain method model that the external force is applied.....	1 3 0
Fig. 132 Displacement in z direction (M) .....	1 3 1
Fig. 133 Displacement in z direction (M) .....	1 3 1
Fig. 134 Residual stress in x direction (M) .....	1 3 1
Fig. 135 Residual stress in x direction (M) .....	1 3 1
Fig. 136 Residual stress in y direction (M) .....	1 3 2
Fig. 137 Residual stress in y direction (M) .....	1 3 2
Fig. 138 Three analysis cases that the external force is applied	1 3 2
Fig. 139 Improved equivalent strain method model that the external force is applied.....	1 3 3
Fig. 140 Displacement in z direction (2M) .....	1 3 3
Fig. 141 Displacement in z direction (2M) .....	1 3 4
Fig. 142 Residual stress in x direction (2M) .....	1 3 4
Fig. 143 Residual stress in x direction (2M) .....	1 3 4
Fig. 144 Residual stress in y direction (2M) .....	1 3 5
Fig. 145 Residual stress in y direction (2M) .....	1 3 5
Fig. 146 Maximum displacement in z direction.....	1 3 7
Fig. 147 Analysis model of 1000x1000x10 .....	1 3 8

# LIST OF TABLES

Table 1 Research on welding deformation .....	6
Table 2 Residual plastic strain of various analysis cases....	2 5
Table 3 Boundary condition on the core element.....	3 8
Table 4 Relationship between degree of restraint and plastic strain.....	5 2
Table 5 Degree of restraint (Planar type) .....	5 3
Table 6 Degree of restraint (Fillet type) .....	5 5
Table 7 Temperature–degree of restraint relation.....	5 7
Table 8 Summary of comparison with the previous study..	7 1
Table 9 Angular distortion results of butt welding (Sato and Terasaki).....	7 3
Table 10 Analysis model dimension and welding condition (t=6mm).....	7 4
Table 11 Angular distortion (t=6mm) .....	7 6
Table 12 Maximum residual stress in x direction (t=6mm)	7 7
Table 13 Maximum residual stress in y direction (t=6mm)	7 8
Table 14 Angular distortion (t=10mm) .....	7 9
Table 15 Maximum residual stress in x direction (t=10mm)	8 0
Table 16 Maximum residual stress in y direction (t=10mm)	8 1
Table 17 Angular distortion (t=15mm) .....	8 2
Table 18 Maximum residual stress in x direction (t=15mm)	8 3
Table 19 Maximum residual stress in y direction (t=15mm)	8 4
Table 20 Angular distortion (t=20mm) .....	8 5
Table 21 Maximum residual stress in x direction (t=20mm)	8 6

Table 22 Maximum residual stress in y direction (t=20mm)	8 7
Table 23 Angular distortion.....	8 9
Table 24 Residual stress in x direction.....	9 0
Table 25 Residual stress in y direction.....	9 1
Table 26 Demension of analysis model.....	9 4
Table 27 Angular distortion (t=8mm) .....	9 5
Table 28 Residual stress in x direction (t=8mm) .....	9 6
Table 29 Residual stress in y direction (t=8mm) .....	9 7
Table 30 Angular distortion (t=15mm) .....	9 8
Table 31 Residual stress in x direction (t=15mm) .....	9 9
Table 32 Residual stress in y direction (t=15mm) .....	1 0 0
Table 33 Angular distortion (t=18mm) .....	1 0 1
Table 34 Residual stress in x direction (t=18mm) .....	1 0 2
Table 35 Residual stress in y direction (t=18mm) .....	1 0 3
Table 36 Angular distortion.....	1 0 5
Table 37 Residual stress in x direction.....	1 0 6
Table 38 Residual stress in y direction.....	1 0 7
Table 39 Maximum deformation in z direction.....	1 0 9
Table 40 B.C. and results of 2D thermal elasto-plastic analysis .....	1 1 8
Table 41 Dimension of analysis model.....	1 2 4
Table 42 Maximum displacement in z direction (0 to 150 MPa) .....	1 2 8
Table 43 Dimension of analysis model.....	1 2 9
Table 44 Analysis results of external constraint model..	1 3 6
Table 45 Comparison of analysis time.....	1 3 9

# NOMENCLATURE

A	Area
a	Length of 1 <sup>st</sup> HAZ area
a	Half breadth
B	Breadth
b	Length of 2 <sup>nd</sup> HAZ area
c	The largest distance from the neutral surface
dS <sub>0</sub>	Initial length of an infinitesimal element
dS <sub>1</sub>	Length of an infinitesimal element in stresses state
dS <sub>2</sub>	Length of an infinitesimal element in stresses–released state
d	Thickness
E	Young’ s modulus
EPA	Elasto–plastic analysis
ESM	Existing equivalent strain methods
h	Thickness
I	Second moment of area
Improved ESM	Improved equivalent strain methods
K <sub>s</sub>	Stiffness of a solid
K <sub>Rx</sub>	Stiffness of a spring (x–direction)
K <sub>Ry</sub>	Stiffness of a spring (y–direction)
k	Degree of restraint
L	Length
M	Moment

$P$	External normal force
$Q$	Heat
$T_0$	Room temperature
$T_{\text{core}}$	Temperature of the core element
$TG$	Temperature gradient
$TG_x$	Temperature gradient in x-direction
$TG_y$	Temperature gradient in y-direction
$TG_z$	Temperature gradient in z-direction
$T_{\text{max}}$	Maximum temperature
$z$	Distance from the neutral surface in z-direction
$\alpha$	Thermal expansion coefficient
$\Delta T$	Temperature change
$\epsilon$	Strain
$\epsilon^e$	Elastic strain
$\epsilon_m$	Maximum absolute value of the strain
$\epsilon^p$	Plastic strain
$\epsilon^p_{x, y, z}$	Plastic Strain acting on core element
$\epsilon_{\text{res}}$	Residual stress
$\epsilon^{\text{th}}$	Thermal strain
$\epsilon_x, \epsilon_y, \epsilon_z$	Strain acting on core element
$\epsilon^*$	Inherent strain
$\theta$	Angular distortion
$\nu$	Poisson ratio

$\sigma$	Stress
$\sigma_{\text{core}}$	Stress of core
$\sigma_{\text{periphery}}$	Stress of periphery
$\sigma_{x, y, z}$	Stress acting on core element
$\sigma_{x2, x3...z2}$	stress acting on periphery elements
$\sigma_0$	Unit stress

# 1. Introduction

## 1.1. Background of this study

Nowadays, most commercial and naval ships are constructed by the block building method in shipyards. The blocks which constitute the ship hull are built in a series of production process and transferred to the pre-erection area for the preparation works including the correction of distortion. The distortion of a block is inevitably induced by welding and is accumulated during the sequential fabrication process.

As the block erection step accounts for about one-third of the whole shipbuilding process, the accuracy of a block's shape and size has a close relation with the overall efficiency of production in the shipyard.

The welding distortions reduce the fabrication accuracy of ship hull blocks and decrease productivity due to lots of correction works. To increase the precision of fabrication, the welding distortion and the exact distortion margin at every fabrication stage should be estimated to meet the allowable tolerances of ship hull blocks.

The prediction and control of welding distortions at the design stage has been an essential task for most shipyards to ensure the higher quality as well as higher productivity in

shipbuilding[1].

The most widely used method is the thermal elastio-plastic analysis method. This method gives relatively accurate result. But it has disadvantageous in computational time because of non-linearity of material. In addition, computation time becomes more extensive when considering the geometric non-linearity.

In order to overcome above difficulties, some efficient approaches to predict the welding distortion of the actual ship hull blocks are needed.

## 1.2. Research Status

The research of welding deformation has begun in 1930's. It was mainly conducted by experiments until computational numerical analysis development.

Analytic research on welding deformation was started in 1950's. Watanabe and Satoh[2], most representative researcher, conducted analytic solution based on elastic theory by imposing strain which cause welding deformation to initial state material. This useful study is the foundation of inherent strain-based equivalent loads.

The research on welding deformation analysis was actively studied after numerical analysis method was generalized by development of computer technology, finite differential method

and finite element method in 1960–1970's. Satoh and Terasaki[3] found the variables related to welding deformation based on heat transfer and thermal elasto–plastic theory, suggested the estimated equation about angular distortion and shrinking deformation by ordering the variables of bead–on welding experimental results. Tall[4] researched one dimensional welding deformation analysis problem. Masubuchi et al.[5] completed 1–dimensional thermal elasto–plastic analysis program based on Tall's method. Fujita and Nommoto[6], Ueda and Yamakawa[7], Masubuchi et al.[5], Masubuchi and Papazoglou[8], and Papazoglou et al.[9] applied FEM to plate's in–plane residual stress analysis about 2–dimensional structure. Okumoto[10] performed calculation on shrinking deformation of assembled beam by fillet welding and residual stress by butt–welding. Although deformation result and residual stress can be calculated by thermal elasto–plastic analysis, it has been limited on large structure analysis due to very long time–consuming analysis.

The equivalent load method which can give final deformation using elastic FE analysis was suggested for analysis of welding deformation on large structure such as ship. The equivalent load method can be divided into experimental method and method based on inherent strain.

The experimental equivalent load method can calculate conversely forces and moments which can gain shrinkage and

angular distortion based on the experiment. This method is suggested by Ueda et al.[11] in 1986, and he induced the moment equation of angular distortion same as Watanabe and Satoh[2]'s experimental estimation equation. Nomoto et al.[12][13] calculated the equivalent load by making up the correlation between angular distortion and heat input and utilized FEM to deformation analysis based on equivalent load method at the first time. In 1996, Kim et al.[14] studied for calculating equivalent load about angular distortion of fillet welding and longitudinal bending. And he assigned the results to Ueda et al.[11]'s suggested equivalent moment equation. In this way, the experimental equivalent load method calculates equivalent load based on the experimental data of welding members. This method can analyze for simple member, but has limited application for complex structure such as ship.

The equivalent load method based on inherent strain calculates the distributed inherent strain surrounding welding area and computes the equivalent loads by integrating the strain on the welding section area. In 1996, Murakawa et al.[15] proposed 1 dimensional bar-spring model which describes the inherent strain as the function of maximum temperature and constraint constant. Thermal elasto-plastic analysis using bar-spring model was performed by Seo and Jang[16] in 1997. Jang et al.[17] proposed disk-spring model which can be used to three dimensional structure analysis using the equivalent load

method based on the inherent strain in 1997. Lee[18] performed welding deformation analysis according to welding sequence for hull plane block in 2002. Kim[19] studied structural analysis considered hardening effect using the equivalent load method based on the inherent strain in 2006.

Recently, Ha[20] proposed the equivalent thermal strain method calculating inherent strain not using the equivalent load. This study can conveniently estimate the deformation using scalar expression thermal strain instead of vector expressed load.

Research status is summarized in Table 1.

Table 1 Research on welding deformation

Approach		Age	Researchers
Method based on elastic theory		1950	Watanabe Sato Fujimoto
Numerical analysis method		1960	Rosenthal Masubuchi Hibbitt Rybicki Argyris
Equivalent load method	Based on experiment	1980	Ueda Nomoto Lee, J. S. Kim, S. I.
	Based on inherent strain	1990	Jang, C. D. Seo, S. I. Ko, D. E.
Equivalent strain method based on inherent strain		recent	Jang, C. D. Ha, Y. S.

### 1.3. Objectives

The main purpose of present study is to propose an efficient approach to predict the welding deformation based on the inherent strain theory combined with the finite element analysis.

Specific goals are as follows.

- i) Development of a quick method to perform analysis
- ii) Development of a method to analysis considering deformation control
- iii) Development of an analytical method precisely predicting both deformation and residual stress
- iv) Validation of a method under the various conditions of butt and fillet welding
- v) Suggestion of the equivalent strain method adaptable to welding model under external constraint

### 1.4. Organization

In Chap. 2, overall process is introduced for equivalent strain method based on inherent strain. The degree of restraint is delineated and defined. The process to perform the welding analysis in a conventional method is also described in Chap. 2. Limitation of the method in previous study is pointed out in Chap. 3. Chapter 4 is devoted to the establishment of the

improved equivalent strain method. A new inherent strain model considering 3 dimensional constraints is proposed to construct the inherent strain chart. The effect of temperature gradient is newly reflected in the inherent strain chart. Improved equivalent strain method, conventional equivalent strain method, and thermal elasto–plastic method are compared with the experimental results in Chap. 5. In Chap. 6, external constraint during cooling stage is taken into account in the improved equivalent strain method. Welding analysis model under external force during cooling stage is idealized as a prismatic member subjected to pure bending. Analytical validation of this is done in Chap. 7. Chapter 8 shows a comparison of the analysis time between improved equivalent method and thermal elasto–plastic method. The conclusion is laid in Chap. 9.

## 2. Equivalent strain method based on inherent strain

### 2.1. Definition of the inherent strain

The inherent strain is defined mechanically as follows: At first, there is a material object that has no stress distribution. When it is under stress by any causes, stress acting on an element of material is accompanied by strains. Then the stress is released by cutting out a small part of material, however, residual and irrecoverable strain may still exist. This strain is regarded as the inherent strain.

It can be explained as three material states shown in Fig. 1. The initial state has no stress distribution (Fig. 1a) inside, and the material experiences stressed condition caused by phenomenon such as thermal strain (Fig. 1b) and the stress is partly released by cutting a part from the material (Fig. 1c) [21].

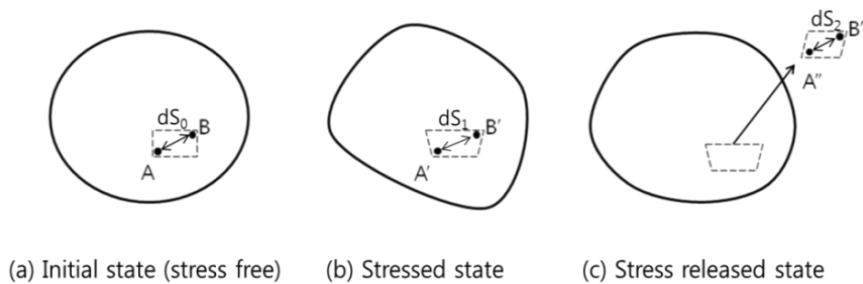


**Fig.1 Definition of the inherent strain**

A small element AB( $dS_0$ ) of material in the initial state is deformed into A'B'( $dS_1$ ) when material get stressed. A'B' is deformed into A''B''( $dS_2$ ) by cutting out from the material to remove the elastic strain. Based on the above definition, the inherent strain( $\epsilon^*$ ) is expressed by subtracting the elastic strain from the total strains as follows.

$$\epsilon^* = \frac{dS_2 - dS_0}{dS_0}$$

The total strain can be divided into the elastic, thermal, and plastic strains,

$$\epsilon = \epsilon^{th} + \epsilon^p + \epsilon^e$$

In the middle of welding process, the inherent strain is the sum of thermal and plastic strains.

$$\epsilon^* = \epsilon - \epsilon^e = \epsilon^{th} + \epsilon^p$$

After welding process, temperature of steel member returns to room temperature and the thermal strain becomes zero. Therefore, the inherent strain is the same as the residual plastic strain[19].

$$\epsilon^* = \epsilon - \epsilon^e = \epsilon^p$$

## 2.2. Welding analysis based on inherent strain

Two contrasting methods, for the prediction of welding distortion and residual stress, have the pros and cons.

One is the thermal elasto-plastic analysis in which the welding is treated as a transient nonlinear problem. Distortion and residual stress induced by welding are generated through three complex processes: i) heat transfer by the heating and cooling, ii) non-uniform temperature distribution and thermal stress, and iii) changes in mechanical properties of the material due to temperature changes. These are mechanical thermal elasto-plastic analyses of large deformation. This method tracks iterative elasto-plastic processes mechanically in accordance with the thermal conductivity. It is known to give relatively accurate result. However, the process is time-consuming due to material non-linearity. In addition, the computational time becomes more longer if geometric non-linearity is taken into account as well.

The other is the inherent strain method in which the distortion and residual stress are computed by elastic analysis imposing the inherent strain as initial strain. Inherent strain method is an economical and simple method in the prediction of welding deformation of large-scaled structure. Inherent strains always remains along weld bead and nearby zone which

undergoes a large thermal cycle. It is considered as a source causing the welding deformation. This method is advantageous in computational time. However, it has a disadvantage that details of the welding condition may not be fully reflected in some cases.

Inherent strain method is again divided into two different methods: equivalent loading method and equivalent strain method. Equivalent loading method is to predict welding deformation by imposing equivalent concentrated loads which are converted from inherent stress remaining along the heat affected zone [17]. This method is simple but its demerit is incapable of predicting welding residual stress. The analysis procedure is summarized in Fig. 2.

In the equivalent strain method, equivalent strain is applied to the model directly instead of the equivalent loads. By omitting the process of calculating the equivalent loads, analysis time is shortened while the results become more accurate. Its strength is to enable the evaluation of welding residual stresses as well as welding deformation. The procedure is explained in Fig. 3.

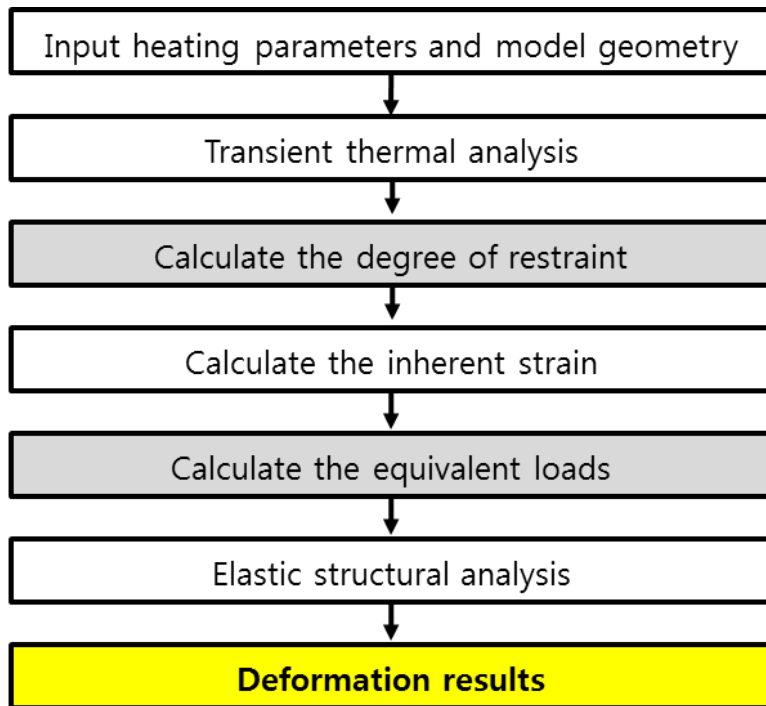


Fig.2 Procedure for prediction of deformation using equivalent loading method

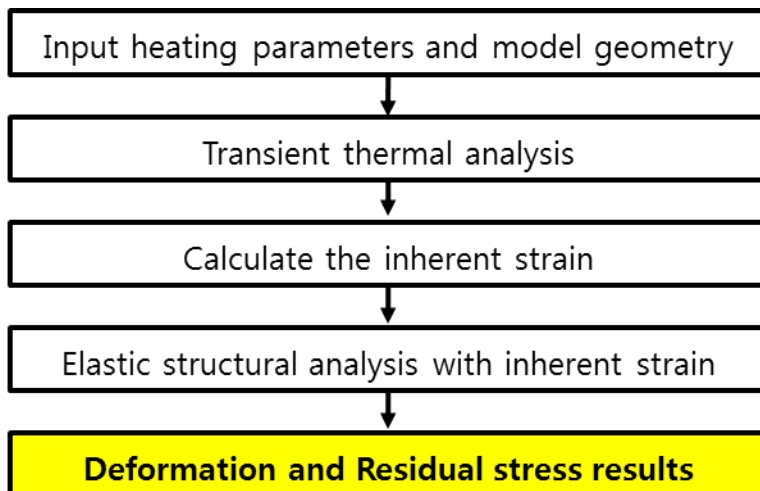


Fig.3 Procedure for prediction of deformation and residual stress using equivalent strain method

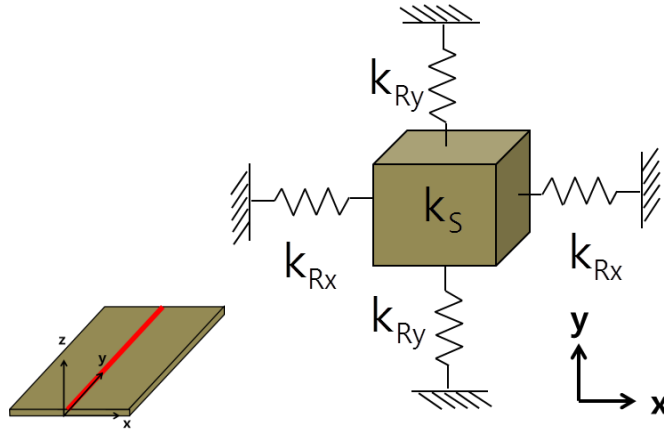
## 2.3. Calculation of the inherent strain in a previous equivalent strain method

### 2.3.1. Simplified inherent strain model for equivalent strain method

Two important factors to determine equivalent strain are the highest temperature and degree of restraint. The highest temperature indicates the maximum temperature that each point in the heat affected region experiences through whole welding time. The degree of restraint represents the level of resistance against the thermal deformation of the welding region. After calculating of the highest temperature and the degree of restraint, inherent strains are determined through an integration process in the inherent strain region. Depending on the way of idealizing heat affected region, the value of inherent strain differs.

In the recent study, the inherent strain distribution can be formulated using a simplified thermal elasto–plastic analysis model as shown in Fig. 4[23]. The welding region, where inherent strain occurs, can be modeled as a solid and springs. In this model, heat affected region is idealized as the solid element (called core), and adjacent regions putting a restraint on the core are idealized spring elements (called periphery). The restraint degree in z–direction (thickness direction) is omitted

since it is assumed to be not significantly effective to the deformation.



Where

$K_s$ : stiffness of a solid

$K_{Rx}$ : Stiffness of a spring (x-direction)

$K_{Ry}$ : Stiffness of a spring (y-direction)

**Fig. 4 Simplified thermal elasto-plastic analysis model**

FE analysis is used to calculate the inherent strain. Temperature-dependent material properties are used for the core and the periphery considered as springs are converted to structural-solid elements which have elastic modulus to induce equivalent restraint as shown in Fig. 5.

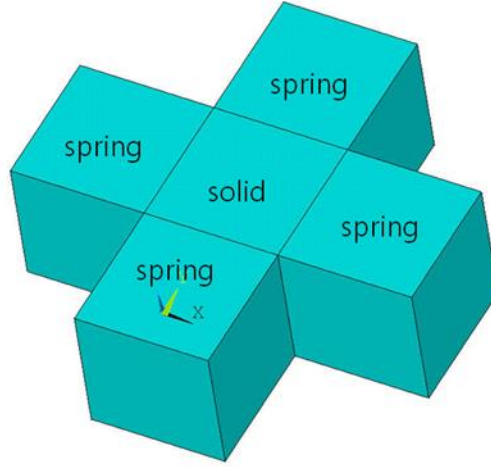


Fig. 5 Simplified thermal elasto-plastic FE analysis model

Elastic modulus of the periphery is determined through the following process.

Assuming that stresses  $\sigma_x = \sigma_y = \sigma$  is applied by the definition of inherent strain and equations of the strains in biaxial stress.

$$\sigma_{core} + \sigma_{periphery} = \sigma$$

$$\varepsilon = \frac{1}{E_{core}}(1 - \nu)\sigma_{core} = \frac{2}{E_{periphery}}\sigma_{periphery} = \frac{1}{E_{core}}(1 - k)(1 - \nu)\sigma$$

$$\sigma_{core} = (1 - k)\sigma$$

$$\sigma_{periphery} = k\sigma$$

$$E_{core} = 2E_{periphery} \frac{k}{(1 - k)(1 - \nu)}$$

### 2.3.2. Inherent strain chart for equivalent strain method

Analysis results are as follows. X-axis is degree of restraint which is divided by 0.01 intervals in the range from 0.01 to 0.99, and y-axis is inherent strain. Each graph is organized according to highest temperature which divided by 50°C in the range from 0 to 2000°C.

The final residual inherent strain after thermal cycle can be determined using the highest temperature and degree of restraints shown in Fig. 6–8[23]. Fig. 6 shows inherent strain chart for butt welding, Fig. 7–8 show inherent strain charts for fillet welding.

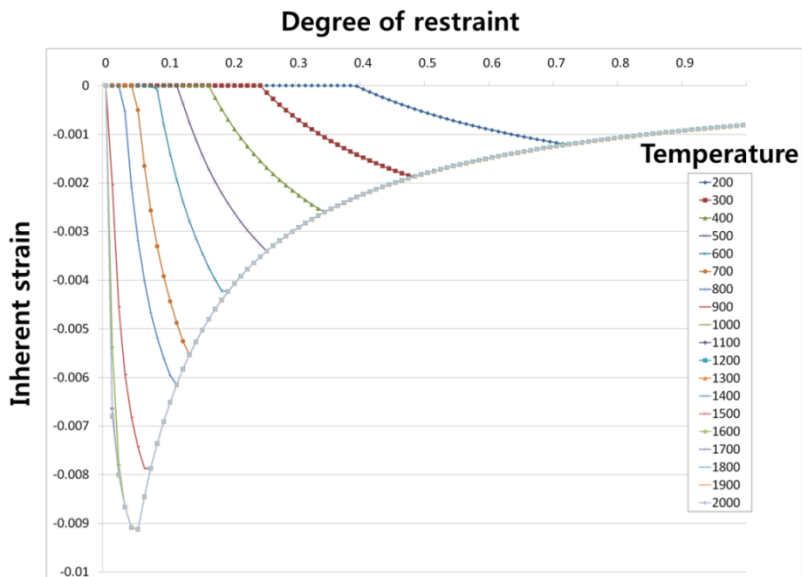


Fig. 6 Inherent strain chart of butt welding

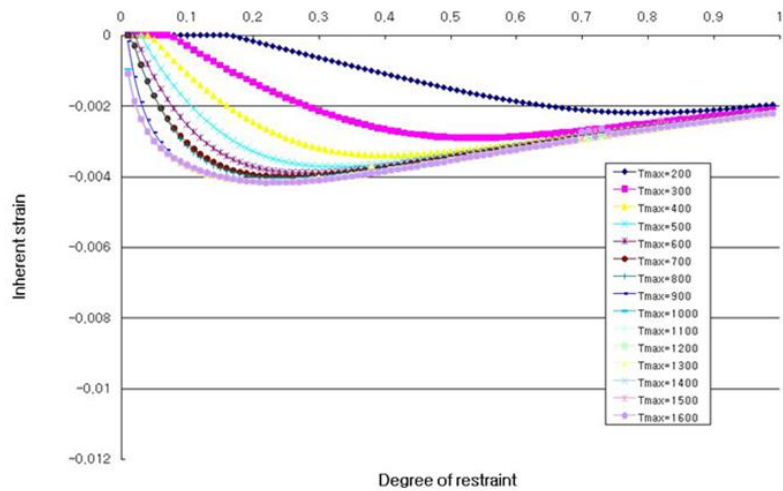


Fig. 7 Inherent strain chart of fillet welding (Vertical direction of weld line)

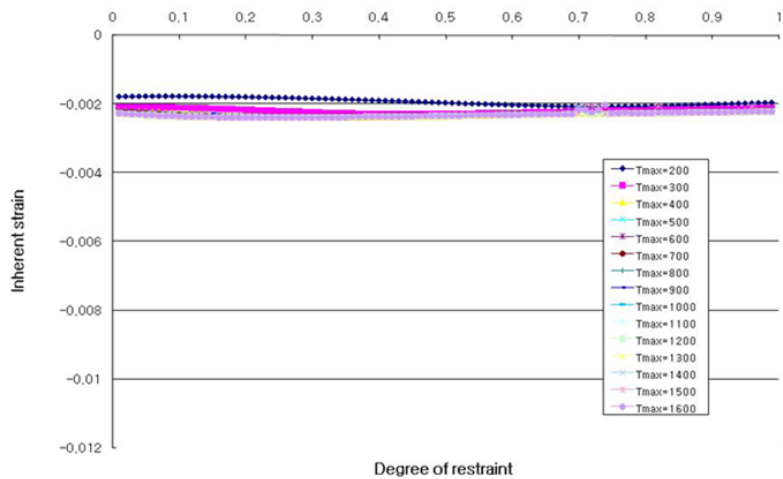


Fig. 8 Inherent strain chart of fillet welding (Weld line direction)

### 2.3.3. Distribution of the highest temperature

The heat transfer analysis is conducted to calculate the temperature distribution of welded structures. The welding heat

source is modeled as a normal–distributed moving heat flux. The highest temperature at each node in the finite element model is calculated by the heat transfer analysis.

#### 2.3.4. Calculation of degree of restraint

The degree of restraint of stiffened panel is determined from the analogy of solid–spring model and the elastic finite element analysis using unit load. This method applies unit loads to points where the inherent strains are inputted. An iterative calculation is needed to find the degree of restrains of all input points.

Fig. 9 shows procedure to calculate equivalent strain.

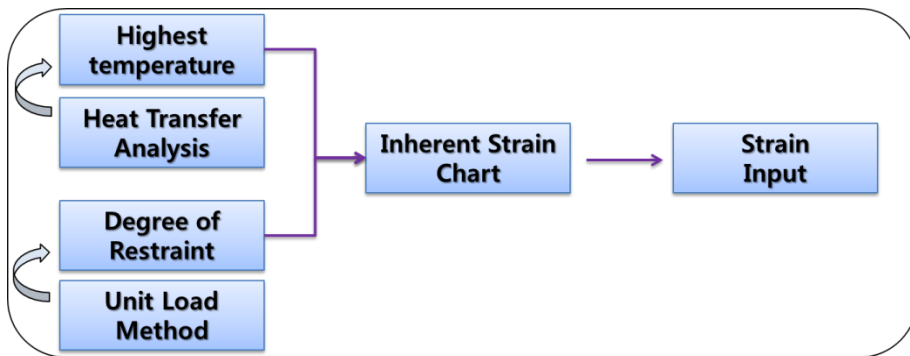


Fig. 9 Calculation of equivalent strain

### 3. Limitation of equivalent strain method in previous study

#### 3.1. Absence of consideration of the temperature distribution

Inherent strain model in previous study is based on the assumption that the inherent strain value is changed in accordance with degree of restraint and the highest temperature. However, beyond a certain temperature, regardless of the maximum temperature, inherent strain value corresponding to the degree of restraint becomes constant.

In a common welding analysis model of steel, the degree of restraint ranges from 0.4 to 0.7 for the most part. In this case, inherent strain has the same value regardless of the highest temperatures as long as it is beyond 300°C. It varies depending on only the degree of restraint as shown in Fig. 10.

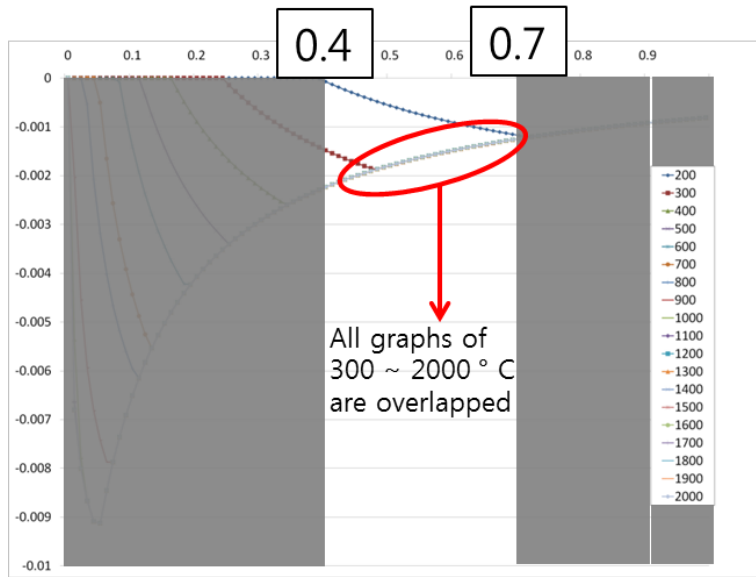


**Fig. 10 Inherent strain chart (0.4–0.7 degree of restraint)**

The temperature of core element increases to the highest temperature ( $T_{\max}$ ) and then returns to room temperature ( $T_0$ ),  $T_0 \rightarrow T_{\max} \rightarrow T_0$ . If  $T_{\max}$  reaches to sufficiently high temperature (300°C at this case), the heating and cooling process of elasto–perfectly plastic model can be divided in four stages as shown in Fig. 11. The first two stages are elastic and plastic process with temperature rising and the last two stages are elastic and plastic process with temperature falling down. The intermediate history is different dependent on the highest temperature. However, the ending pathway is the same independent of the highest temperature.

While the temperature rises to 450°C and drops to room temperature, plastic strain varies along the path  $O \rightarrow A \rightarrow B'$

→ C' → C. OA is an elastic interval. Compressive elastic strain increases and the plastic strain begins at A. Compressive plastic strain grows constantly in AB'. As cooling starts, elastic strain occurs again in B'C', which is the twice the length of OA. In this stage, compressive elastic strain changes into tensile strain gradually and elastic tensile strain arrives at the limit, point C'. Then compressive plastic strain decreases along the same slope as that of AB', and eventually reaches the point C.

Since a slope of the plastic deformation section and the length of the elastic deformation section is the same, the residual plastic strain is also the same as long as the highest temperature is over 300°C.

Considering material non-linearity, shape of the graph is altered without any fundamental change even if it does not correspond to the experimental results or thermal elasto-plastic analysis results.

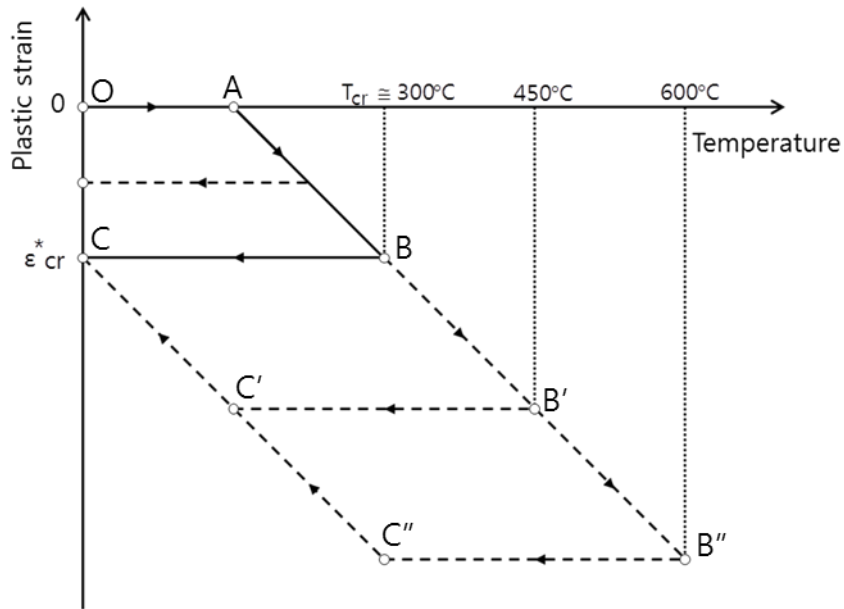


Fig. 11 Thermal history of plastic strain

Fig. 12 shows the highest temperature and residual plastic strain distributions of same FE model with different heat input. Each case has the same degree of restraint at the same node, but plastic strain distribution is different depending on the highest temperature. The inherent strain chart obtained from the existing equivalent method is not able to cover this difference.

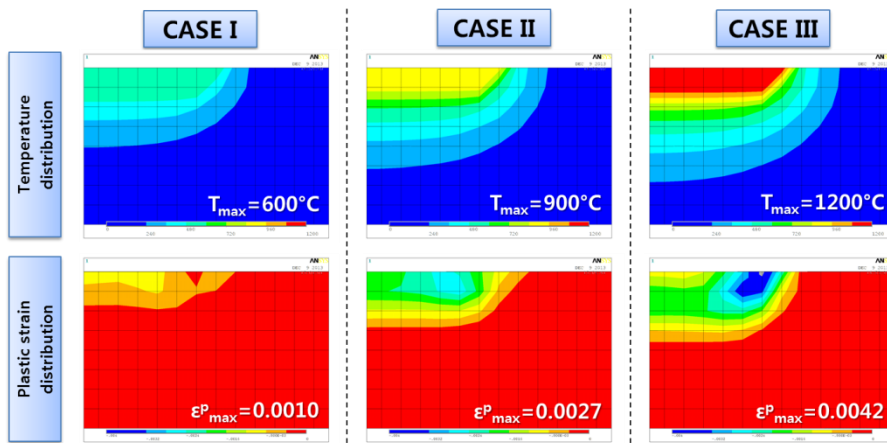


Fig. 12 Temperature and residual plastic strain distributions of same FE model with different heat input

Furthermore, plastic strain value differs according to the distribution of surrounding temperature even if degree of restraint and the highest temperature are exactly the same as depicted in Fig. 13.

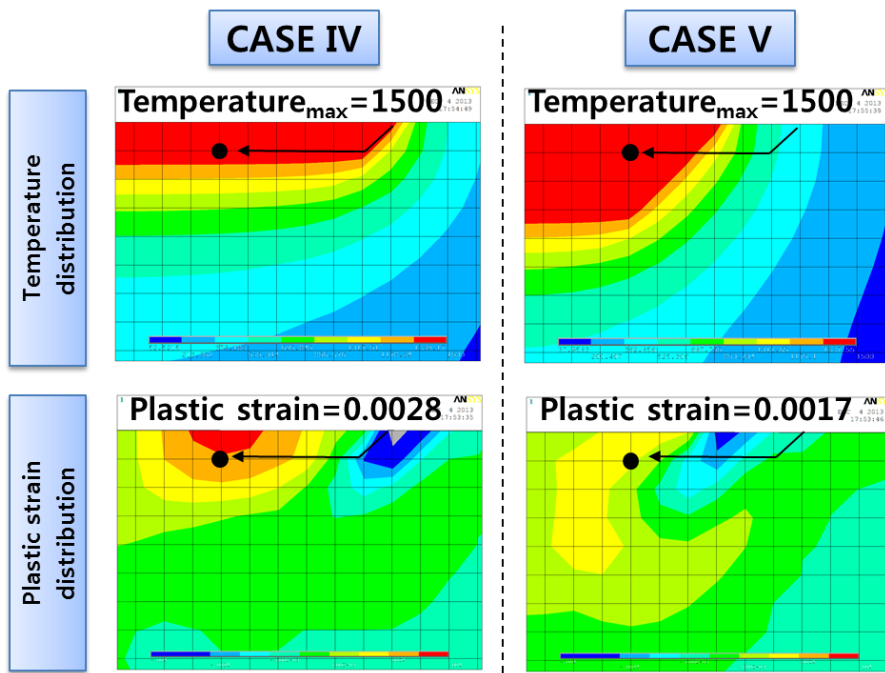


Fig. 13 Temperature and residual plastic strain distributions of same point with same degree of restraint and highest temperature

Table 2 Residual plastic strain of various analysis cases

Analysis Case	Degree of restraint	Highest temperature(°C)	Residual plastic strain
I	0.57	600	0.0010
II	0.57	900	0.0027
III	0.57	1200	0.0042
IV	0.57	1500	0.0028
V	0.57	1500	0.0017

The contents of Fig.12–13 are summarized in Table 2. All values listed in Table 2 are those measured at the same position. At this position of case I, II and III, residual plastic strains are 0.0010, 0.0027 and 0.0042 respectively. Since the critical temperature is 300°C, the residual plastic strain is not supposed to be different in these cases according to the existing equivalent strain method. At least, plastic strains have to be identical in case IV and V, but not even similar. These results mean that residual strain cannot be evaluated accurately by only two factors, degree of restraint and the highest temperature.

This is because the inherent strain model uses the assumption of equivalent loading method improperly. Welding model is completely divided into two regions of heat affected region and the periphery in the equivalent loading method. Then, the effect of all inherent strains is represented by a single load applied to heat affected region. At this time, it is assumed that temperature gradient of the periphery is neglected as shown in Fig. 14.



**Fig. 14 Concept of welding model in equivalent loading method**



**Fig. 15 Actual temperature distributions**

In the equivalent inherent strain method, equivalent strains are inputted directly instead of equivalent loads. Therefore, continuity of the actual temperature distribution should be considered as shown in Fig. 15. Temperature and inherent strain are distributed continuously from the region of heat input to the region free from the heat input. In order to find the inherent strain of elements, it should be taken into account even temperature dependent characteristics of the periphery.

### **3.2. Repetitive calculation of degree of restraint**

As mentioned, the whole model is divided into independent regions when calculating the degree of restraint as shown in Fig. 16. Here, distinction between heat affected region and the

periphery depends on welding conditions, shape of structure or analysis location. Moreover, the existing equivalent inherent strain method requires a calculation of the degree of restraint along a line in the vicinity of the welding line where inherent strains are to be inputted. In addition, it needs to be calculated over thickness direction.

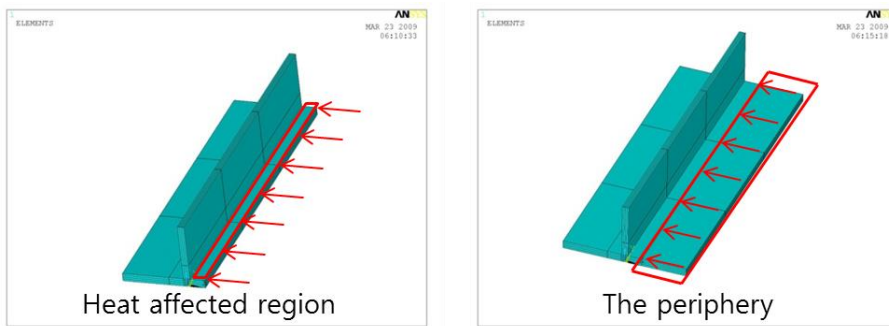


**Fig. 16 Heat affected region and the periphery**

This requires a repetitive calculation at all positions that inherent strain values are applied to for all welding cases. In case of a complex welding model such as Fig. 17, a lot of calculation of the degree of restraints should be carried out. For a different welding process, different FE analysis for unit load method may be required separately.

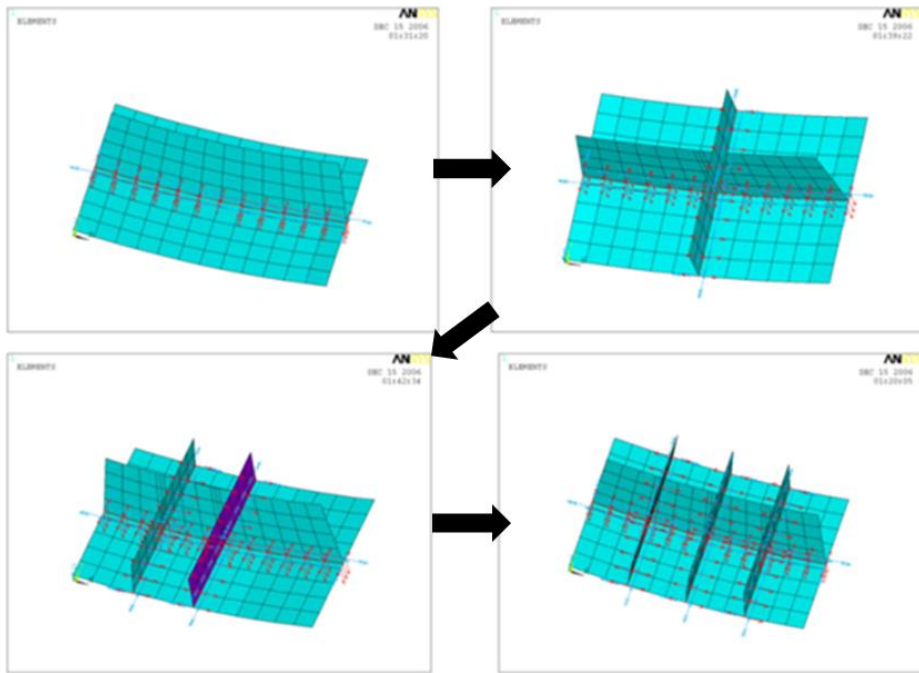


Fig. 17 Complex welding analyses

### 3.3. Strain input

Inherent strain of each node can be read from the inherent strain chart. However, it would be quite inefficient to input inherent strain values for all nodes of FE model that experience high weld temperature. Therefore, a method to input equivalent strain values to some representative nodes is needed for a practical purpose.

First, heat affected zone is divided into high temperature zone and low temperature zone. High temperature zone is defined as a region of twice the leg length in transverse in-plane direction, perpendicular to the weld line. Low temperature zone is defined as the region which experiences temperature

higher than 100°C excluding the high temperature zone as depicted in Fig. 18.

Average strain value is calculated in each region and at each layer across the thickness. Then, for each layer, a node in the middle of each zone is selected as the representative node and the averaged strain value is imposed there.

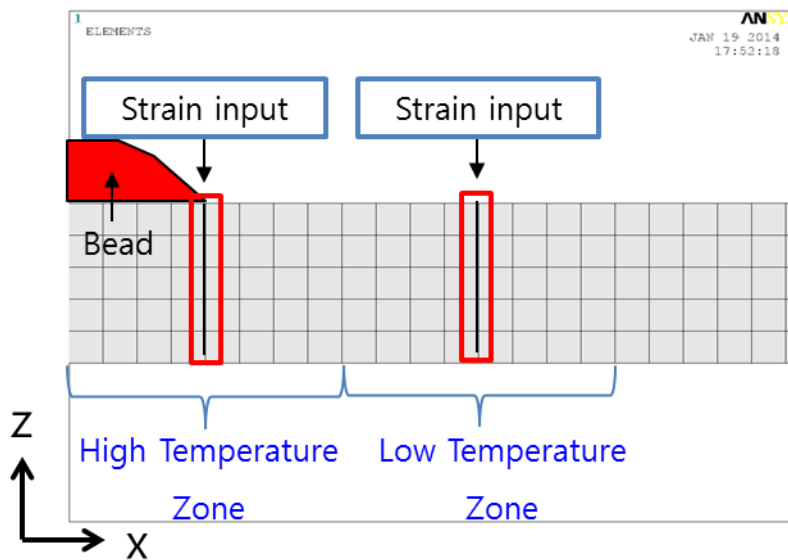


Fig. 18 Strain input

The average strain value of each layer is substituted to thermal strain and applied to the representative node. If assuming the thermal expansion coefficient,  $\alpha$ , as 1.0, inherent strain is the same as the temperature given by Eq. (3-1). Therefore, inherent strain can be applied in the form of temperature, and it spreads around like a heat transfer from a

heat source.

$$\varepsilon_{res} = \alpha \Delta T = \Delta T \quad (3-1)$$

This approach is expected to enable to spread the strain values applied to the representative nodes out to the neighboring nodes like interpolation or extrapolation.

Contrary to the expectation, actual heat transfer result is different from the interpolation. Fig. 19 shows actually applied thermal input obtained from one step of heat transfer analysis executed prior to elastic FE analysis.

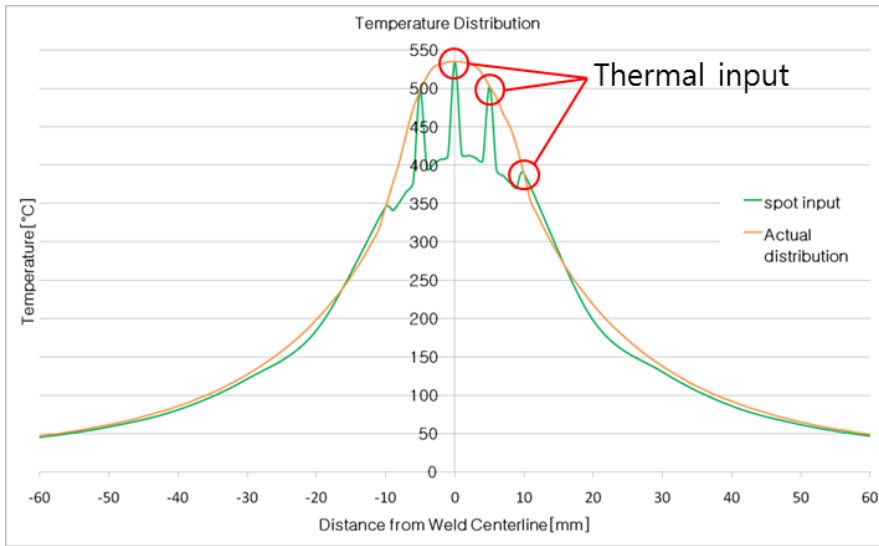


**Fig. 19 Temperature distributions between spot input model and actual model**

This leads to a result which does not properly fulfill the re-distribution of strain as shown in Fig. 20. Stresses and

strains are concentrated in the input positions.

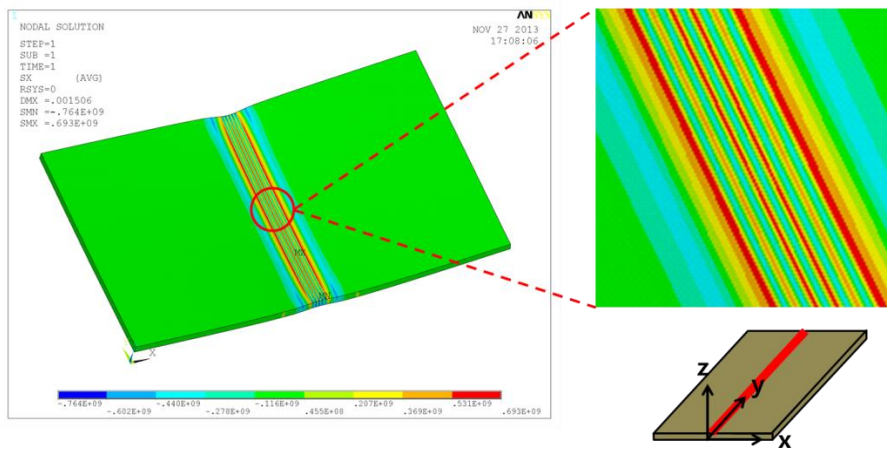


Fig. 20 Residual stress distribution (x-direction)

## 4. Improved equivalent strain method considering the temperature distribution

### 4.1. Improved solid–spring model

When a small part of material expands or shrinks by temperature gradient due to welding, restraint force acts largely on the horizontal plane rather than the vertical plane of the force direction as shown in Fig. 21.

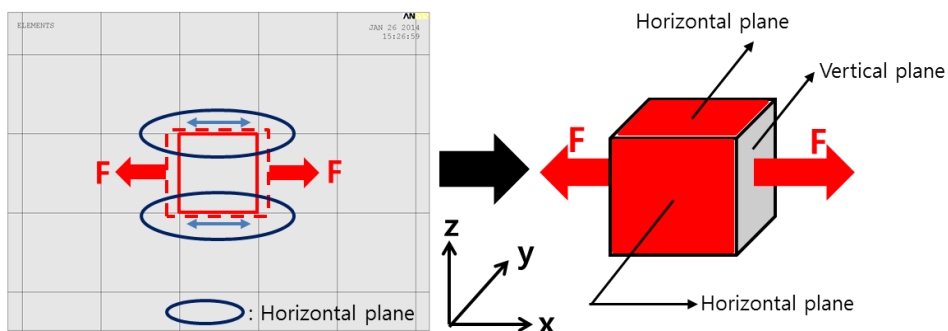


Fig. 21 Working surface of the restraint

As shown in Fig. 22, under the condition that the load in the same direction is applied and Poisson's ratio of the model is zero, an element on the left is subject to resistance from the normal surface shared by two vertically adjacent elements. However, an element on the right is free from the resistance of periphery subject to this load.

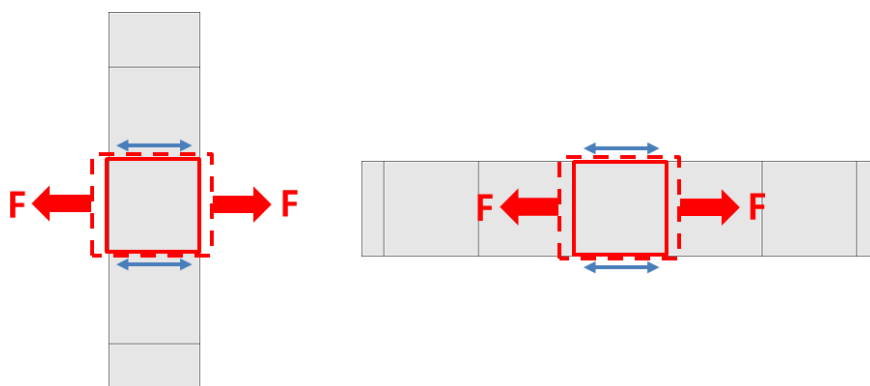


Fig. 22 The extreme cases of working surface of restraint

This means that the resistance to the force which drives to expand or shrink in the lateral would increase when the rigidity of two vertically attached elements becomes greater.

#### 4.1.1. Restraint positions of solid–spring model

As discussed above, the proposed restraint model is closer to the actual phenomenon and more intuitive by placing proper elements matching with actual restraint than the previous model. Process to modify the restraining position of the existing model and to generate FE model is shown in Fig.23–26. All elements, except RBE elements, are in the form of a regular hexahedron. The modification in one dimension is extended into two dimensions and three dimensions.

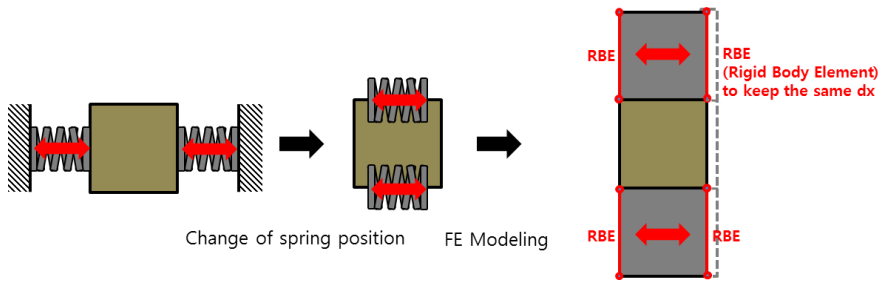


Fig. 23 Uniaxial restraints model

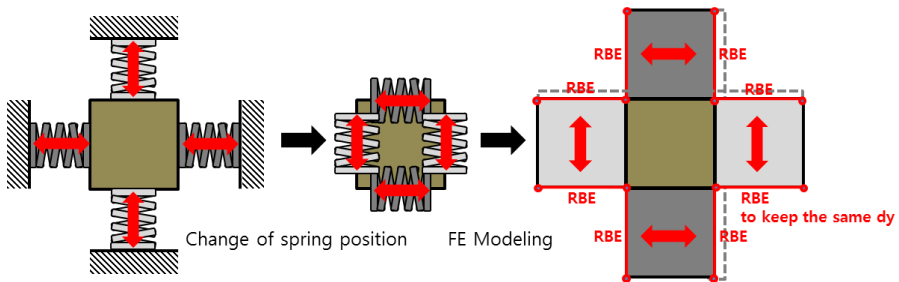


Fig. 24 Biaxial restraints model

One dimensional inherent strain model expressing uniaxial restraint is shown in Fig. 23. It can be simply extended to biaxial restraint model as shown in Fig. 24 by adding spring elements acting in orthogonal direction. The horizontally attached elements affects the vertical behavior and the vertically attached elements the horizontal behavior.

Likewise, restraining forces against x-directional force act dominantly on faces perpendicular to y and z-axis in a three dimensional model. This is also the same to the other axes.

Three dimensional inherent strain model is shown in Fig. 26.  
 Fig. 27 represents its disassembled view.

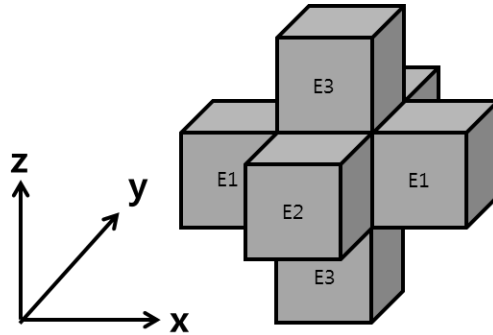


Fig. 25 Tri-axial restraints model

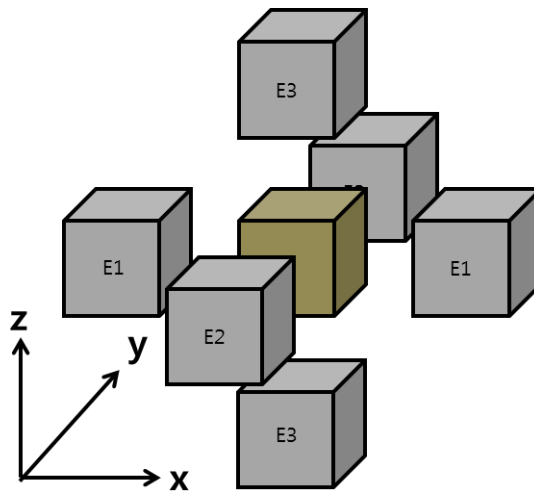


Fig. 26 Disassembled view of tri-axial restraints model

Mainly restraining elements against the expansion of core element in each of three directions are marked in Fig. 27.

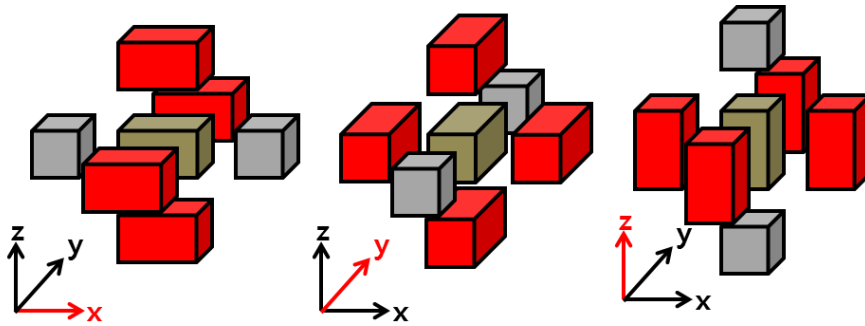


Fig. 27 Restraining elements for the each load direction

#### 4.1.2. Boundary condition of solid–spring model

A solid–spring model is considered to be axially symmetric. One of two faces normal to each axis is fixed and the other is allowed to move freely to the axis. This boundary condition prevents a rigid body motion without disturbing intended structural behavior. Boundary condition adopted in this analysis is depicted in Fig. 28 and Table 3.

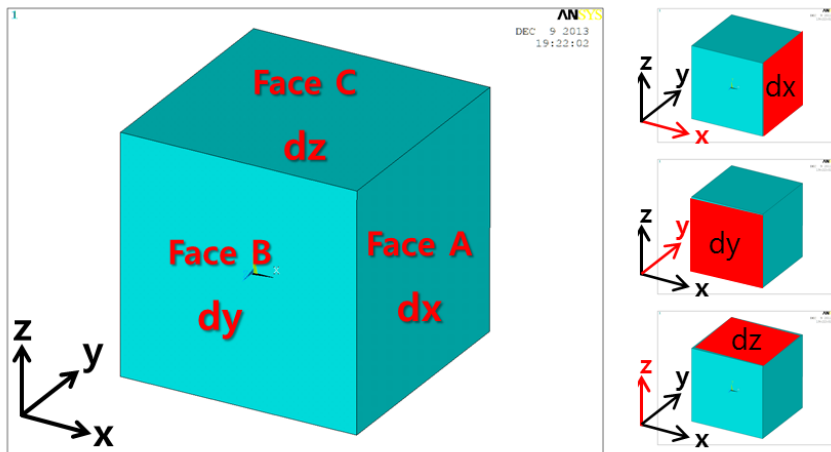


Fig. 28 Boundary condition on the core element

Table 3 Boundary condition on the core element

	Face A	Face B	Face C
dx	×	Free	Free
dy	Free	×	Free
dz	Free	Free	×

Under this boundary condition, core element behavior by heating and cooling is as shown in Fig. 29–30.

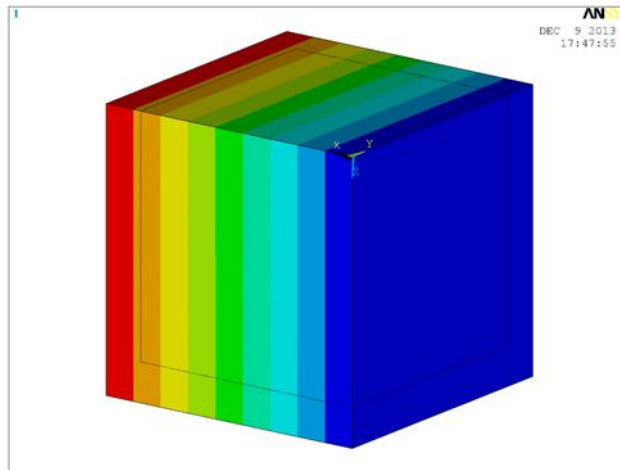


Fig. 29 Expansion of core element

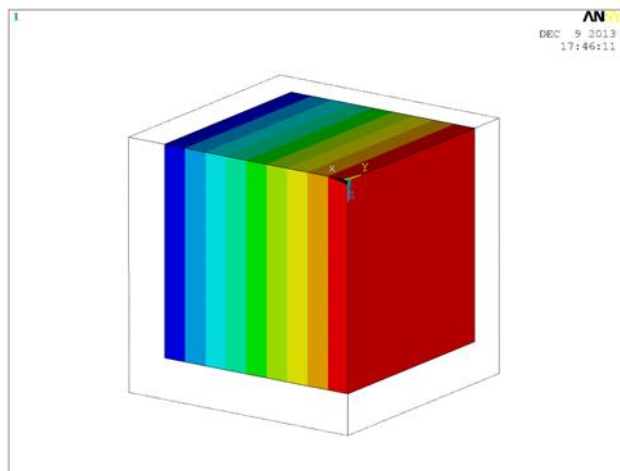


Fig. 30 Shrinkage of core element

#### 4.1.3. Calculation of elastic modulus of the periphery elements

Elastic modulus of the periphery to induce equivalent restraint is determined through the following process.

The left box of Fig. 31 contains a core element without restraint and the right box of Fig. 32 is a core element subject to restraints by the neighboring elements. If each system is under the same tri-axially identical unit stress  $\sigma_0$ , the degree of restraint can be expressed by the ratio of strain( $\varepsilon'$ ) of a core element subject to restraint by the periphery to that( $\varepsilon_0$ ) without restraint. Degree of restraint is defined as follows.

$$\text{Degree of restraint } k = \frac{\varepsilon_0 - \varepsilon'}{\varepsilon_0}$$
$$(1 - k) \varepsilon_0 = \varepsilon' \quad (4-1)$$

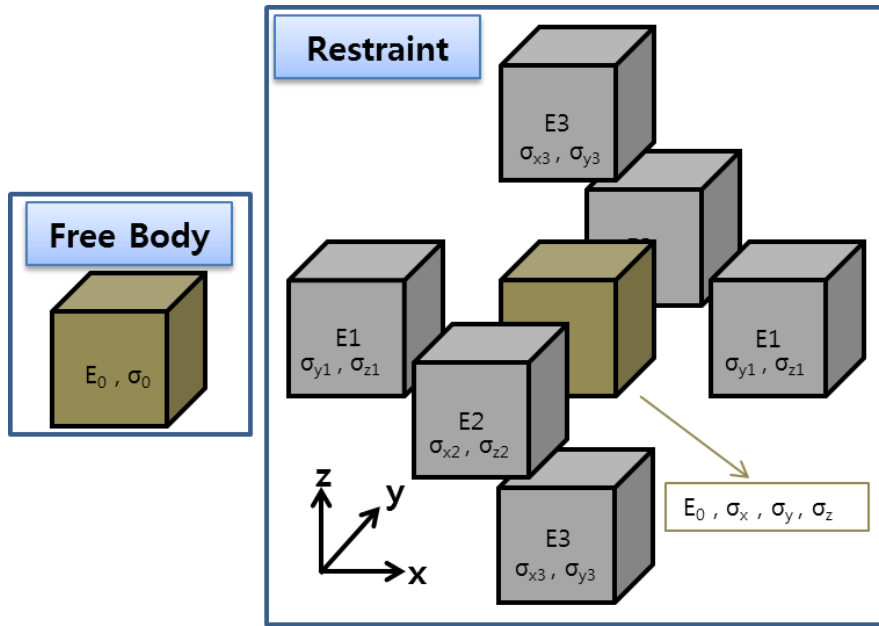


Fig. 31 Definition of stress

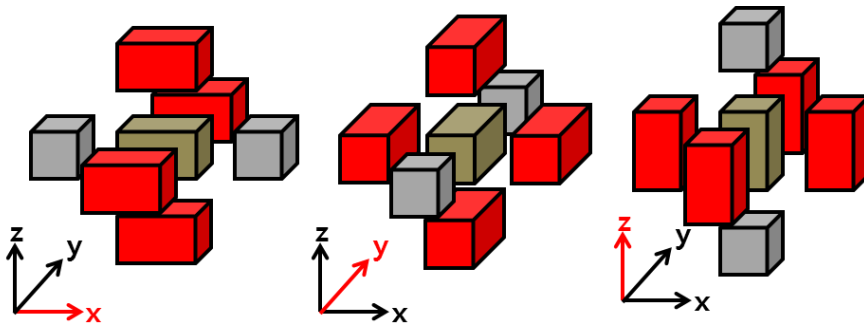


Fig. 32 Restraint element for the each load direction

Based on the definition of the restraint model as represented in Fig. 32, unit stress  $\sigma_0$  applied to the model is divided to the unknown stress, such as  $\sigma_{x2}, \sigma_{x3}, \sigma_{y3}, \dots, \sigma_{z2}$ . Thus, the equation of equilibrium is,

$$\begin{aligned}
\sigma_0 &= \sigma_x + 2(\sigma_{x2} + \sigma_{x3}) \\
&= \sigma_y + 2(\sigma_{y3} + \sigma_{y1}) \\
&= \sigma_z + 2(\sigma_{z1} + \sigma_{z2})
\end{aligned}$$

$\sigma_0$  = unit stress

$\sigma_x, \sigma_y, \sigma_z$  = stress of a core element

$\sigma_{x2}, \sigma_{x3}, \sigma_{y3}, \dots, \sigma_{z2}$  = stress of periphery elements

Definitions of the above-defined stresses are illustrated in Fig. 31. The index, 1, 2 and 3 in the subscript indicates the position of restraining elements which are attached perpendicular to x, y, z-axis, respectively. The character, x, y, and z represents the direction of stress of each element.

An element of material subjected to normal stresses  $\sigma_x$ ,  $\sigma_y$ , and  $\sigma_z$  acting in three mutually perpendicular directions is said to be in a state of tri-axial stress. If the material follows Hooke's law, the relationship between the normal stresses and normal strains can be obtained. Strains induced by the stresses  $\sigma_x$ ,  $\sigma_y$ , and  $\sigma_z$  acting independently are superimposed to obtain the resultant strains. Thus, following equations are derived in tri-axial stress:

$$\epsilon_x = \frac{1}{E} [\sigma_x - \nu(\sigma_y + \sigma_z)]$$

$$\epsilon_y = \frac{1}{E} [\sigma_y - \nu(\sigma_z + \sigma_x)]$$

$$\epsilon_z = \frac{1}{E} [\sigma_z - \nu(\sigma_x + \sigma_y)]$$

In these equations, the standard sign conventions are used; That is, tensile stress  $\sigma$  and extensional strain  $\epsilon$  are positive.

In a special case of  $\sigma_x = \sigma_y = \sigma_z = \sigma$ , The resulting equations are simplified to an equation (4-2).

$$\epsilon = \frac{1}{E} [(1 - 2\nu)\sigma] \quad (4-2)$$

Eq. (4-1) is applied to each axis direction of the model shown in Fig. 31,

$$\begin{aligned} \epsilon_{0x} &= \frac{1}{E_0} (1 - 2\nu)\sigma \\ \epsilon_{0y} &= \frac{1}{E_0} (1 - 2\nu)\sigma \\ \epsilon_{0z} &= \frac{1}{E_0} (1 - 2\nu)\sigma \end{aligned} \quad (4-3)$$

$$\begin{aligned} \epsilon'_x &= \frac{1}{E_0} [\sigma_x - \nu(\sigma_y + \sigma_z)] \\ \epsilon'_z &= \frac{1}{E_0} [\sigma_z - \nu(\sigma_x + \sigma_y)] \\ \epsilon'_y &= \frac{1}{E_0} [\sigma_y - \nu(\sigma_z + \sigma_x)] \end{aligned} \quad (4-4)$$

Substituting Eq. (4-3) and (4-4) into Eq. (4-1), definition of degree of restraint, then Eq. (4-5) can be obtained as follows.

$$\begin{aligned}
\frac{1}{E_0} [\sigma_x - \nu(\sigma_y + \sigma_z)] &= \frac{1}{E_0} (1 - k_x)(1 - 2\nu)\sigma_0 \\
\frac{1}{E_0} [\sigma_y - \nu(\sigma_z + \sigma_x)] &= \frac{1}{E_0} (1 - k_y)(1 - 2\nu)\sigma_0 \\
\frac{1}{E_0} [\sigma_z - \nu(\sigma_x + \sigma_y)] &= \frac{1}{E_0} (1 - k_z)(1 - 2\nu)\sigma_0
\end{aligned} \tag{4-5}$$

Since the strain of core element is the same as those of periphery elements as explained by the definition of restraint model, the following equations are derived as follows.

$$\begin{aligned}
\varepsilon'_x &= \frac{1}{E_0} [\sigma_x - \nu(\sigma_y + \sigma_z)] = \frac{1}{E_2} (\sigma_{x2} - \nu\sigma_{z2}) = \frac{1}{E_3} (\sigma_{x3} - \nu\sigma_{y3}) \\
\varepsilon'_y &= \frac{1}{E_0} [\sigma_y - \nu(\sigma_z + \sigma_x)] = \frac{1}{E_3} (\sigma_{y3} - \nu\sigma_{x3}) = \frac{1}{E_1} (\sigma_{y1} - \nu\sigma_{z1}) \\
\varepsilon'_z &= \frac{1}{E_0} [\sigma_z - \nu(\sigma_x + \sigma_y)] = \frac{1}{E_1} (\sigma_{z1} - \nu\sigma_{y1}) = \frac{1}{E_2} (\sigma_{z2} - \nu\sigma_{x2})
\end{aligned} \tag{4-6}$$

Now clearing the variables  $\sigma_x$ ,  $\sigma_y$  and  $\sigma_z$ ,  $\sigma_{x2}$ ,  $\sigma_{x3}$ ,  $\sigma_{y3}$ ,  $\dots$ ,  $\sigma_{z2}$  by solving simultaneously the equations of (4-4) and (4-5), elastic moduli of the periphery to induce equivalent restraint are defined as follows.

$$\begin{aligned}
E_1 = f_1(k_x, k_y, k_z) &= \frac{\frac{Y + vZ}{Z + vY} - v}{Y} \times \frac{\frac{X + vZ}{Z + vX} C + \frac{X + vY}{Y + vX} B - A}{\frac{X + vZ}{Z + vX} + \frac{X + vY}{Y + vX} \frac{Y + vZ}{Z + vY}} \times E_0 \\
E_2 = f_1(k_x, k_y, k_z) &= \frac{\frac{Z + vX}{X + vZ} - v}{Z} \times \frac{\frac{Y + vX}{X + vY} A + \frac{Y + vZ}{Z + vY} C - B}{\frac{Y + vX}{X + vY} + \frac{Y + vZ}{X + vY} \frac{Z + vX}{X + vZ}} \times E_0 \\
E_3 = f_1(k_x, k_y, k_z) &= \frac{\frac{X + vY}{Y + vX} - v}{X} \times \frac{\frac{Z + vY}{Y + vZ} B + \frac{Z + vX}{X + vZ} A - C}{\frac{Z + vY}{Y + vZ} + \frac{Z + vX}{X + vZ} \frac{X + vY}{Y + vX}} \times E_0
\end{aligned}$$

Where

$$\begin{aligned}
A &= \frac{1}{2} \frac{(1 - v) k_x + v(k_y + k_z)}{1 + v} & X &= \frac{1}{E_0} (1 - k_x)(1 - 2v) \\
B &= \frac{1}{2} \frac{(1 - v) k_y + v(k_z + k_x)}{1 + v} & Y &= \frac{1}{E_0} (1 - k_y)(1 - 2v) \\
C &= \frac{1}{2} \frac{(1 - v) k_z + v(k_x + k_y)}{1 + v} & Z &= \frac{1}{E_0} (1 - k_z)(1 - 2v)
\end{aligned}$$

## 4.2. Degree of restraint determination

### 4.2.1. Inherent strain of the elements subjected to tri-axial stress.

Degree of restraint of welding model is also expressed in the same manner as the inherent model: by the ratio of a core element strain under restraint ( $\varepsilon'$ , Fig. 33b) by periphery to that without restraint ( $\varepsilon_0$ , Fig. 33a).

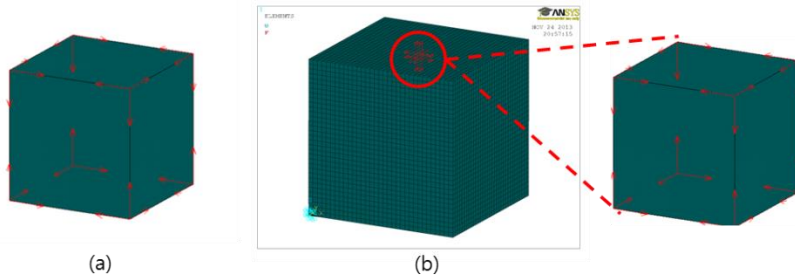


Fig. 33 Unit load method of welding model

The noticeable point is that plastic strain does not occur when element has isotropic degree of restraint in all direction. If stresses acting on the element in all axial directions are the same ( $\sigma_x = \sigma_y = \sigma_z = \sigma$ ), from equation (4-2),

$$\varepsilon = \frac{1}{E} [(1 - 2\nu)\sigma]$$

When plastic yielding occurs, Poisson's ratio is 0.5. Therefore plastic strain is always zero as follows.

$$\epsilon^p = \frac{1}{E} [(1 - 2 \times 0.5)\sigma] = 0$$

This fact is also confirmed in FE analysis. Thermal history of strain is shown in Fig. 34 and Fig. 35 in case of  $k=0.4$  and 0.5 in all axial directions. Thermal and elastic strain varies depending on the temperature changes but plastic strain is zero in all intervals. In any degree of restraint defined as a value between 0.01–0.99, the plastic strain does not occur in this case, regardless of the thermal history.

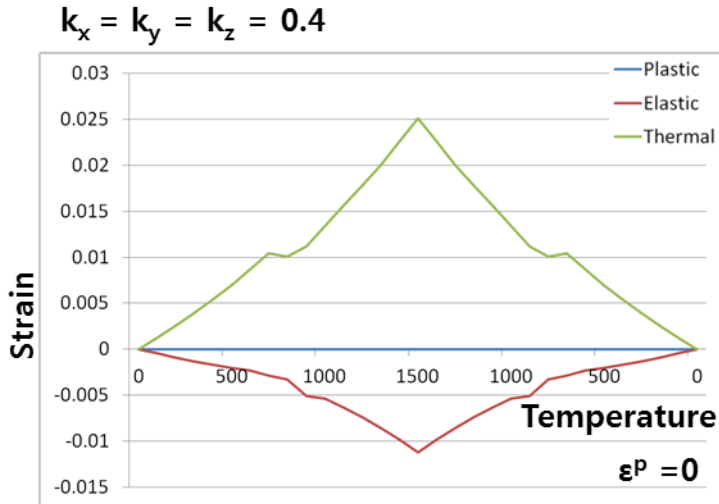


Fig. 34 Thermal history of strain, CASE I

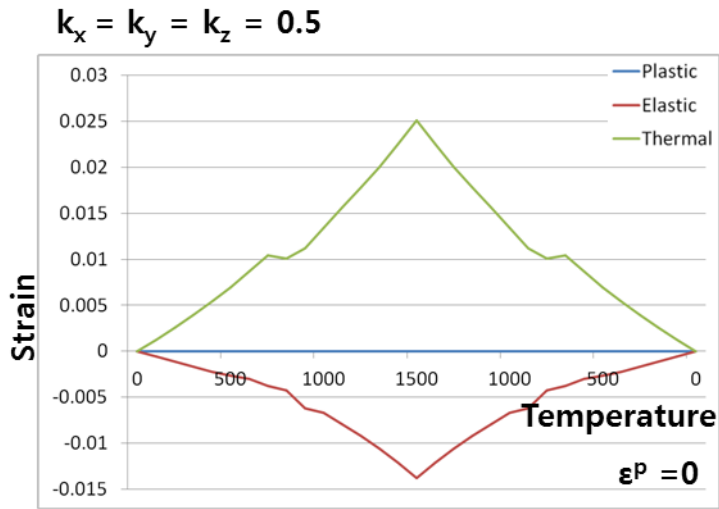


Fig. 35 Thermal history of strain, CASE II

If axial degrees of restraints are different from each other, it causes different axial stresses and plastic strain can occur during the thermal process. The following three cases make the degree of restraint in z direction different from those of x and y directions while maintaining the latter two values the same.

The differences are set small in Case III and IV while relatively larger difference in Case V. The resultant absolute plastic strains in x and y directions become larger as the difference in the degree of restraints increases as illustrated in Fig. 36, 38, and 40. The same tendency for the plastic strain in z direction is observed in Fig. 37, 39 and 41.

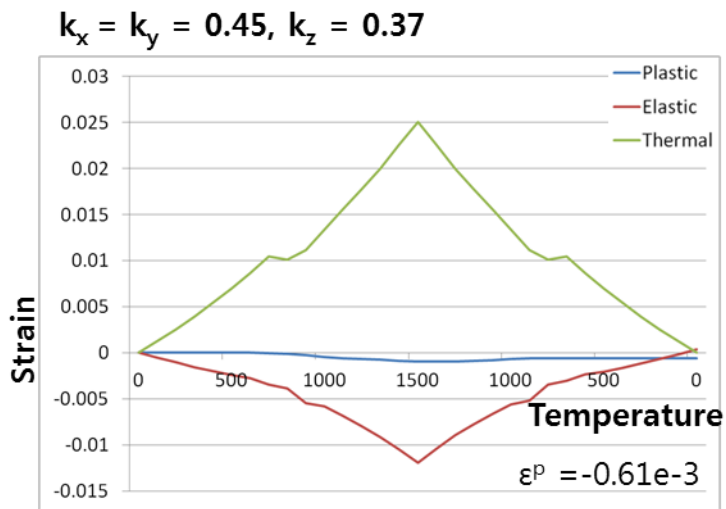


Fig. 36 Thermal history of strain, CASE III (x,y-direction)

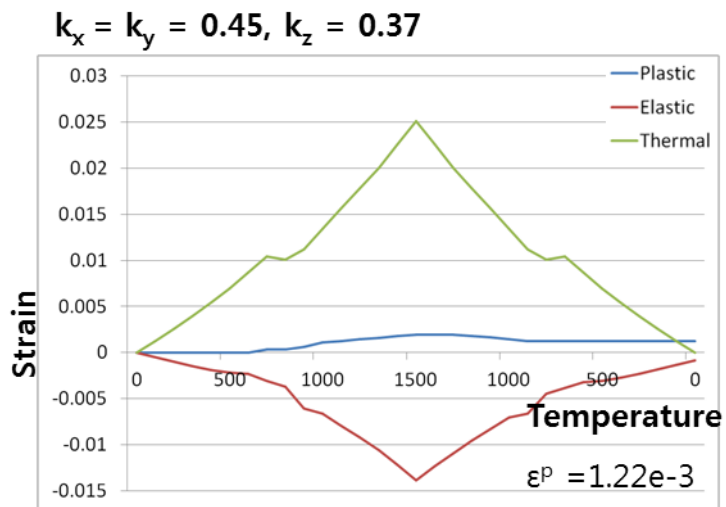


Fig. 37 Thermal history of strain, CASE III (z-direction)

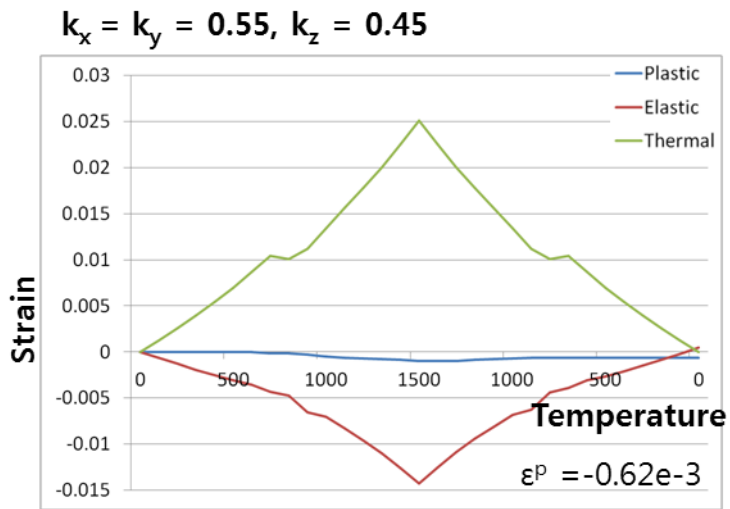


Fig. 38 Thermal history of strain, CASE IV (x,y-direction)

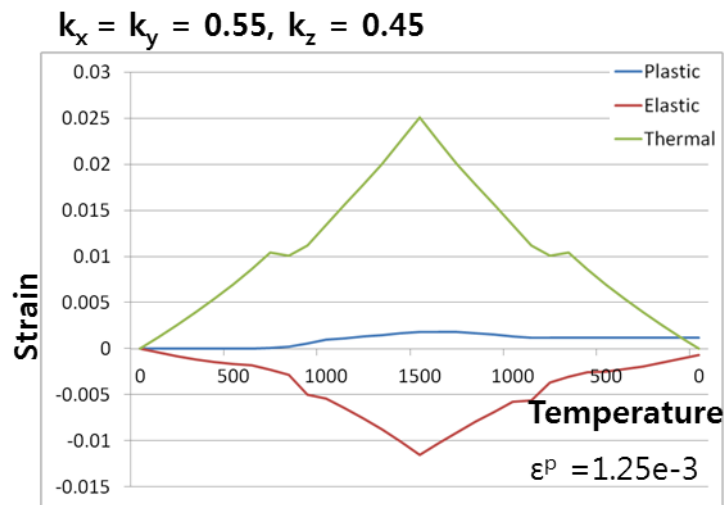


Fig. 39 Thermal history of strain, CASE IV (z-direction)

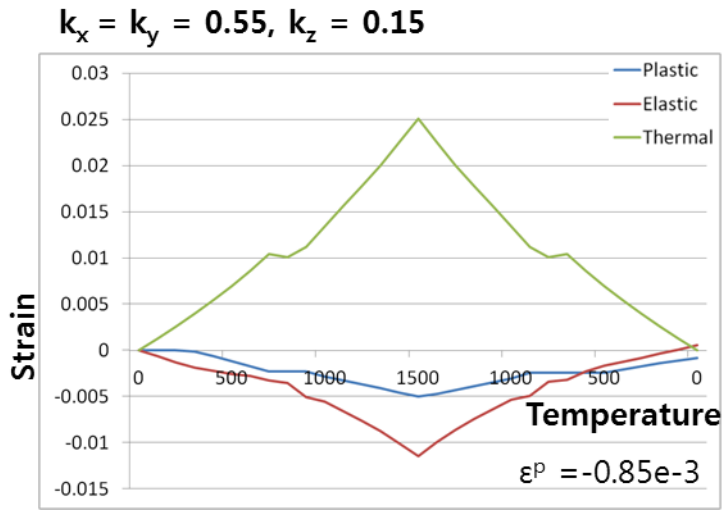


Fig. 40 Thermal history of strain, CASE V (x,y-direction)

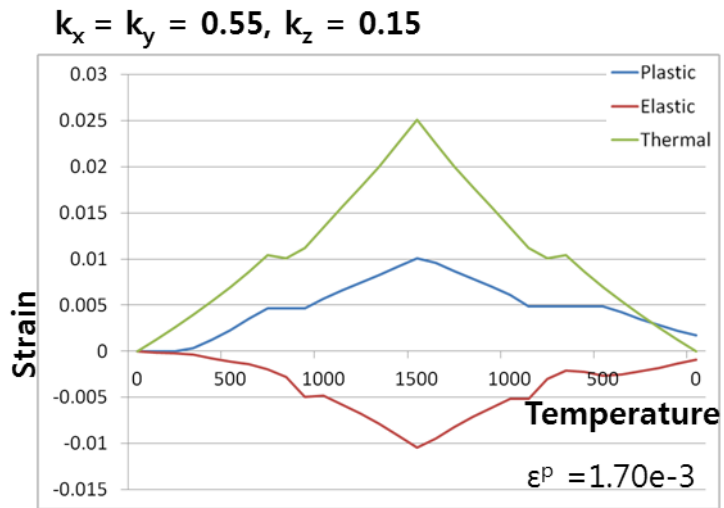


Fig. 41 Thermal history of strain, CASE V (z-direction)

The results of five cases shown in Fig. 34–41 are summarized in Table 4. It can be concluded that the residual plastic strain become larger as the difference in degree of

restraints increases.

Table 4 Relationship between degree of restraint and plastic strain

	$k_x, k_y$	$k_z$	$ k_x - k_z $	$\varepsilon_x^p, \varepsilon_y^p$	$\varepsilon_z^p$
CASE I	0.4	0.4	0	0	0
CASE II	0.5	0.5	0	0	0
CASE III	0.45	0.37	0.08	-0.61e-3	1.22e-3
CASE IV	0.55	0.45	0.10	-0.62e-3	1.25e-3
CASE V	0.55	0.15	0.40	-0.85e-3	1.70e-3

#### 4.2.2. Degree of restraint in room temperature

In the previous section, the residual plastic strain is found to be dependent on the difference of three axial degrees of restraints. Here, for a plate structure, actual degrees of restraints are calculated across thickness as depicted in Fig. 42. As long as element size is sufficiently small, all degrees of restraints are the same at any locations as listed in Table 5. The only element in the surface has different value of degree of restraint from other elements. Even for the element, the difference between the degree of restraint of in-plane direction and thickness direction is very small.

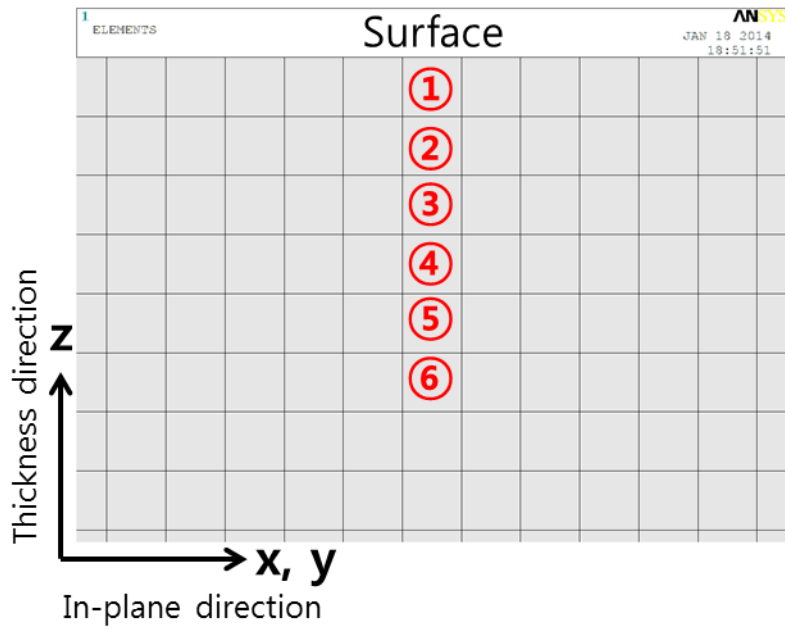


Fig. 42 Degree of restraint calculate location (Planar type)

Table 5 Degree of restraint (Planar type)

Location	Degree of restraint		Ratio (In-plane / Thickness)
	In-plane direction, x,y	Thickness direction, z	
①	0.39	0.43	0.91
②	0.56	0.56	1
③	0.57	0.57	1
④	0.57	0.57	1
⑤	0.57	0.57	1
⑥	0.57	0.57	1
⋮	⋮	⋮	⋮

In a fillet type joint as shown in Fig. 43, the degree of restraints are calculated along in-plane direction. In the similar way, the degrees of restrains are slightly different depending on the locations, however, the difference between in-plane direction and thickness direction is zero or quite small as shown in Table 6.

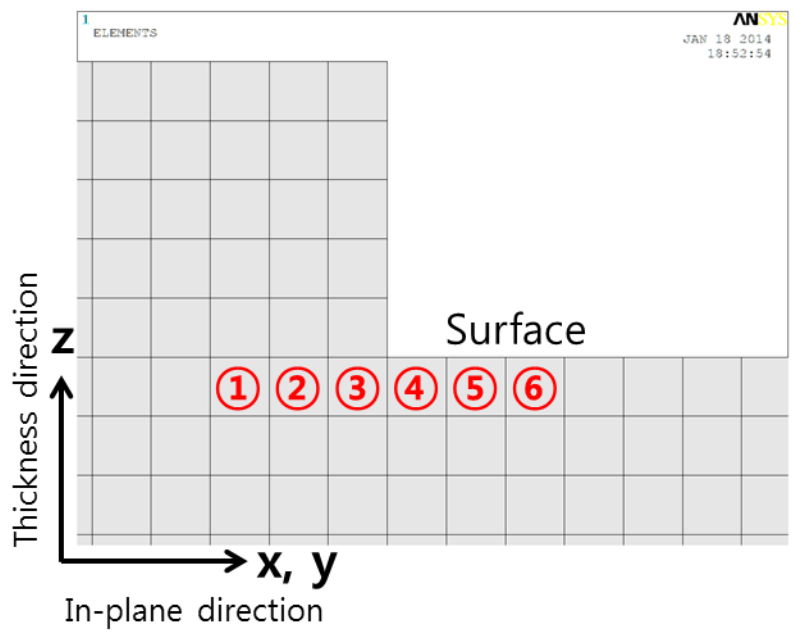


Fig. 43 Degree of restraint calculate location (Fillet type)

Table 6 Degree of restraint (Fillet type)

Location	Degree of restraint		Ratio (In-plane / Thickness)
	In-plane direction, x,y	Thickness direction, z	
⋮	⋮	⋮	⋮
①	0.57	0.57	1
②	0.57	0.57	1
③	0.54	0.54	1
④	0.44	0.49	0.90
⑤	0.40	0.43	0.93
⑥	0.39	0.43	0.91
⋮	⋮	⋮	⋮

#### 4.2.3. Changes in degree of restraint due to temperature

Thus, a value of 0.57 is to be used as degree of restraint value in all axial directions at room temperature regardless of the shape of the analysis model and analysis position for a calculation of inherent strain using the improved solid–spring model.

Even if there is no significant difference among three axial degrees of restraints and plastic strain does not occur when element has isotropic degree of restraint, residual plastic strains still remain after welding process. This is because the

degree of restraint varies due to temperature changes in welding process as shown in Fig. 44 and Table 7. That is, different temperature distributions along three axes can cause a difference in three axial restraints and it can induce the residual plastic strain as identified in the previous section.

Therefore, it is necessary to take into account the changes in degree of restraints induced by different temperature gradients along three axial directions. This requires the consideration of temperature-dependent material property of the peripheral elements to reflect the continuous changes in the degree of restraints during welding process.

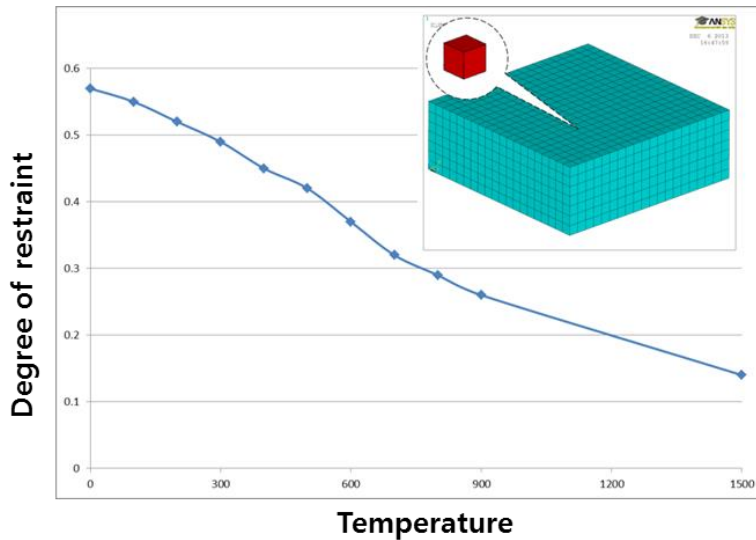


Fig. 44 Temperature–degree of restraint relation

As listed in Table 7, the degree of restraint decreases as the temperature increases due to the degradation of elastic

modulus.

Table 7 Temperature–degree of restraint relation

Temperature (°C)	E (GPa)	Poisson's Ratio	Degree of restraint
0	206	0.29	0.57
100	201	0.31	0.55
200	198	0.33	0.52
300	191	0.35	0.49
400	181	0.37	0.45
500	175	0.39	0.42
600	163	0.41	0.37
700	121	0.43	0.32
800	80.3	0.44	0.26
900	39.2	0.45	0.26
⋮	⋮	⋮	⋮
1500	13.2	0.48	0.14

### 4.3. Inherent strain chart considering temperature gradient

#### 4.3.1. Definition of thermal gradient TG

The temperature gradient is represented by an index, named TG, hereafter. TG is a value which is greater than 0 and less than or equal to 1. For example, if there is no temperature gradient, then  $TG=1$ . The temperature gradient is in inverse proportion to TG value.

TG can represent relative magnitude of temperature between the core element and the periphery element. For example, when the temperature of a core element is  $500^{\circ}\text{C}$  and TG value is 1, the temperature of each periphery element is  $500^{\circ}\text{C}$ , as shown in Fig. 45. When TG value is 0.7, the temperature of each periphery element is shown in Fig. 46. The periphery element of right hand side has 30% lower temperature in comparison with the temperature of the core element ( $T_{core} \times 0.7$ ) while the periphery element of left hand side 30% higher temperature.

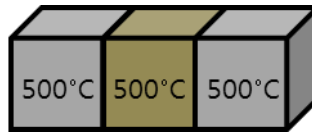


Fig. 45 Temperature gradient at  $TG=1$

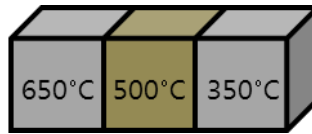


Fig. 46 Temperature gradient at  $TG=0.7$

Fig. 47 shows a heating and cooling process of 2D inherent strain model at the highest temperature of  $1000^{\circ}\text{C}$ ,  $TG_x$  and  $TG_y$  are 0.8 and 0.5, respectively.

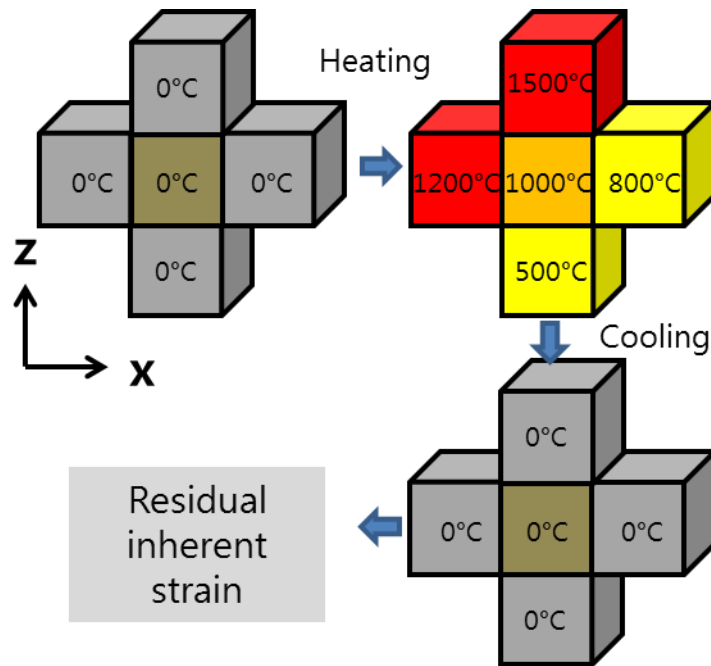


Fig. 47 Temperature gradient at  $TG_x=0.8$ ,  $TG_y=0.5$

#### 4.3.2. Application of TG to welding model

How to apply TG to an actual welding analysis model can be explained in Fig. 48. Welding analysis model is divided into two regions, i.e. 1<sup>st</sup> and 2<sup>nd</sup> heat affected areas, depending on the level of temperature variation. Then TG is determined by average temperature gradient of each region.

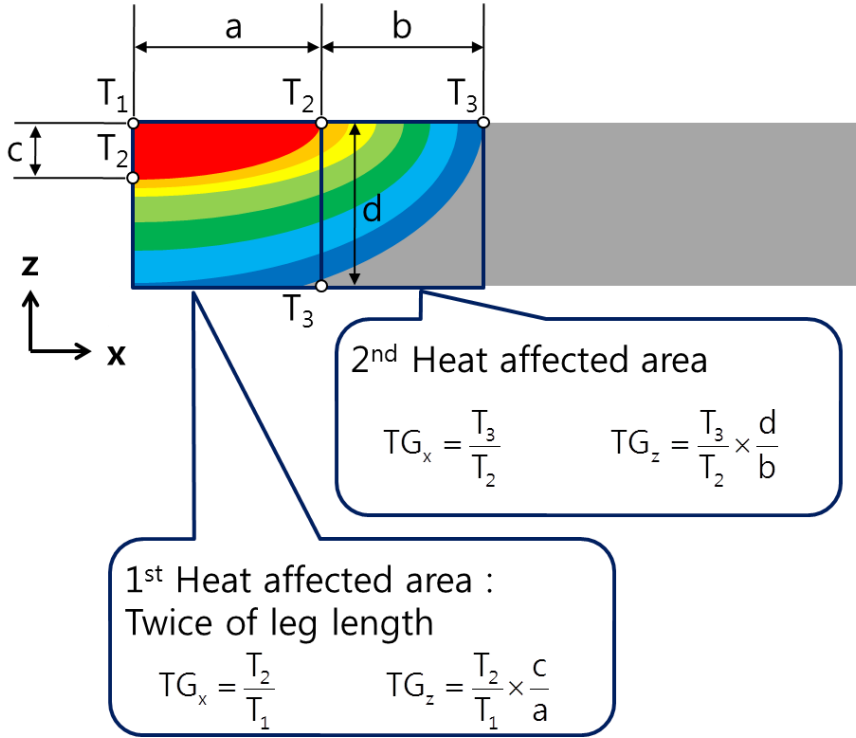


Fig. 48 Definition of TG in the thermal analysis model

In an example where temperature distribution on a cross section obtained from a heat transfer analysis like Fig. 49, the procedure to calculate TG is as follows.

First,  $TG_x$  of 1<sup>st</sup> heat affected area is calculated using two temperatures  $T_1$  and  $T_2$  on upper surface.  $T_1$  is the temperature at the center point of the weld line and  $T_2$  is the temperature at a point located twice leg length, 'a', far from the center point. Since  $TG_x$  of 1st heat affected area is defined by the ratio of  $T_1$  and  $T_2$ , it is 0.83 in this example.

Second,  $TG_z$  of 1st heat affected area can be calculated by multiplying the value of ' $c/a$ ' to  $TG_x$ . ' $c$ ' is the distance between

the center point on the top surface to the point of  $T_2$  along the center line. Here,  $TG_z$  is 0.25.

Like this, relative temperature gradients of x direction and z direction are defined.  $TG_y$ , temperature gradient in weld line direction, is set as 1.0 because temperature gradient is quite gentle due to the movement of heat source along the welding line.  $TG$  can be obtained in the same way in the 2<sup>nd</sup> heat affected area.

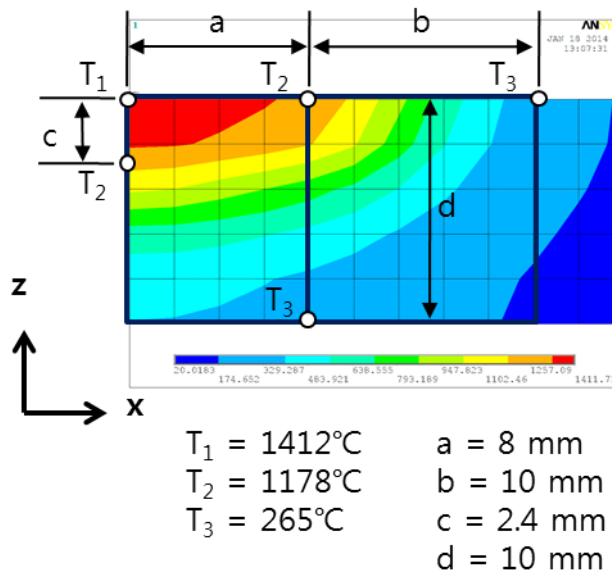


Fig. 49 Example model of finding TG

#### 4.3.3. Inherent strain chart

Improved inherent strain charts obtained by applying the new solid-spring model and considering the effect of the

temperature gradient are illustrated in Fig. 50–52. The x, y, and z-axis represent  $TG_x$ ,  $TG_y$ , and inherent strain, respectively.

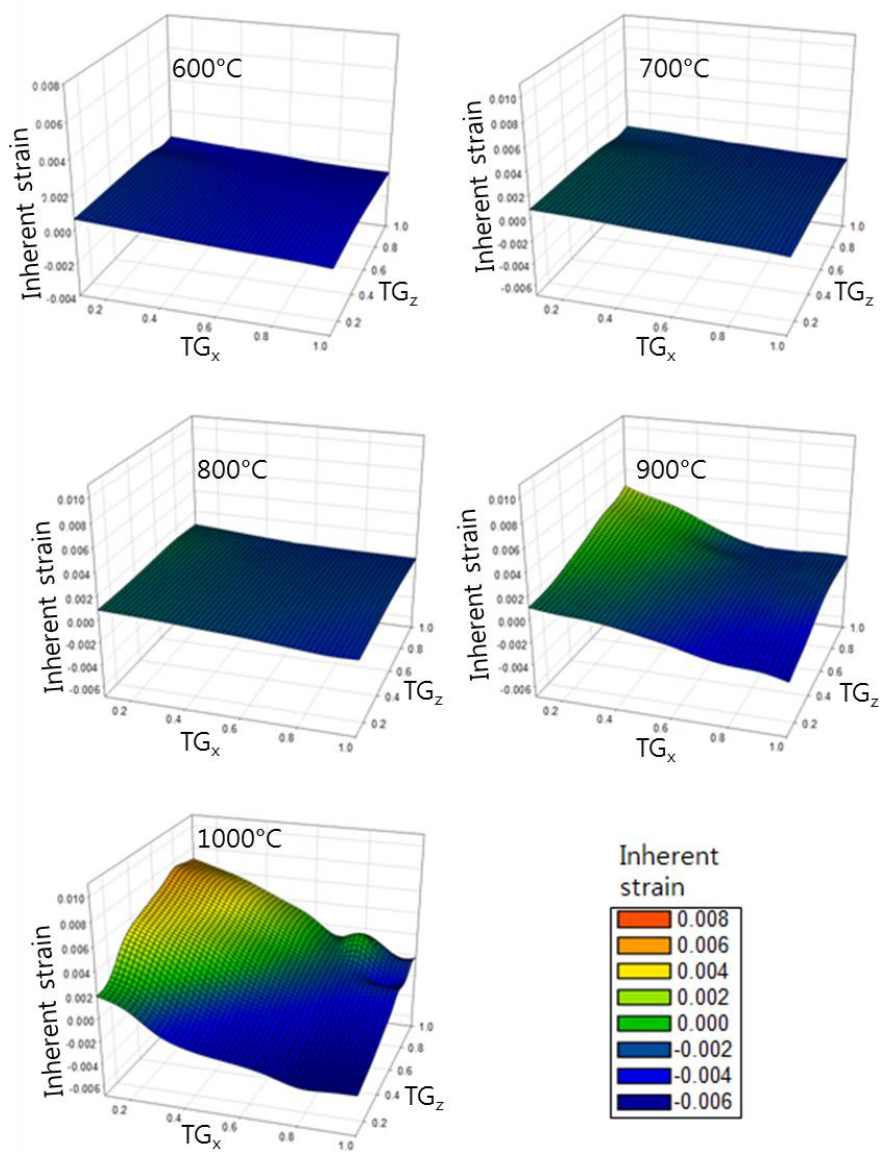


Fig. 50 Inherent strain chart (at highest temperature 600–1000°C of the core element)

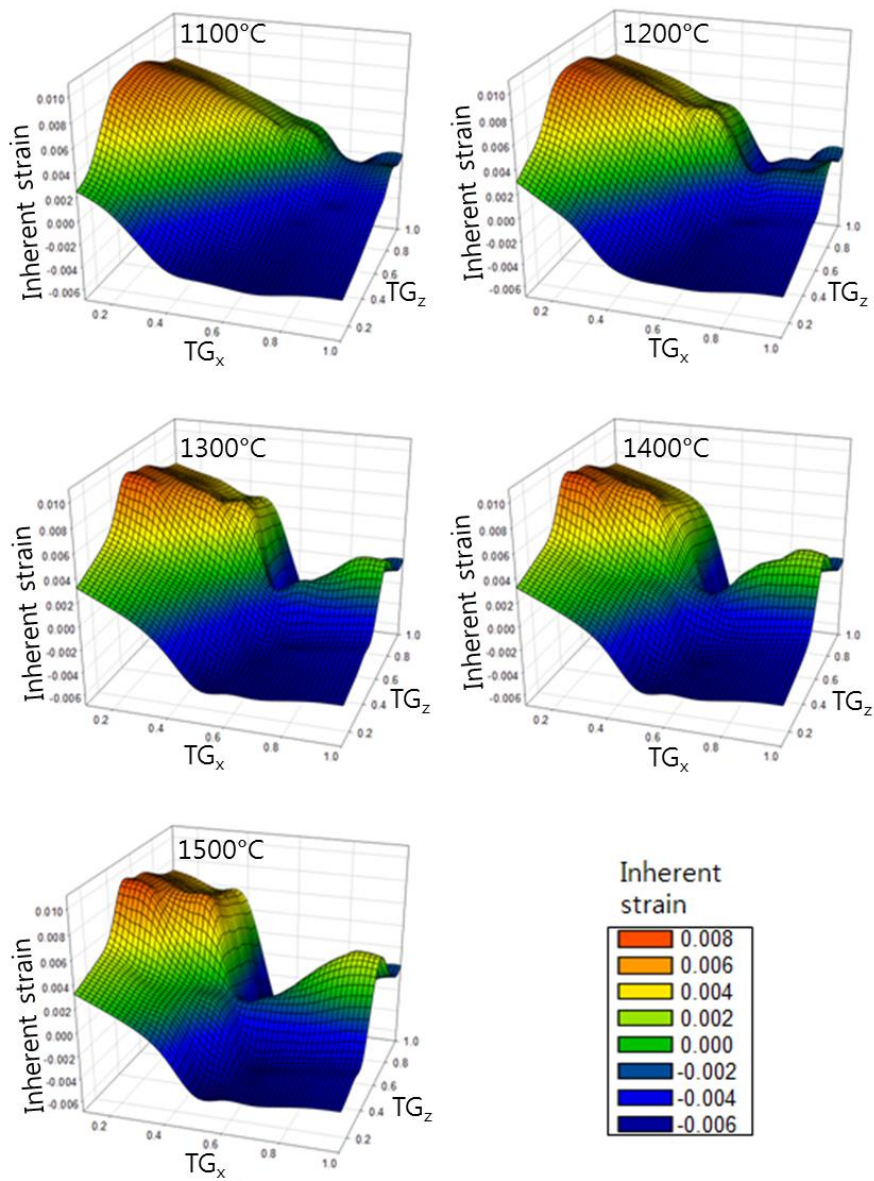
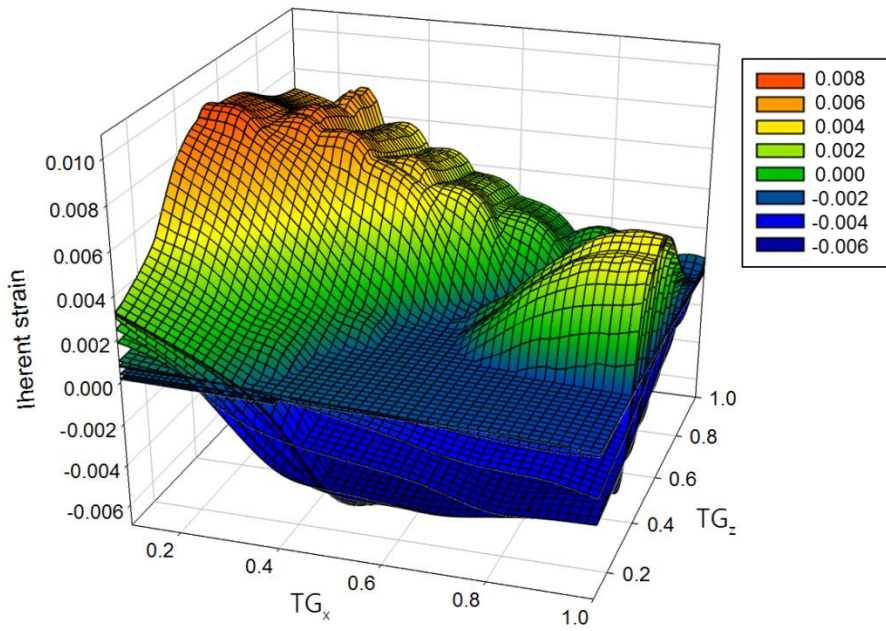


Fig. 51 Inherent strain chart (at highest temperature 1100–1500° C of the core element)



**Fig. 52 Inherent strain chart**

Fig.52 displays overlapped strain charts for all the highest temperatures. By and large, the compressive plastic strain tends to increase as  $TG_x$  gets larger and  $TG_z$  smaller, and vice versa. Fig. 53 and Fig. 54 show inherent strain–highest temperature curve at 0.4 of  $TG_z$  and that at 0.4 of  $TG_x$ , respectively. Inherent strain shifts toward positive direction as  $TG_x$  becomes larger, and negative direction as  $TG_z$  becomes larger.

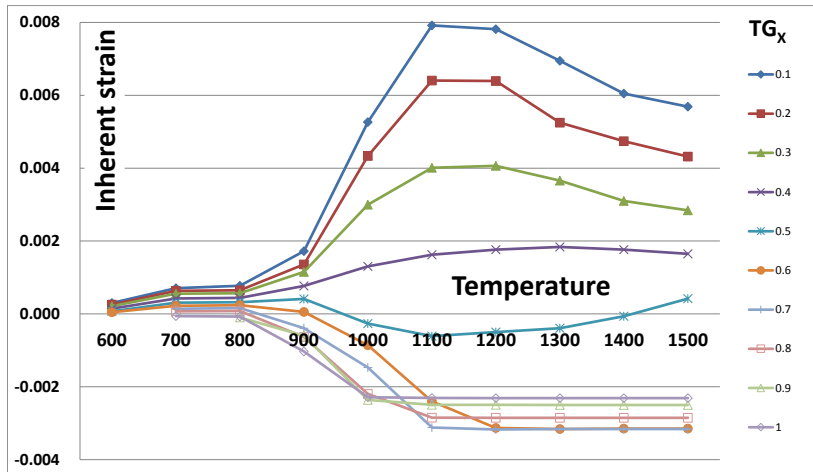


Fig. 53 Inherent strain curve at  $TG_z = 0.4$

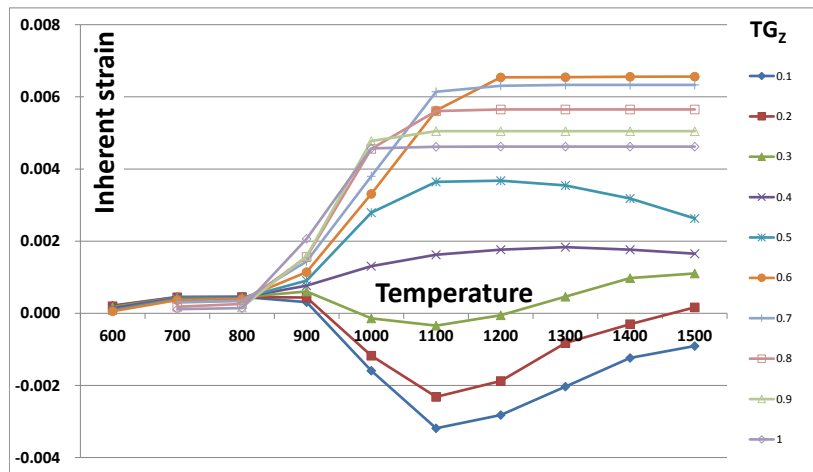


Fig. 54 Inherent strain curve at  $TG_x = 0.4$

## 4.4. Strain input

Next step is to calculate welding deformation in an elastic FE analysis. Prior to the analysis, a heat transfer analysis for a heat flux modeled according to the welding condition needs to

be performed. From this analysis, the highest temperature, and temperature gradients in transverse direction and thickness direction are calculated and the corresponding inherent strain values are read from the inherent strain charts.

The inherent strain is inputted in form of temperature and a simple one step heat transfer analysis is performed to spread the temperature out to the surroundings. Then an elastic FE analysis is carried out to compute welding deformation subjected to the distributed thermal load. In this research, strains are imposed on the top and bottom surfaces as shown in Fig. 55. It can make the distributed inherent strain obtained from the simple heat transfer analysis close to the actual strain distribution.

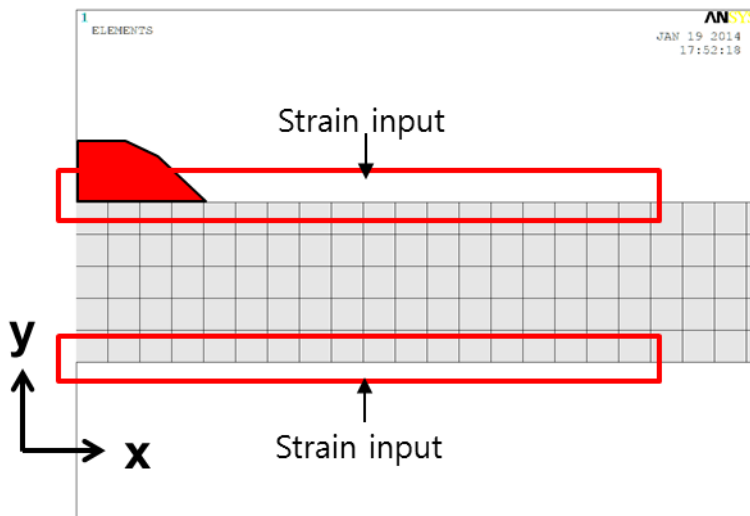


Fig. 55 Strain input point

Compared with the previous method (Fig. 56b and Fig. 57b), this approach (Fig. 56c and Fig. 57c) provides strain distribution much more similar to the actual welding condition (Fig. 56a and Fig. 57a). Input locations and transfer directions are shown in Fig. 56, and the results are shown in Fig. 57.

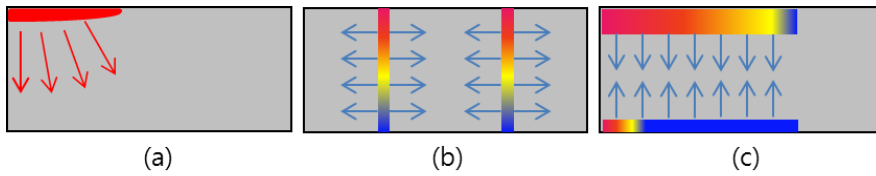


Fig. 56 Heat transfer direction

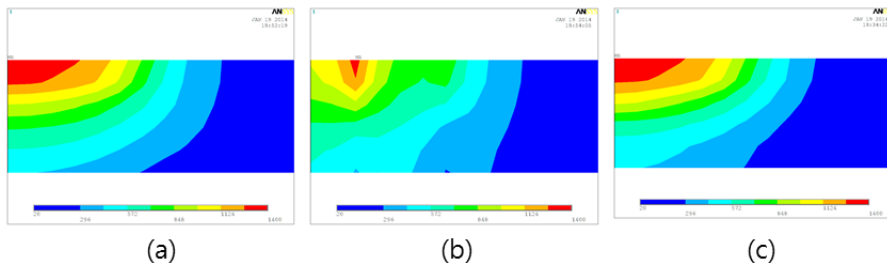


Fig. 57 Heat transfer results

#### 4.5. Welding analysis procedure based on improved equivalent strain method

Fig. 58 shows welding analysis procedure based on improved equivalent strain method. There is no need for elasto–plastic nonlinear analysis which takes a lot of time.

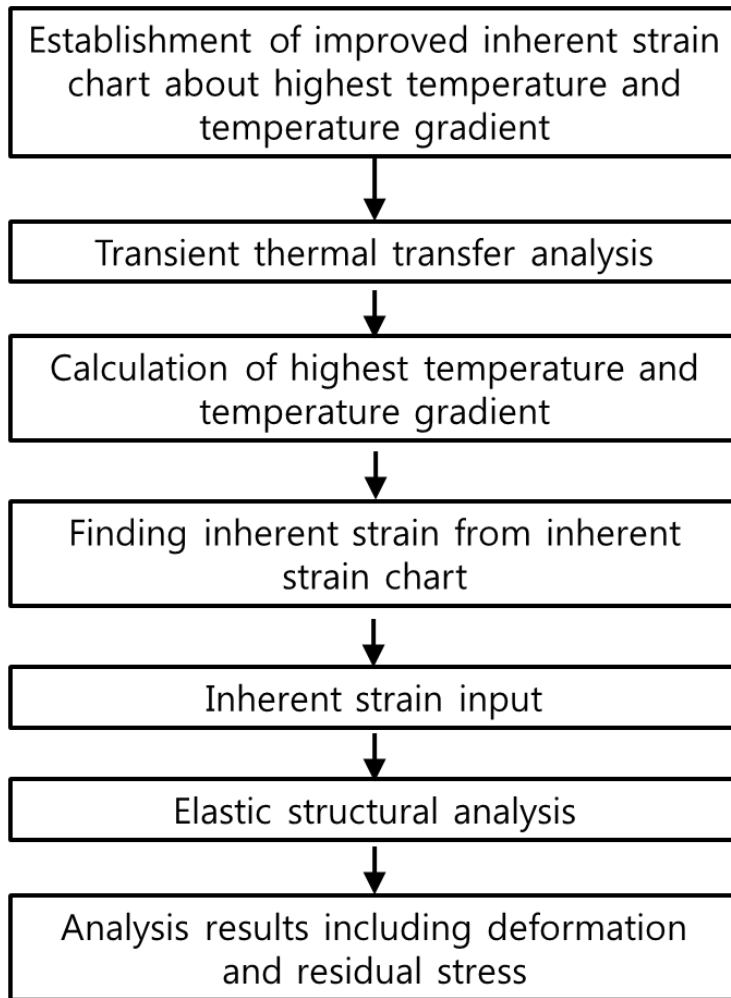


Fig. 58 Welding analysis procedure using improved inherent strain method

#### 4.6. Summary of comparison with the previous study

Table 8 shows features and difference between the two

equivalent strain methods in this study and previous study.

Table 8 Summary of comparison with the previous study

	Existing equivalent strain method	Improved equivalent strain method
How to restrain unit model	<ul style="list-style-type: none"> <li>- Using the spring of displacement direction</li> <li>- Disregarding Restraint in thickness direction</li> </ul>	<ul style="list-style-type: none"> <li>- Restrained by the rigidity to the direction of displacement of the peripheral element</li> <li>- 3dimensional restraint</li> </ul>
How to create inherent strain chart	<ul style="list-style-type: none"> <li>- Considering difference of degree of restraint in axial direction at room temperature</li> <li>- Disregarding changes in degree of restraint due to temperature gradient</li> <li>- Disregarding changes in rigidity of the periphery due to temperature gradient</li> </ul>	<ul style="list-style-type: none"> <li>- Degree of restraint at room temperature is fixed (0.57)</li> <li>- Considering changes in degree of restraint due to temperature gradient</li> <li>- Considering changes in rigidity of the periphery due to temperature gradient</li> </ul>

## 5. Welding analysis using improved equivalent strain method

### 5.1. Butt welding

The experimental data of Sato and Terasaki is used for butt welding analysis model. Satoh and Terasaki[2] found the variables related to welding deformation based on heat transfer and thermal elasto-plastic theory, suggested the estimated equation about angular distortion and shrinking deformation by ordering the variables of butt welding experimental result. From this data, angular distortion for GMAW of mild steel is compared with the analysis results in this study. The experimental results are organized by welding parameter  $Q/h^2$  as shown in Fig. 59 and Table 9. Fig. 59 also indicates analysis results based on improved equivalent strain method in four models which refer to the experimental data.

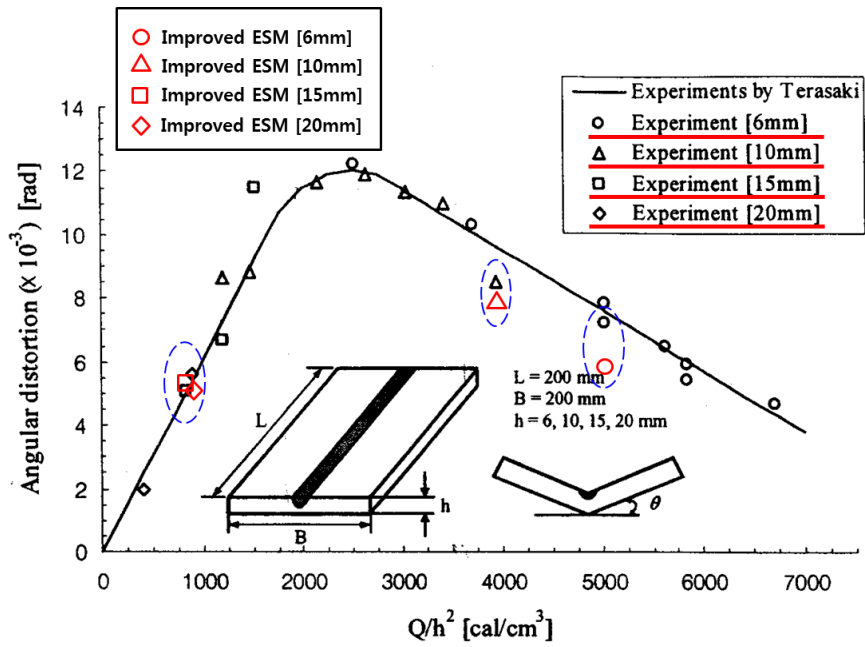


Fig. 59 Comparison with experiment (Sato and Terasaki[2])

Table 9 Angular distortion results of butt welding (Sato and Terasaki)

Welding parameter [cal/cm <sup>3</sup> ]	Angular distortion [rad]
$0 \leq \frac{Q}{h^2} \leq 1700$	$\theta = 6.0 \times 10^{-6} \times \frac{Q}{h^2}$
$1700 \leq \frac{Q}{h^2} \leq 3000$	$\theta = 2.65 \times 10^{-9} \times \left(\frac{Q}{h^2}\right)^2$ $+ 1.34 \times 10^{-5} \times \left(\frac{Q}{h^2}\right) - 0.005$
$3000 \leq \frac{Q}{h^2} \leq 7000$	$\theta = 2.17 \times 10^{-6} \times \frac{Q}{h^2} + 0.018$

Based on the experimental data, the analyses of the plate thickness in the range from 6 to 20 are performed. The results

of thermal elasto–plastic analysis (EPA), existing equivalent strain method (ESM) and improved equivalent strain method (Improved ESM) are compared with experimental data. Welding conditions and detailed dimensions of the welding models are listed in Table 10. Analysis models are symmetric with regard to center line.

**Table 10 Analysis model dimension and welding condition (t=6mm)**

Dimension			Heat
Width [mm]	Length [mm]	Thickness [mm]	$Q/h^2$ [cal/cm <sup>3</sup> ]
200	200	6	4880
		10	3830
		15	800
		20	870

Analysis results are described in Section 5.1.1 to 5.1.4. The results in each section are sorted in order of displacement in z direction, residual stress in x and y direction (Fig.60–83, Table 11–22). Each result is sorted again in order of the figure, graph and table. Figures depict the distribution shape of model, graphs show distribution of values in the x direction which are

measured at  $y=L/2$  in top of plate. Maximum values are listed in table.

### 5.1.1 Comparison of 6mm plate

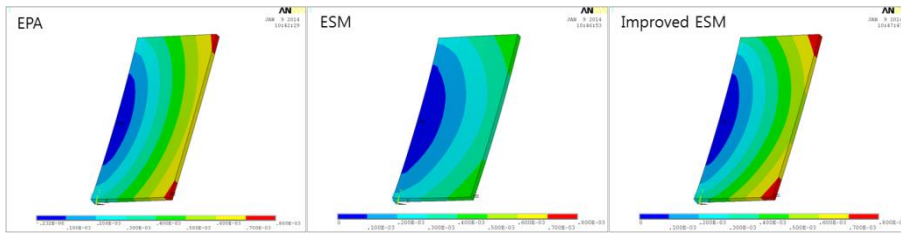


Fig. 60 Displacement in z direction (t=6mm)

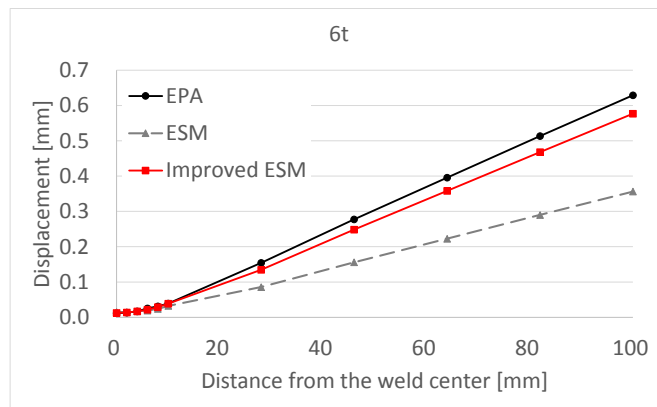


Fig. 61 Displacement in z direction (t=6mm)

Table 11 Angular distortion (t=6mm)

	Experiment	EPA	ESM	Improved ESM
Angular distortion	7.47 [10 <sup>-3</sup> rad]	6.28 [10 <sup>-3</sup> rad]	3.56 [10 <sup>-3</sup> rad]	5.77 [10 <sup>-3</sup> rad]
Ratio	-	0.84	0.48	0.77

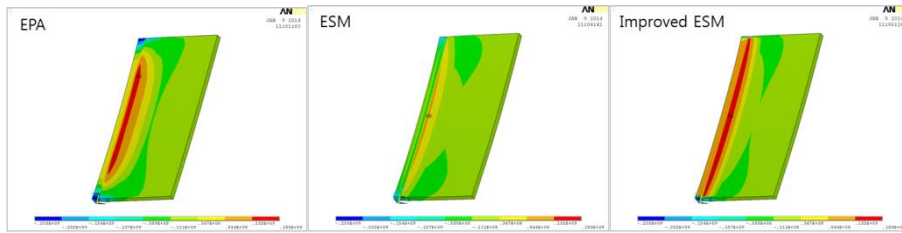


Fig. 62 Residual stress in x direction (t=6mm)

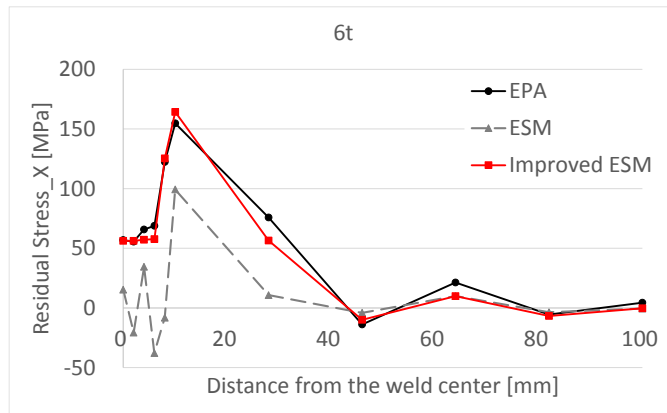


Fig. 63 Residual stress in x direction (t=6mm)

Table 12 Maximum residual stress in x direction (t=6mm)

	EPA	ESM	Improved ESM
Residual Stress (x)	154 [MPa]	99.3 [MPa]	181 [MPa]
Ratio	-	0.64	1.18

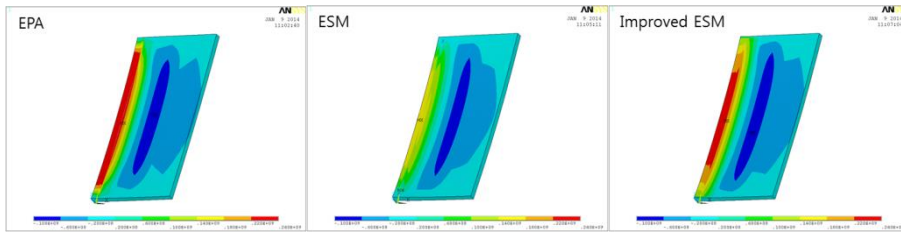


Fig. 64 Residual stress in y direction (t=6mm)

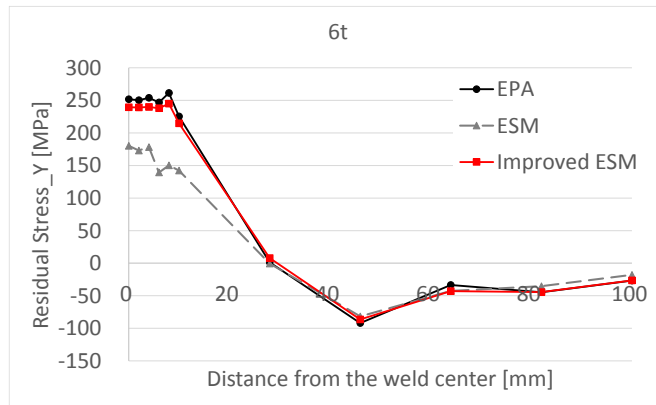


Fig. 65 Residual stress in y direction (t=6mm)

Table 13 Maximum residual stress in y direction (t=6mm)

	EPA	ESM	Improved ESM
Residual Stress (y)	262 [MPa]	186 [MPa]	245 [MPa]
Ratio	-	0.71	0.94

### 5.1.2 Comparison of 10mm plate

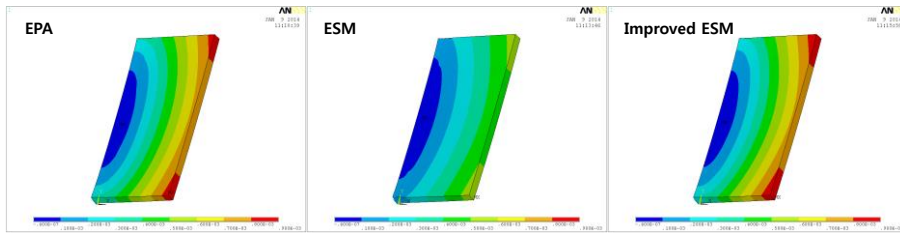


Fig. 66 Displacement in z direction (t=10mm)

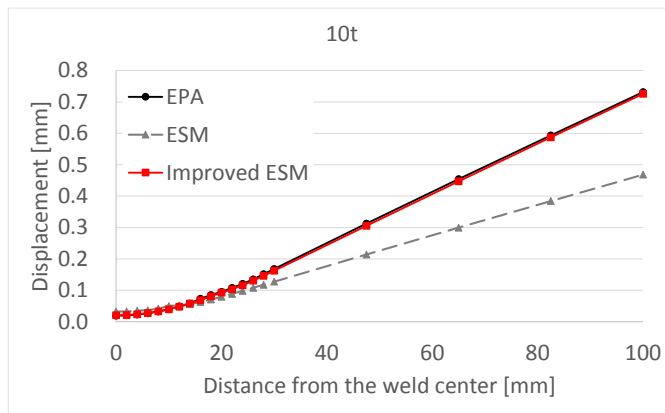


Fig. 67 Displacement in z direction (t=10mm)

Table 14 Angular distortion (t=10mm)

	Experiment	EPA	ESM	Improved ESM
Angular distortion	8.64 [10-3rad]	7.31 [10-3rad]	4.46 [10-3rad]	7.63 [10-3rad]
Ratio	-	0.85	0.52	0.88

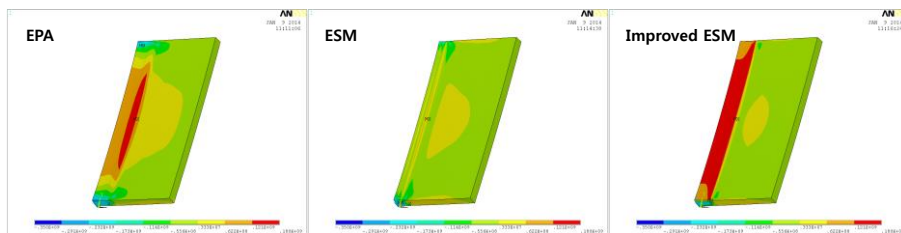


Fig. 68 Residual stress in x direction (t=10mm)

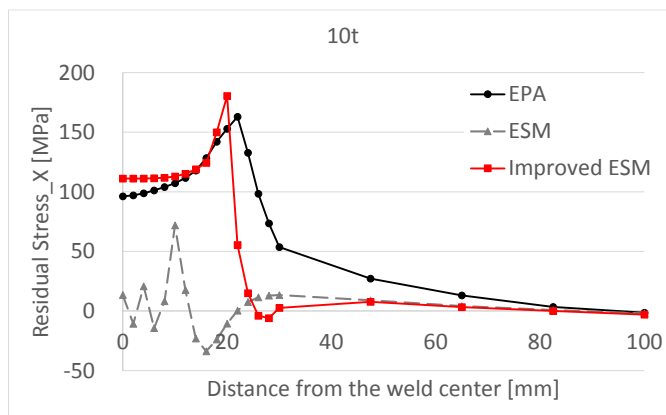


Fig. 69 Residual stress in x direction (t=10 mm)

Table 15 Maximum residual stress in x direction (t=10mm)

	EPA	ESM	Improved ESM
Residual Stress (x)	163 [MPa]	71.9 [MPa]	180 [MPa]
Ratio	-	0.44	1.10

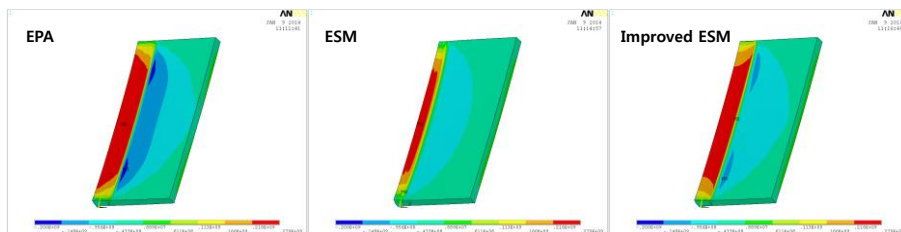


Fig. 70 Residual stress in y direction (t=10mm)

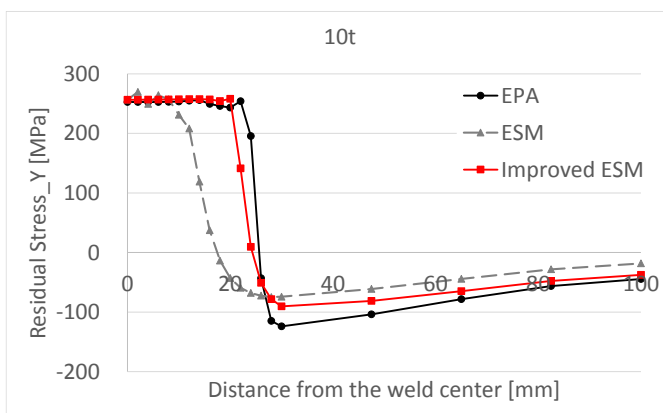


Fig. 71 Residual stress in y direction (t=10mm)

Table 16 Maximum residual stress in y direction (t=10mm)

	EPA	ESM	Improved ESM
Residual Stress (y)	267 [MPa]	270 [MPa]	258 [MPa]
Ratio	-	1.01	0.97

### 5.1.3 Comparison of 15mm plate

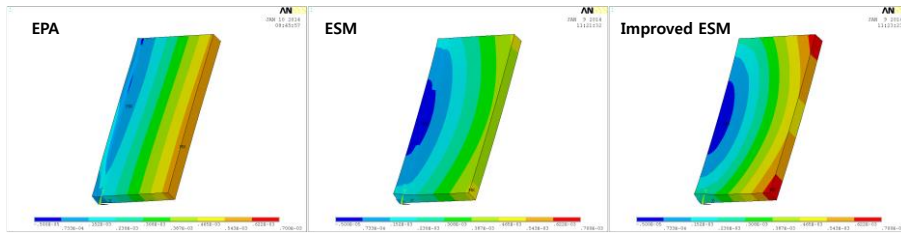


Fig. 72 Displacement in z direction (t=15mm)

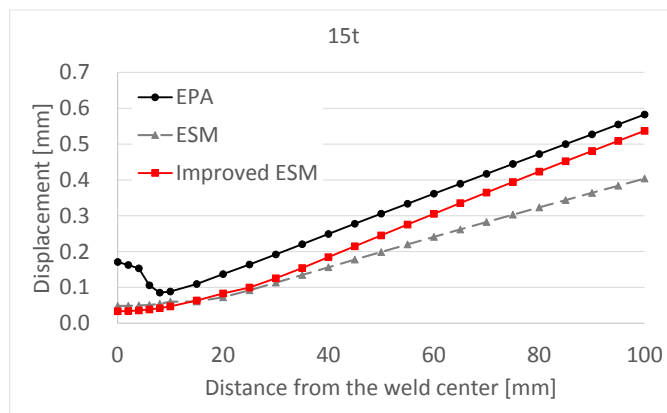


Fig. 73 Displacement in z direction (t=15mm)

Table 17 Angular distortion (t=15mm)

	Experiment	EPA	ESM	Improved ESM
Angular distortion	5.24 [10 <sup>-3</sup> rad]	5.82 [10 <sup>-3</sup> rad]	4.76 [10 <sup>-3</sup> rad]	5.38 [10 <sup>-3</sup> rad]
Ratio	-	1.11	0.91	1.03

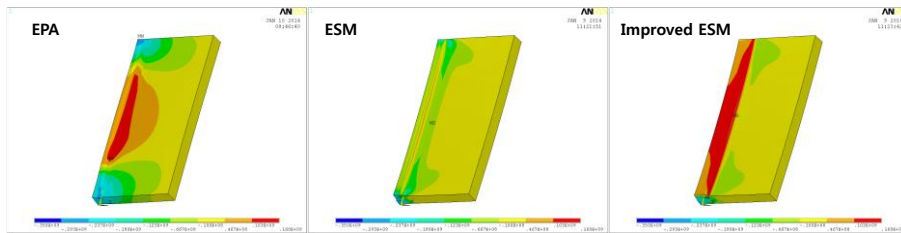


Fig. 74 Residual stress in x direction (t=15mm)

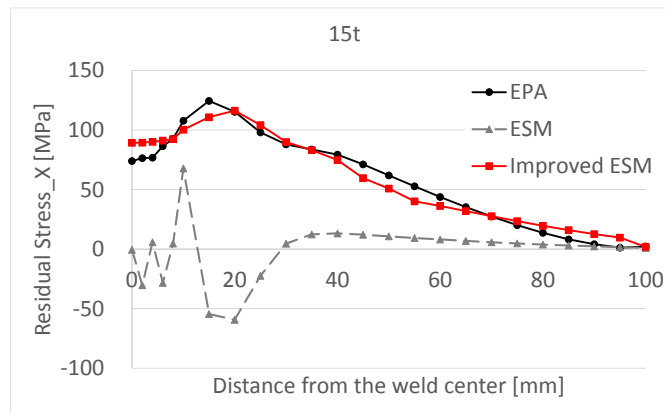


Fig. 75 Residual stress in x direction (t=15mm)

Table 18 Maximum residual stress in x direction (t=15mm)

	EPA	ESM	Improved ESM
Residual Stress (x)	140 [MPa]	114 [MPa]	163 [MPa]
Ratio	-	0.841	1.16

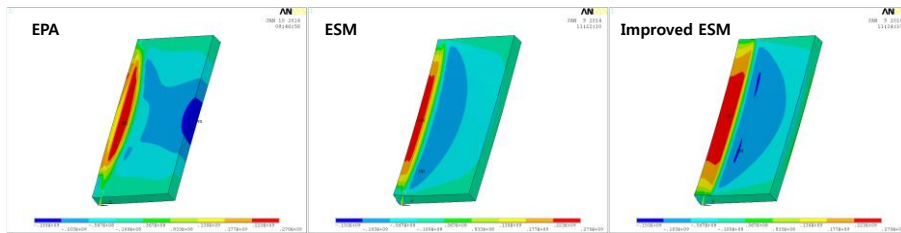


Fig. 76 Residual stress in y direction (t=15mm)

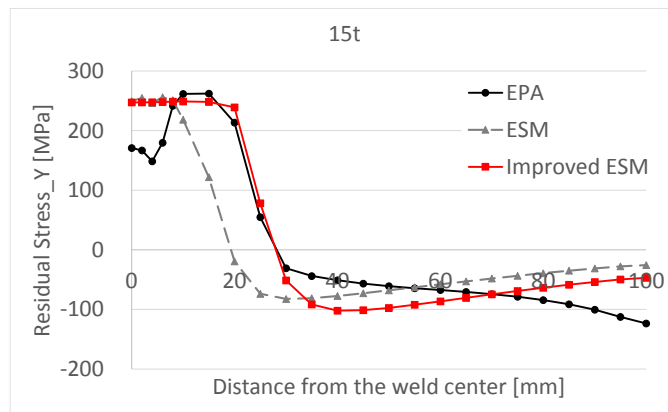


Fig. 77 Residual stress in y direction (t=15mm)

Table 19 Maximum residual stress in y direction (t=15mm)

	EPA	ESM	Improved ESM
Residual Stress (y)	268 [MPa]	268 [MPa]	249 [MPa]
Ratio	-	1.00	0.93

### 5.1.4 Comparison of 20mm plate

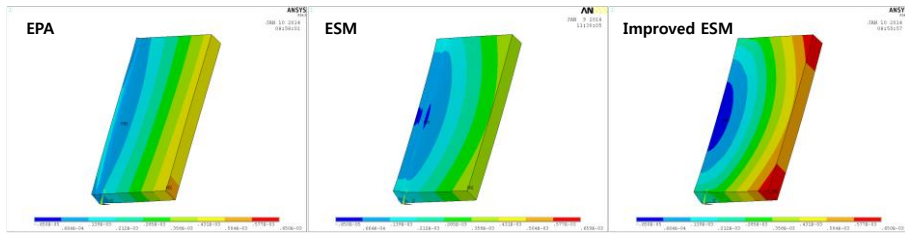


Fig. 78 Displacement in z direction (t=20mm)

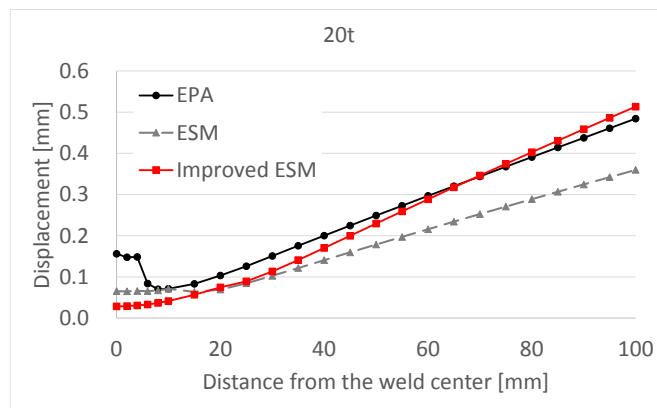


Fig. 79 Displacement in z direction (t=20mm)

Table 20 Angular distortion (t=20mm)

	Experiment	EPA	ESM	Improved ESM
Angular distortion	5.76 [10 <sup>-3</sup> rad]	4.84 [10 <sup>-3</sup> rad]	3.92 [10 <sup>-3</sup> rad]	5.13 [10 <sup>-3</sup> rad]
Ratio	-	0.84	0.68	0.89

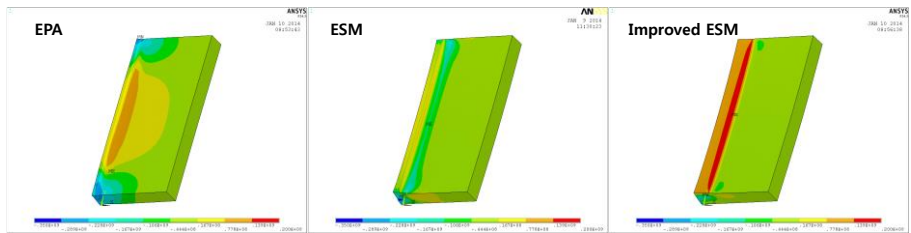


Fig. 80 Residual stress in x direction (t=20mm)

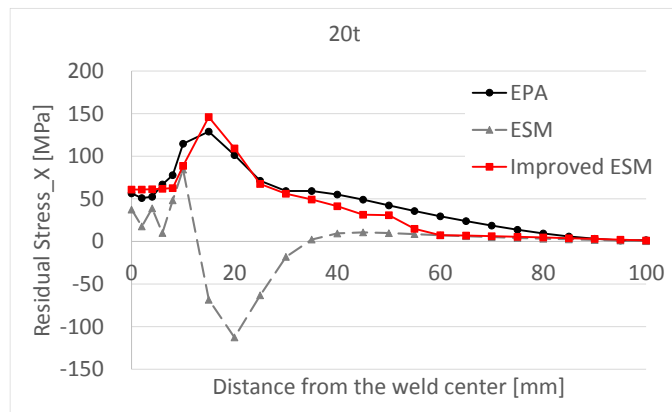


Fig. 81 Residual stress in x direction (t=20mm)

Table 21 Maximum residual stress in x direction (t=20mm)

	EPA	ESM	Improved ESM
Residual Stress (x)	131 [MPa]	202 [MPa]	164 [MPa]
Ratio	-	1.54	1.25

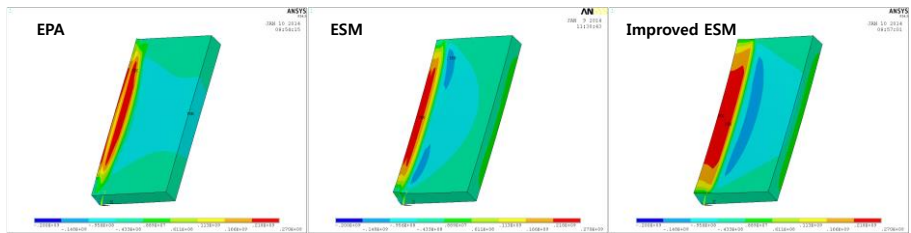


Fig. 82 Residual stress in y direction (t=20mm)

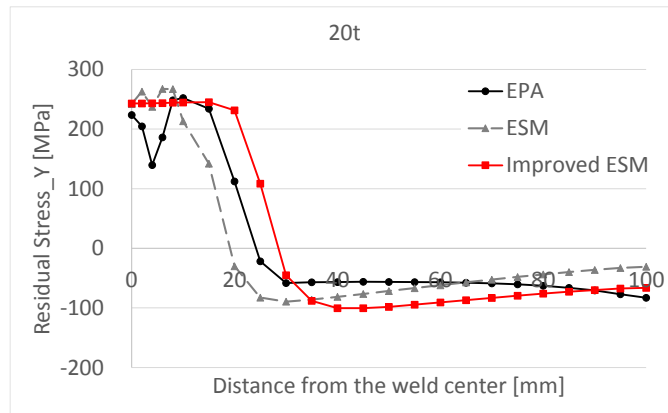


Fig. 83 Residual stress in x direction (t=20mm)

Table 22 Maximum residual stress in y direction (t=20mm)

	EPA	ESM	Improved ESM
Residual Stress (y)	255 [MPa]	269 [MPa]	271 [MPa]
Ratio	-	1.05	1.06

### 5.1.5 Summary and discussion

Analysis results are summarized in Fig. 84 and Table 23–25. Experimental result and analysis result based on Improved ESM in case of a 6mm thin plate show a difference 23%, slightly larger than other cases. But the error between the experiment and EPA is also the largest in case of a 6mm thin plate. Excluding this, both Improved ESM and EPA are in good agreement with experimental results. Only the results of existing ESM are quite different with the other methods and experimental data. Because there is a limit to simulate strain distribution for the reasons discussed in Chap. 3.

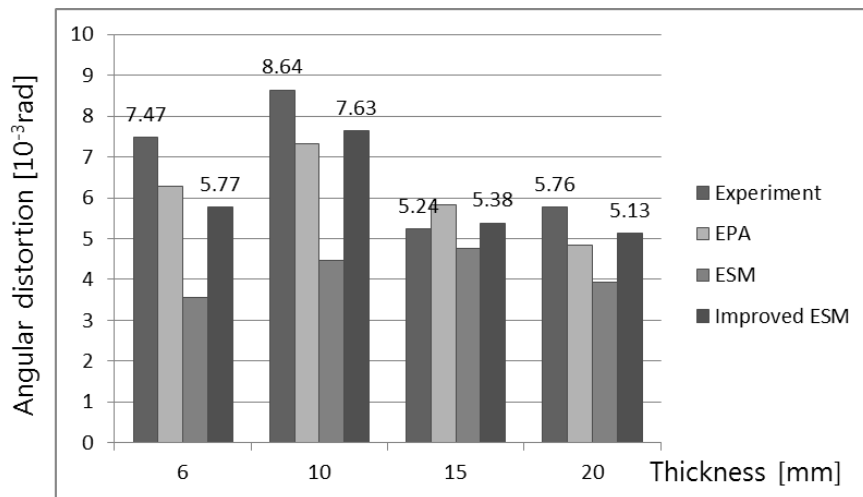


Fig. 84 Angular distortion

Table 23 Angular distortion

Thickness	Comparison	Experiment	EPA	ESM	Improved ESM
6mm	Angular distortion [10 <sup>-3</sup> rad]	7.47	6.28	3.56	5.77
	Ratio	-	0.84	0.48	0.77
10mm	Angular distortion [10 <sup>-3</sup> rad]	8.64	7.31	4.46	7.63
	Ratio	-	0.85	0.52	0.88
15mm	Angular distortion [10 <sup>-3</sup> rad]	5.24	5.82	4.76	5.38
	Ratio	-	1.11	0.91	1.03
20mm	Angular distortion [10 <sup>-3</sup> rad]	5.76	4.84	3.92	5.13
	Ratio	-	0.84	0.68	0.89

Table 24 Residual stress in x direction

Thickness	Comparison	EPA	ESM	Improved ESM
6mm	Residual stress (x) [MPa]	154	99.3	181
	Ratio	-	0.65	1.18
10mm	Residual stress (x) [MPa]	163	71.9	180
	Ratio	-	0.44	1.10
15mm	Residual stress (x) [MPa]	140	114	163
	Ratio	-	0.81	1.16
20mm	Residual stress (x) [MPa]	131	202	164
	Ratio	-	1.54	1.25

Table 25 Residual stress in y direction

Thickness	Comparison	EPA	ESM	Improved ESM
6mm	Residual Stress (y) [MPa]	262	186	248
	Ratio	-	0.71	0.94
10mm	Residual stress (y) [MPa]	267	270	258
	Ratio	-	1.01	0.97
15mm	Residual stress (y) [MPa]	268	268	249
	Ratio	-	1.00	0.93
20mm	Residual stress (y) [MPa]	255	269	271
	Ratio	-	1.05	1.06

## 5.2 Fillet welding

The experimental data of Kim(1996) is used for fillet welding analysis model. The experimental results are organized by welding parameter  $Q/h^{1.5}$  as shown in Fig. 85. It also indicates analysis results based on improved equivalent strain method in four models which refer to the experimental data.

Based on the experimental data, the analysis results of plate thickness in the range from 8 to 18 are performed. The results of thermal elasto-plastic analysis (EPA), existing equivalent strain method (ESM) and improved equivalent strain method (Improved ESM) are compared with experimental data, in the same way as in Section 5.1. Analysis models are symmetric with regard to center line. Welding conditions and detailed dimensions of the welding models are listed in Table 25.

$$\theta = 9.75 \left( \frac{Q}{h^{1.5}} \right) \exp \left( -0.834 \left( \frac{Q}{h^{1.5}} \right)^{2/3} \right) \times 10^{-4} [rad]$$

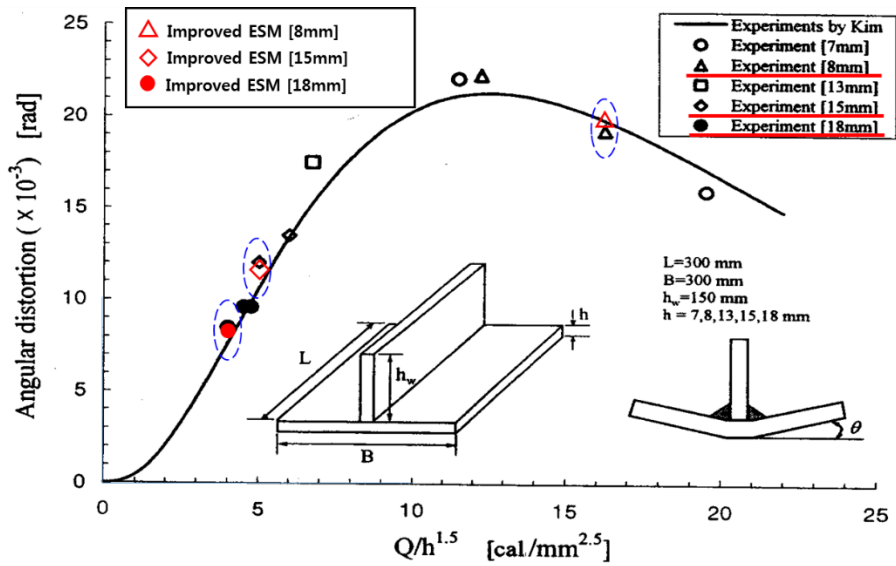


Fig. 85 Comparison with experiment (Kim)

Analysis results are described in Section 5.2.1 to 5.2.3. The results in each section are sorted in order of displacement in  $z$  direction, residual stress in  $x$  and  $y$  direction (Fig.86–103, Table 27–35). Each result is sorted again in order of the figure, graph and table. Figures depict the distribution shape of model, graphs show distribution of values in the  $x$  direction which are measured at  $y=L/2$  in top of plate. Maximum values are listed in table.

Table 26 Demension of analysis model

Dimension			Heat
Width [mm]	Length [mm]	Thickness [mm]	$Q/h^{1.5}$ [cal/mm <sup>2.5</sup> ]
300	300	8	16
		15	5
		18	4

### 5.2.1 Comparison of 8mm plate

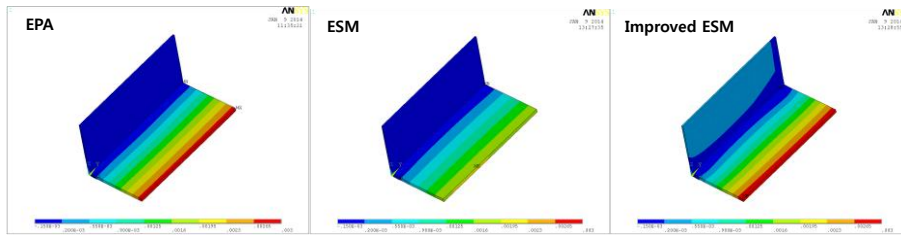


Fig. 86 Displacement in z direction (t=8mm)

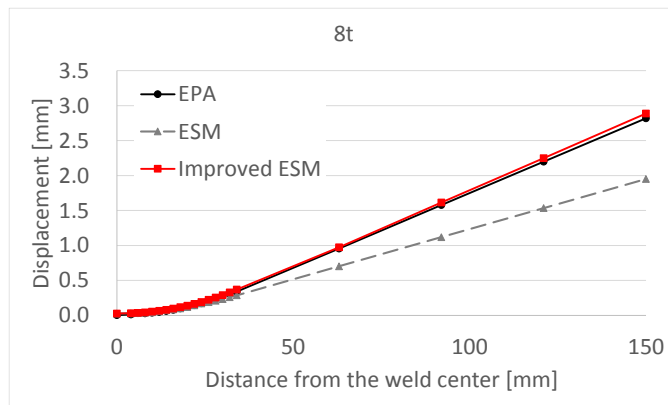


Fig. 87 Displacement in z direction (t=8mm)

Table 27 Angular distortion (t=8mm)

	Experiment	EPA	ESM	Improved ESM
Angular distortion	13.99 [10 <sup>-3</sup> rad]	18.87 [10 <sup>-3</sup> rad]	13.03 [10 <sup>-3</sup> rad]	19.81 [10 <sup>-3</sup> rad]
Ratio	-	0.99	0.69	1.04

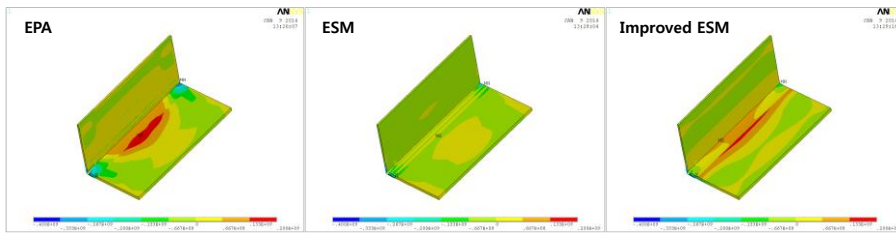


Fig. 88 Residual stress in x direction (t=8mm)

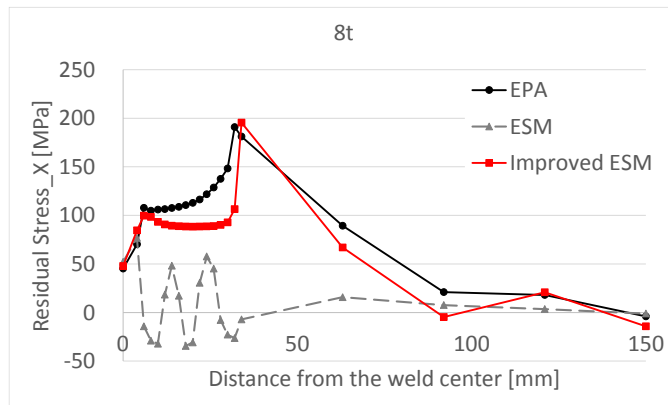


Fig. 89 Residual stress in x direction (t=8mm)

Table 28 Residual stress in x direction (t=8mm)

	EPA	ESM	Improved ESM
Residual stress (x)	201 [MPa]	113 [MPa]	212 [MPa]
Ratio	-	0.56	1.05

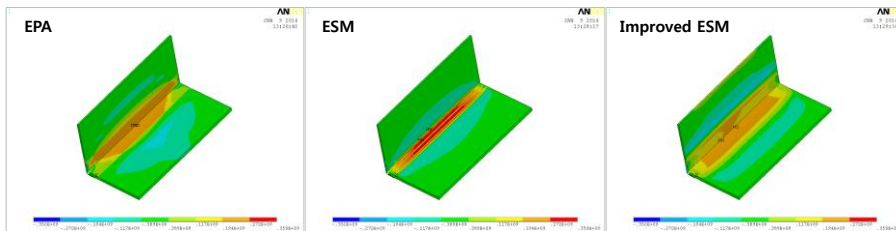


Fig. 90 Residual stress in y direction (t=8mm)

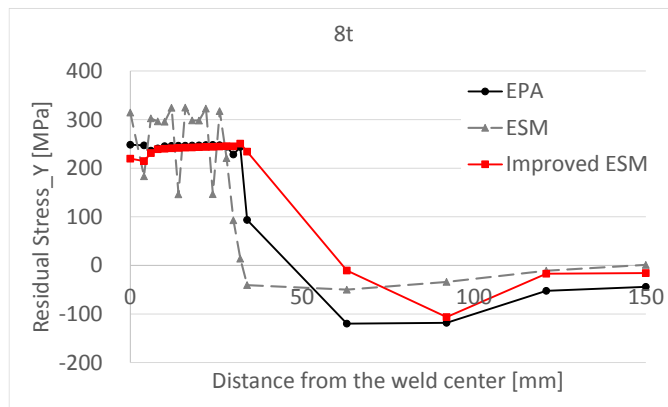


Fig. 91 Residual stress in y direction (t=8mm)

Table 29 Residual stress in y direction (t=8mm)

	EPA	ESM	Improved ESM
Residual stress (y)	268 [MPa]	332 [MPa]	270 [MPa]
Ratio	-	1.24	1.01

### 5.2.2 Comparison of 15mm plate

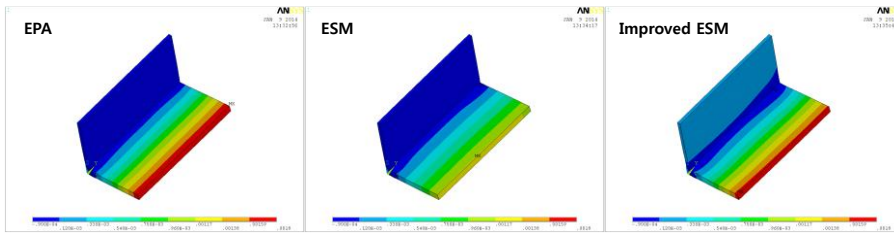


Fig. 92 Displacement in z direction ( $t=15\text{mm}$ )

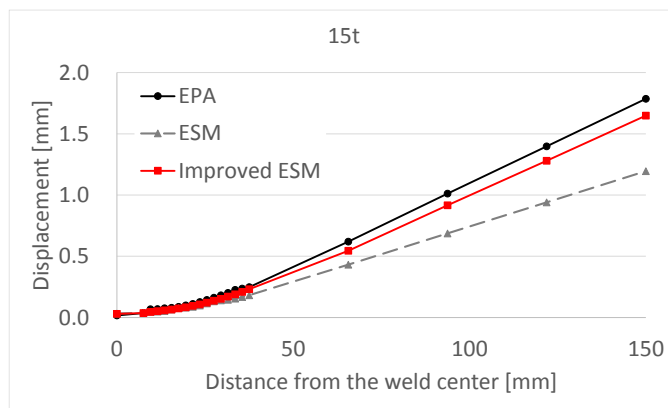


Fig. 93 Displacement in z direction ( $t=15\text{mm}$ )

Table 30 Angular distortion ( $t=15\text{mm}$ )

	Experiment	EPA	ESM	Improved ESM
Angular distortion	11.90 [ $10^{-3}$ rad]	11.98 [ $10^{-3}$ rad]	7.97 [ $10^{-3}$ rad]	11.39 [ $10^{-3}$ rad]
Ratio	-	1.01	0.67	0.96

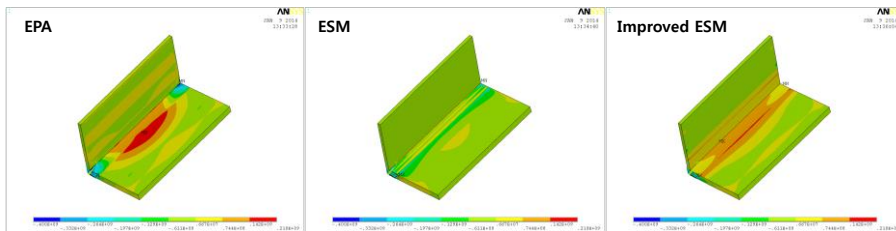


Fig. 94 Residual stress in x direction (t=15mm)

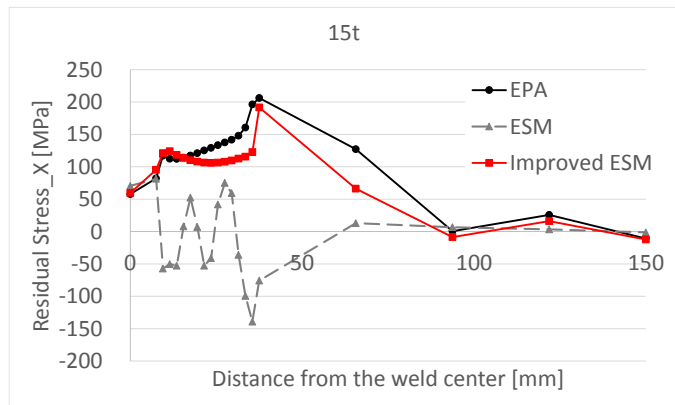


Fig. 95 Residual stress in x direction (t=15mm)

Table 31 Residual stress in x direction (t=15mm)

	EPA	ESM	Improved ESM
Residual stress (x)	208 [MPa]	169 [MPa]	157 [MPa]
Ratio	-	0.81	0.75

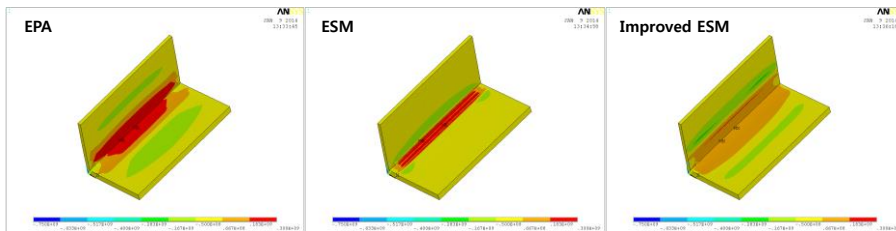


Fig. 96 Residual stress in y direction (t=15mm)

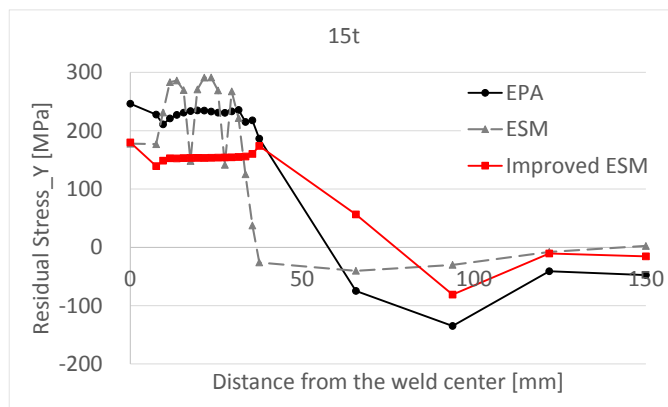


Fig. 97 Residual stress in y direction (t=15mm)

Table 32 Residual stress in y direction (t=15mm)

	EPA	ESM	Improved ESM
Residual stress (y)	283 [MPa]	272 [MPa]	239 [MPa]
Ratio	-	0.96	0.84

### 5.2.3 Comparison of 18mm plate

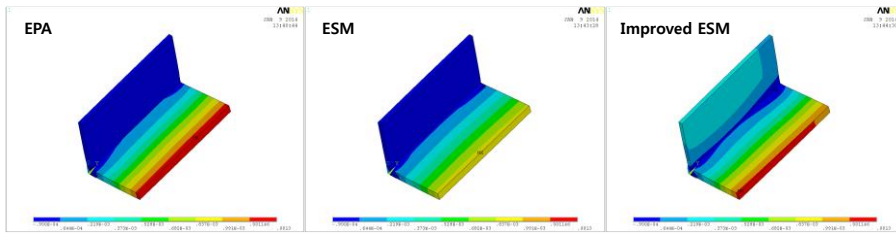


Fig. 98 Displacement in z direction (t=18mm)

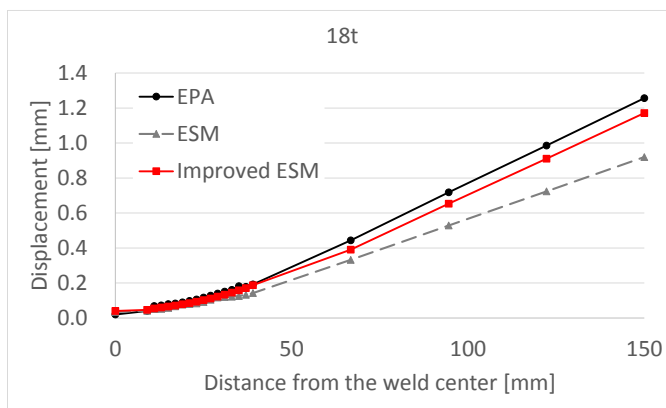


Fig. 99 Displacement in z direction (t=18mm)

Table 33 Angular distortion (t=18mm)

	Experiment	EPA	ESM	Improved ESM
Angular distortion	8.42 [10 <sup>-3</sup> rad]	8.39 [10 <sup>-3</sup> rad]	6.14 [10 <sup>-3</sup> rad]	8.05 [10 <sup>-3</sup> rad]
Ratio	-	1	0.73	0.96

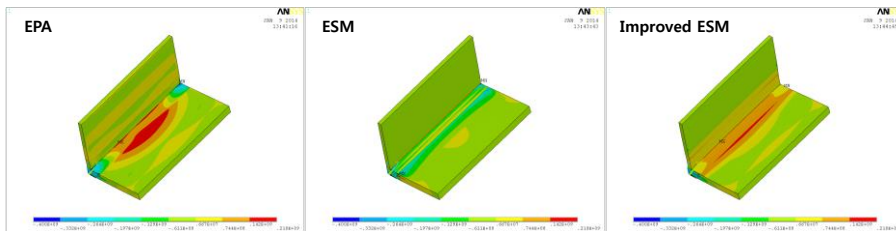


Fig. 100 Residual stress in x direction (t=18mm)

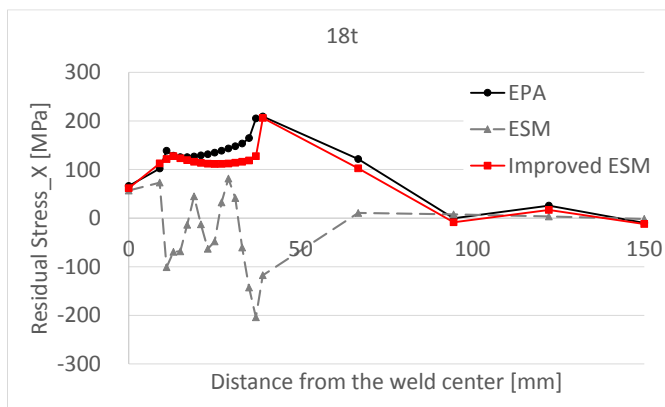


Fig. 101 Residual stress in x direction (t=18mm)

Table 34 Residual stress in x direction (t=18mm)

	EPA	ESM	Improved ESM
Residual stress (x)	211 [MPa]	206 [MPa]	200 [MPa]
Ratio	-	0.98	0.95

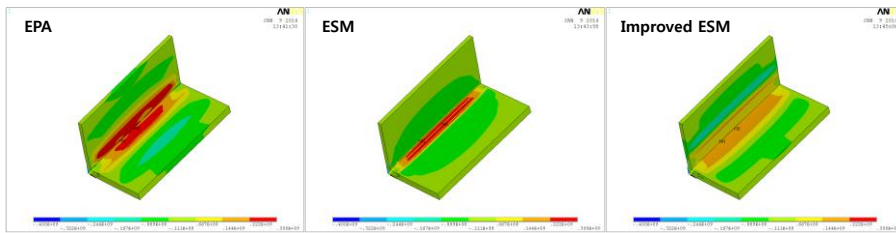


Fig. 102 Residual stress in y direction (t=18mm)

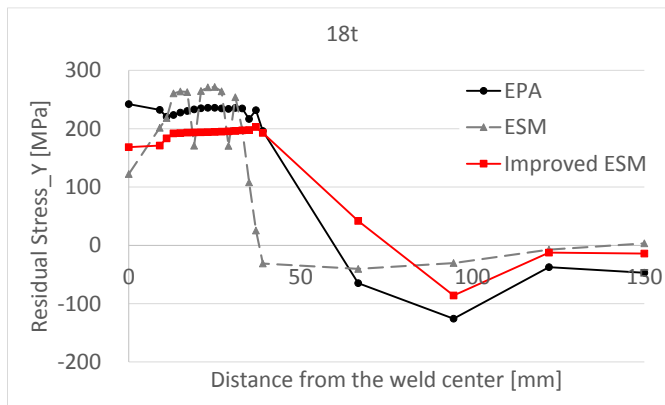


Fig. 103 Residual stress in y direction (t=18mm)

Table 35 Residual stress in y direction (t=18mm)

	EPA	ESM	Improved ESM
Residual stress (y)	283 [MPa]	272 [MPa]	239 [MPa]
Ratio	-	0.96	0.84

## 5.2.4 Summary and discussion

Analysis results are summarized in Fig. 104 and Table 36–38. Angular distortions computed by analysis based on Improved ESM are in good agreement with those of experimental data within the error of 5%. The results of existing ESM are quite different with that of other methods and experimental data.

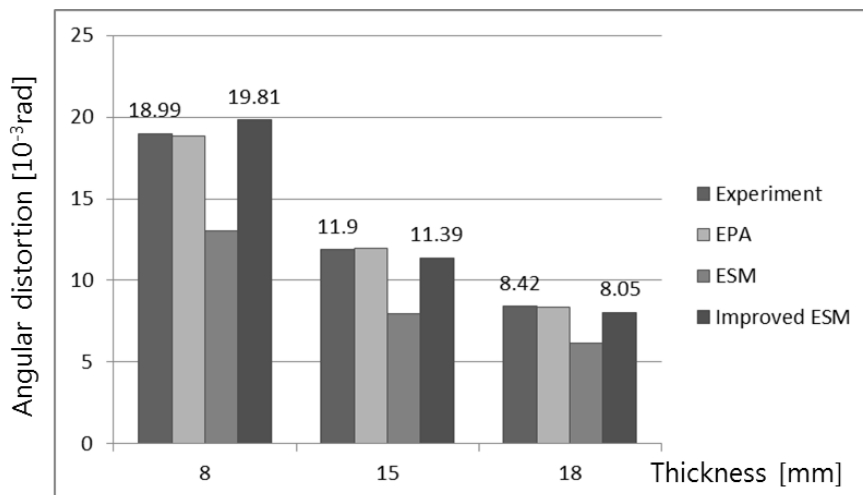


Fig. 104 Angular distortion

Table 36 Angular distortion

Thickness	Comparison	Experiment	EPA	ESM	Improved ESM
8mm	Angular distortion [10 <sup>-3</sup> rad]	18.99	18.87	13.03	19.81
	Ratio	-	0.99	0.69	1.04
15mm	Angular distortion [10 <sup>-3</sup> rad]	11.9	11.98	7.97	11.39
	Ratio	-	1.01	0.67	0.96
18mm	Angular distortion [10 <sup>-3</sup> rad]	8.42	8.39	6.14	8.05
	Ratio	-	1	0.73	0.96

Table 37 Residual stress in x direction

Thickness	Comparison	EPA	ESM	Improved ESM
8mm	Residual stress (x) [MPa]	201	113	212
	Ratio	-	0.56	1.05
15mm	Residual stress (x) [MPa]	208	169	157
	Ratio	-	0.81	0.75
18mm	Residual stress (x) [MPa]	211	206	200
	Ratio	-	0.98	0.95

Table 38 Residual stress in y direction

Thickness	Comparison	EPA	ESM	Improved ESM
8mm	Residual stress (y) [MPa]	268	332	270
	Ratio	-	1.24	1.01
15mm	Residual stress (y) [MPa]	272	292	280
	Ratio	-	1.07	1.03
18mm	Residual stress (y) [MPa]	283	272	239
	Ratio	-	0.96	0.84

## 6. Welding analysis considering external constraint during cooling

### 6.1. The effect of external constraint in welding

In this section, four analysis models are compared with each other. They were divided by external constraint condition, whether or not the external constraint is applied to analysis model when heating and cooling, respectively. These analyses are carried out to identify the effect of the constraint on the residual deformation. Constraints have been removed in the final stage of all the analysis case. Additional boundary condition is illustrated in Fig. 105 and analysis results are shown in Table 39 and Fig. 106.

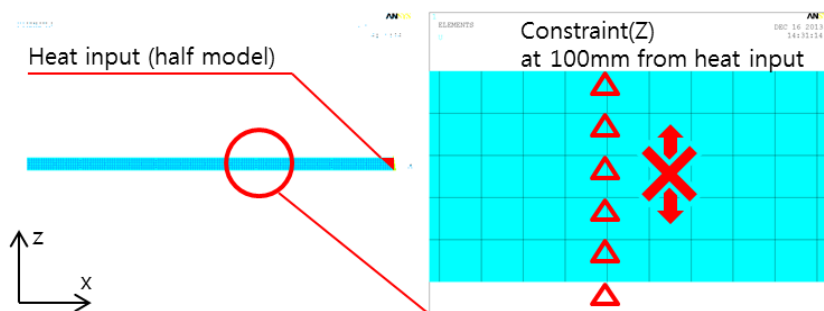


Fig. 105 Constraint condition

Table 39 Maximum deformation in z direction

	Constraint stage		Max. deform.(mm)
	Heating	Cooling	
CASE I	X	X	0.724
CASE II	O	O	1.051
CASE III	O	X	1.751
CASE IV	X	O	0.467

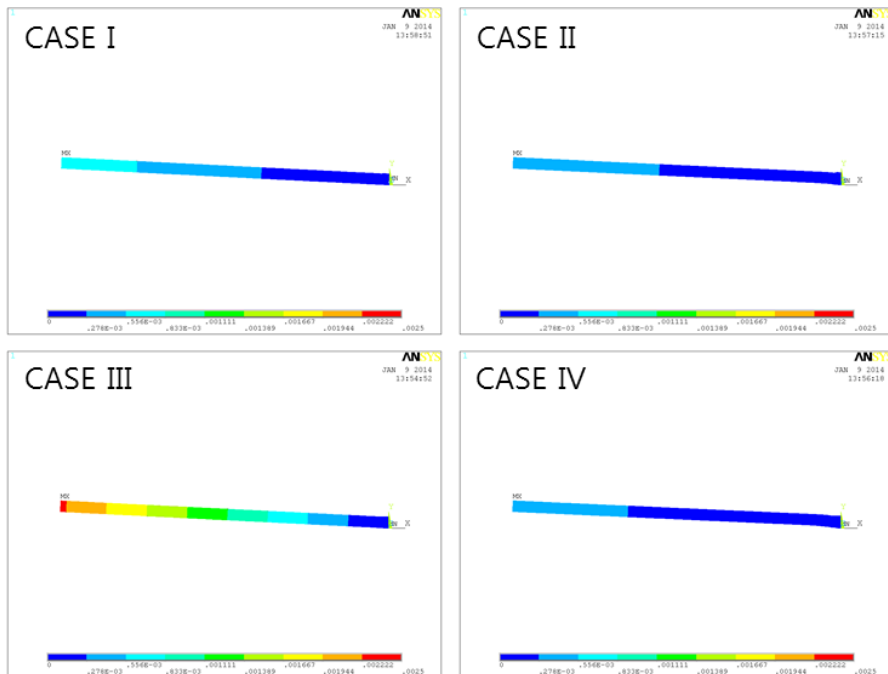


Fig. 106 Deformation in z direction

As is well known, to suppress deformation during cooling stage is a positive effect to reduce the residual deformation. On the contrary, residual deformations of Case III are larger than

the case of no external constraint. The result of CASE II veered between the results of CASE III and CASE IV.

## **6.2. Simplifying of welding analysis considering external constraint during cooling**

Basically, heat induces a thermal stress and strain as shown in Fig. 107 (a). Here both sides of the plate are not heated. So the heated region expands and creates reaction force. Because of this reaction, the heated area is inflated convexly as shown in Fig. 107 (b). After this, the heated area is cooled by water or air, which induces shrinkage of the expanded region and generates contraction force as shown in Fig. 107 (c). Finally, due to the shrinkage the angular distortion is induced as shown in Fig. 107 (d). This slope is caused by the steel temperature gradient due to heating, which induces the different amount of expansion and shrinkage of the plate in the local area and creates angular distortion. If the heat distribution is constant along the thickness, the amount of thermal stress remains the same across the thickness, which leads to the same amount of expansion and shrinkage of the plate along the thickness. Therefore, the residual deformation remains constant thickness-wise and no angular distortion will be induced.

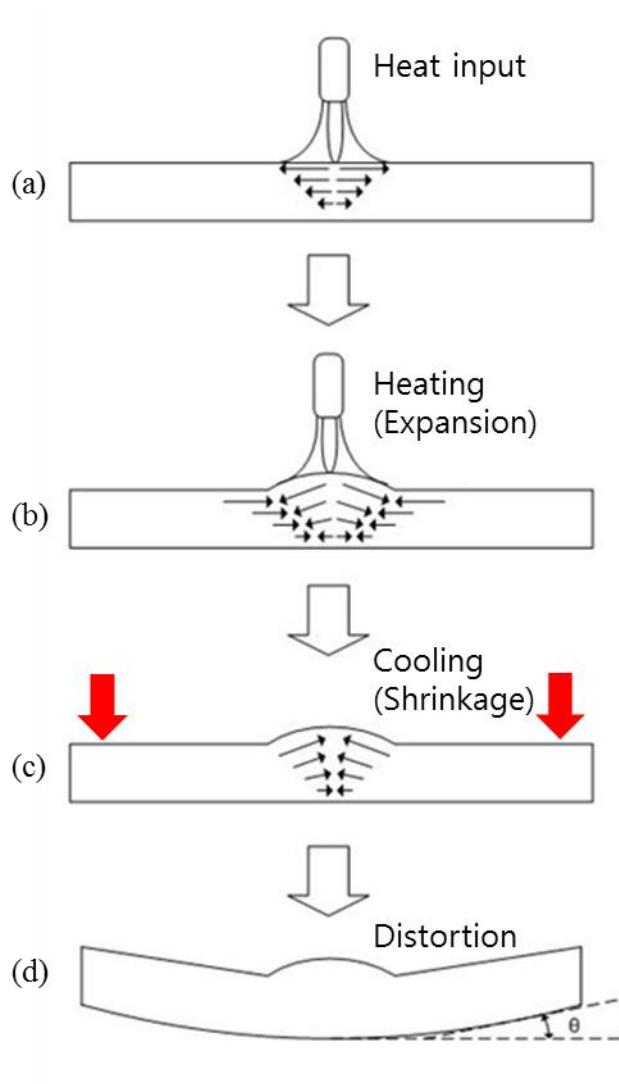


Fig. 107 Welding deformation algorithm

Now an analysis model, which undergo normal force  $P$  during cooling (Fig. 107 (c) and Fig. 108) at distance of 'a' from the weld line, can be simplified.

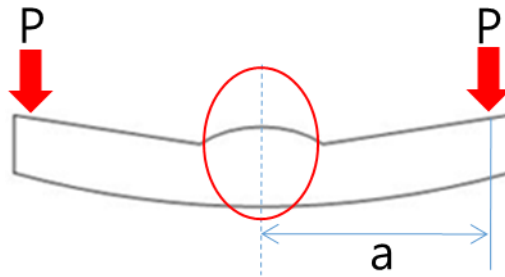


Fig. 108 Analysis model subjected to external load

Assume that  $M$  is the moment acting on the welded region by the external normal force  $P$ ,

$$M = Pa$$

Also assume that this welding analysis model is a prismatic member subjected to pure bending, external force  $P$  can be substitute the stress in  $x$  direction, which varies linearly along the thickness direction as shown in Fig. 109.

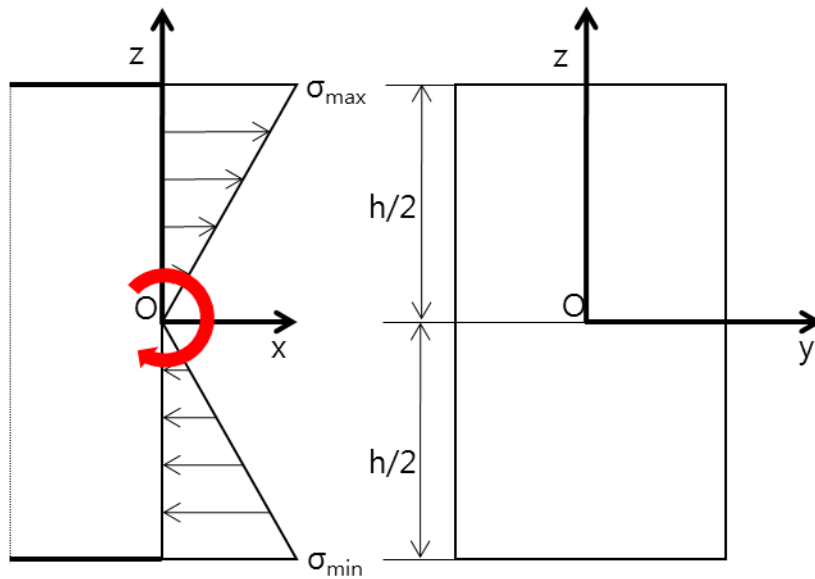


Fig. 109 A cross sectional view of simplified concept model

The derivation is as follows.

The conditions of equilibrium of the cross section area of the member require that the internal force in the section be equivalent to the couple  $M$ . Thus, the internal forces in any cross section of a symmetric member in pure bending are equivalent to a couple.

A couple  $M$  actually consists of two equal and opposite forces. The sum of the components of these forces in any direction is therefore equal to zero. Moreover, the moment of the couple is the same about any axis perpendicular to its plane, and is zero about any axis contained in that plane. Selecting arbitrarily the  $y$  axis as shown in Fig. 109, the equivalence of the elementary internal forces and of the couple  $M$  is expressed

by writing that the sums of the components and of the moments of the elementary force are equal to the corresponding components and moments of the couple M:

$$\text{X components: } \int \sigma_x dA = 0 \quad (6-1)$$

$$\text{Moments about y axis: } \int -z\sigma_x dA = M \quad (6-2)$$

$$\text{Moments about z axis: } \int y\sigma_x dA = 0 \quad (6-3)$$

The longitudinal normal strain  $\epsilon_x$  varies linearly with the distance  $z$  from the neutral surface.

$$\epsilon_x = -\frac{z}{c}\epsilon_m \quad (6-4)$$

The strain  $\epsilon_m$  is the maximum absolute value of the strain,  $c$  is the largest distance from the neutral surface which corresponds to either the upper or the lower surface of the member.

Assuming the material to be homogeneous, and denoting by  $E$  its modulus of elasticity,

$$\sigma_x = E\epsilon_x \quad (6-5)$$

Recalling Eq. (6-4), and multiplying both members of that equation by  $E$ ,

$$E\varepsilon_x = -\frac{z}{c}(E\varepsilon_m)$$

or, using Eq. (6-5),

$$\sigma_x = -\frac{z}{c}\sigma_m \quad (6-6)$$

Where  $\sigma_m$  denotes the maximum absolute value of the stress. This stress distribution is pictured in Fig. 109 for the case in which the bending moment  $M$  is negative and the beam bends with negative curvature. When the curvature is negative, the stresses  $\sigma_x$  are tension above the neutral surface and compression below it. In the figure, compressive stresses are indicated by arrows pointing toward the cross section and tensile stresses are indicated by arrows pointing away from the cross section.

Now recall Eq. (6-2), which was derived with respect to an arbitrary horizontal  $y$  axis,

$$\int -z\sigma_x dA = M \quad (6-2)$$

Specifying that the  $y$  axis should coincide with the neutral axis of the cross section,  $\sigma_x$  can be substituted from Eq. (6-6) into (6-2) and write

$$\int (-y) \left( -\frac{y}{c} \sigma_m \right) dA = M$$

Or

$$\frac{\sigma_m}{c} \int y^2 dA = M \quad (6-7)$$

In the case of pure bending the neutral axis passes through the centroid of the cross section,  $I$  is the moment of inertia, or second moment, of the cross section with respect to a centroidal axis perpendicular to the plane of the couple  $M$ . Solving Eq. (6-7) for  $\sigma_m$ ,

$$\sigma_m = \frac{Mc}{I} \quad (6-8)$$

Substituting for  $\sigma_m$  from Eq. (6-8) into Eq. (6-6), the normal stress at any distance  $z$  from the neutral axis is obtained:

$$\sigma_x = -\frac{Mz}{I} \quad (6-10)$$

Finally, welding analysis under external normal force during cooling idealized as a problem under compressive or tensile stress in  $x$  direction depending on location of constraint, magnitude of constraint, and applied location in thickness direction.

## 6.3. Identification of assumption

In this section, welding analysis is performed to verify whether it is valid to simply regard the normal external constraint force  $P$  as  $M$ , the moment acting on the welded region.

Analysis results of the model which is acting external force during cooling are shown in Fig. 110. Each case has different external loading conditions but in terms of the moment which is simply calculated, all cases can be seen as the same condition. Assume that welding analysis models as prismatic members subjected to pure bending, external forces induce the identical moment,  $0.3 \text{ kN} \cdot \text{m}$  at the weld. Results of the three cases as depicted in Fig. 110 are in good agreement with each other.

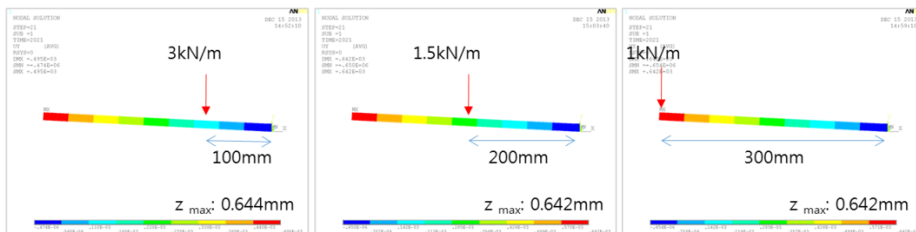


**Fig. 110 Analysis results of the model that external force is acting during cooling**

Table 40 shows the results of analysis of more cases. They are also in good agreement with each other. For several models

that induce the same moment by changing the magnitude and position of vertical force, average error is about 1% which is very small.

Table 40 B.C. and results of 2D thermal elasto–plastic analysis

Moment (Nm)	Distance (mm)	Force (N)	$z_{\max}$ (Disp.) (mm)	Ratio
300	100	3000	0.644	1
	200	1500	0.642	0.997
	300	1000	0.642	0.997
600	100	6000	0.563	1
	200	3000	0.559	0.993
	300	2000	0.558	0.991
900	100	9000	0.481	1
	200	4500	0.475	0.988
	300	3000	0.473	0.983

#### 6.4. Inherent strain model considering external constraint during cooling

Inherent strain model and the procedure to obtain the inherent strain are basically identical to that of improved

equivalent strain method, except that the additional compressive or tensile stress in x direction is applied in cooling stage. This is due to the assumption in section 6.2. Constraint has been removed in final stage.

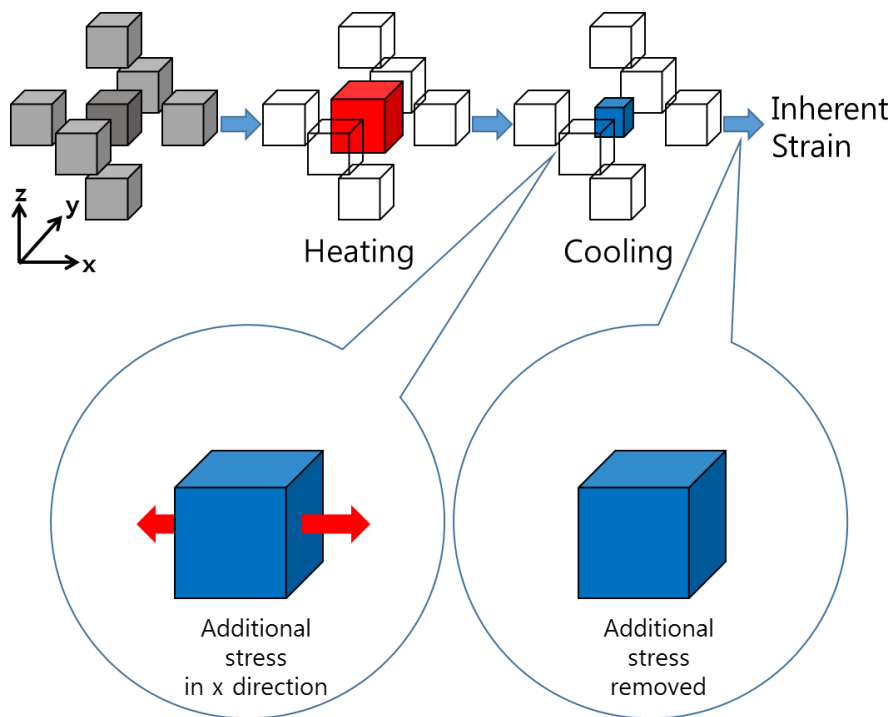


**Fig. 111 Inherent strain model considering external constraint during cooling**

Fig. 112–114 display Improved inherent strain charts considering external constraint during cooling. As compressive stress increases, the residual plastic strain also increases in the positive direction and vice versa.

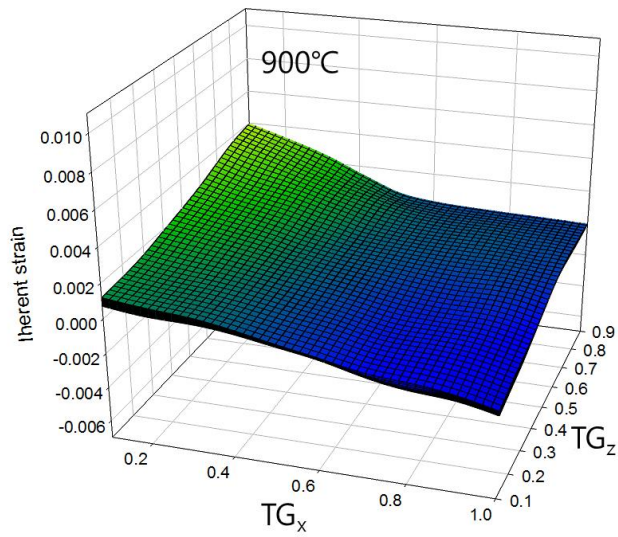


Fig. 112 Inherent strain chart considering external constraint during cooling (900°C)

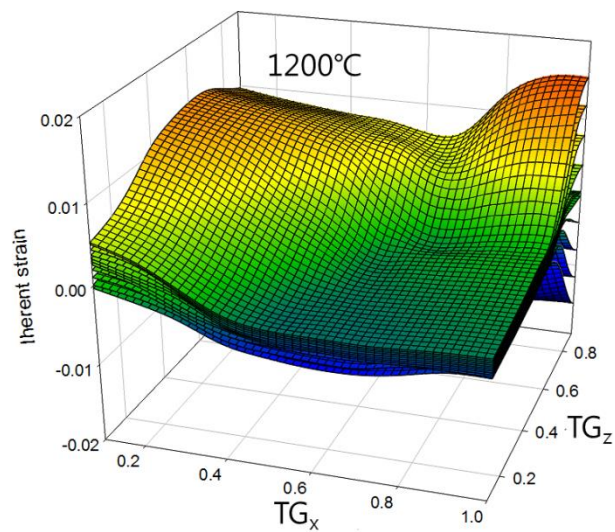
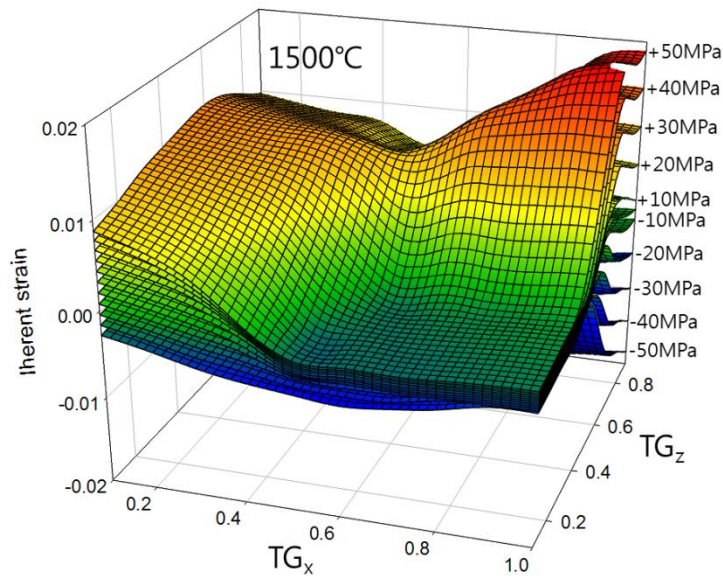


Fig. 113 Inherent strain chart considering external constraint during cooling (1200°C)



**Fig. 114 Inherent strain chart considering external constraint during cooling ( $1500^{\circ}\text{C}$ )**

Under tensile stress during cooling stage, the force is applied to the opposite direction for shrink. Then, the restraint is getting stronger and the inherent strain decreases. On the other hand, the restraint is weakened under compressive stress during cooling stage. It is results of the force applied to direction for shrink. Then, the inherent strain increases.

Tensile and compressive stress affects to top and bottom side of welding plate, respectively. Inherent strain in upper side increases while inherent strain in lower side decreases. Consequentially the slope of inherent strain along the thickness direction becomes gentle as illustrated in Fig. 115.

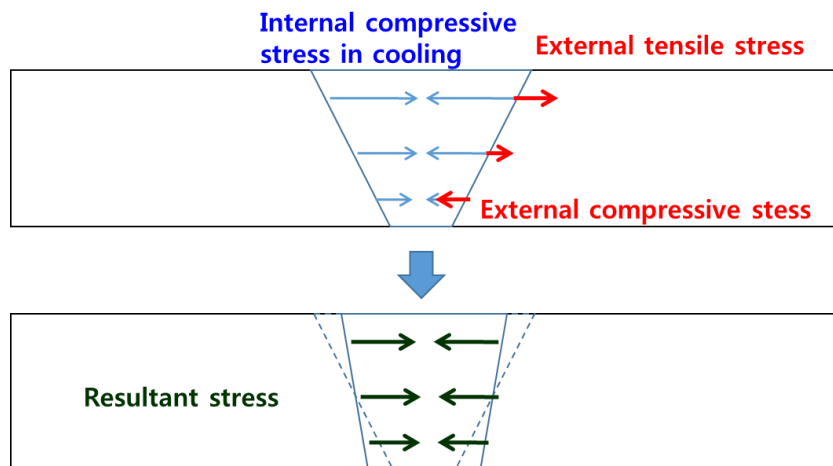


Fig. 115 Mechanism of restraint degree regarding external force during cooling

## 7. Comparison of the welding analysis considering external constraint during cooling stage

### 7.1. Analysis considering various external force

The analyses of six cases which have different welding conditions are performed. One is done in general condition without external constraint. The other five are the cases of condition that vertical forces on work piece at both sides during cooling stage as depicted in Fig. 116. The forces induce the stress in transverse direction, maximum value of 30, 60, 90, 120, and 150 MPa. In each case, the welding distortions calculated by two different methods (Elasto–plastic analysis: EPA, Improved equivalent strain method: Improved ESM) are compared. Dimensions for analysis model are listed in Table 41. Analysis results of deformation are depicted in Fig. 117–128. Each result is sorted again in order of figure and graph. Figures depict the distribution shape of the model, graphs show distribution of values in the x direction which are measured at  $y=L/2$  in top of plate.

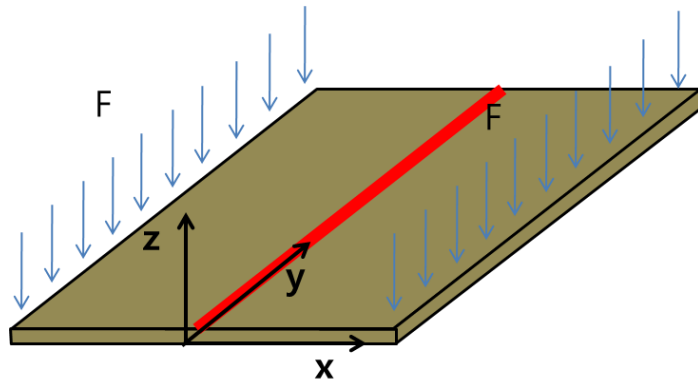


Fig. 116 Analysis cased that force is applied on both ends,  
perpendicular to the weld line

Table 41 Dimension of analysis model

Length	500 mm
Width	1000 mm
Thickness	20 mm

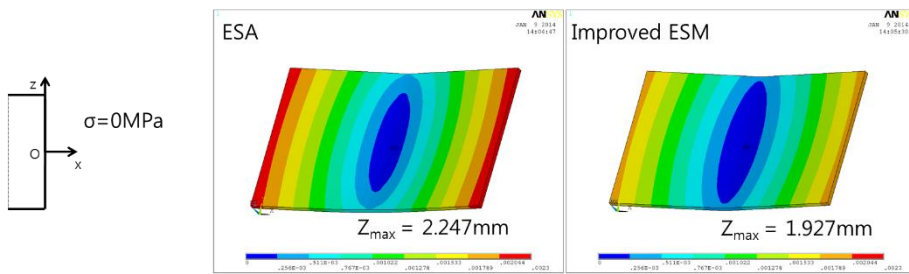


Fig. 117 Displacement in  $z$  direction (0 MPa)

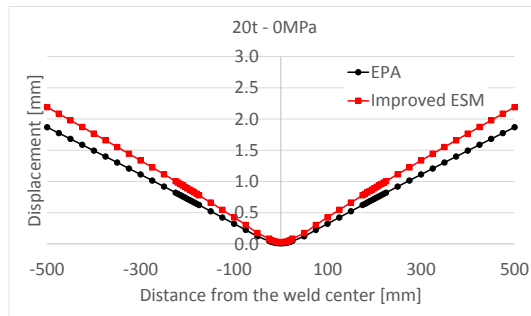


Fig. 118 Displacement in  $z$  direction (0 MPa)

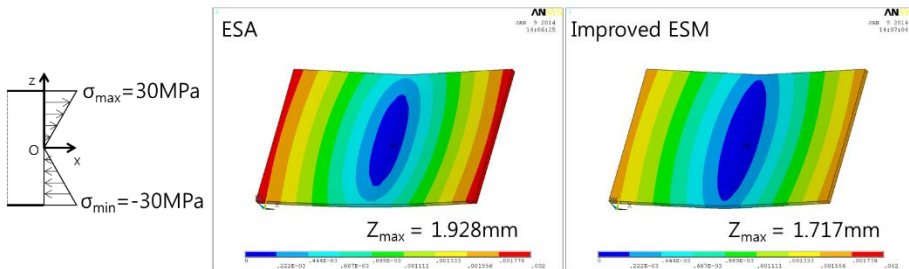


Fig. 119 Displacement in  $z$  direction (30 MPa)

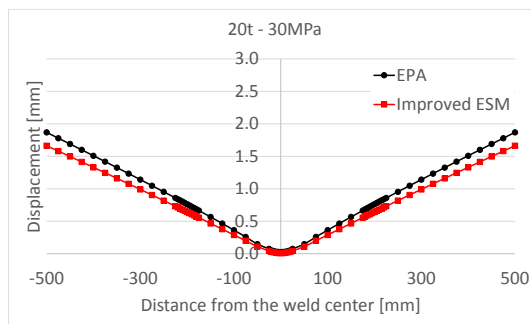


Fig. 120 Displacement in  $z$  direction (30 MPa)

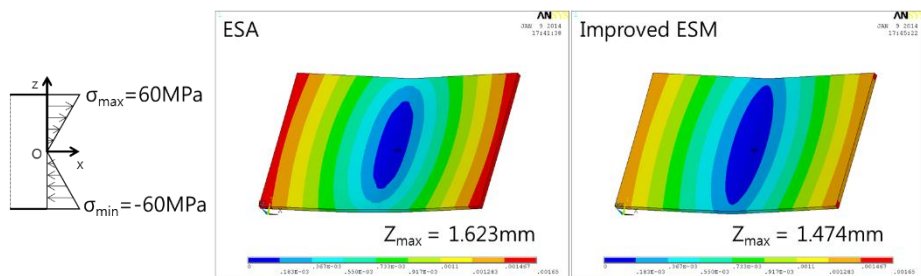


Fig. 121 Displacement in z direction (60 MPa)

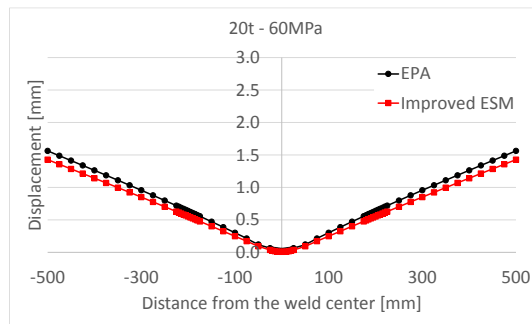


Fig. 122 Displacement in z direction (60 MPa)

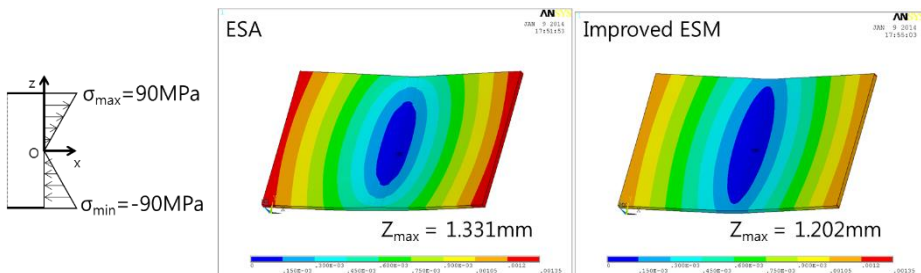


Fig. 123 Displacement in z direction (90 MPa)

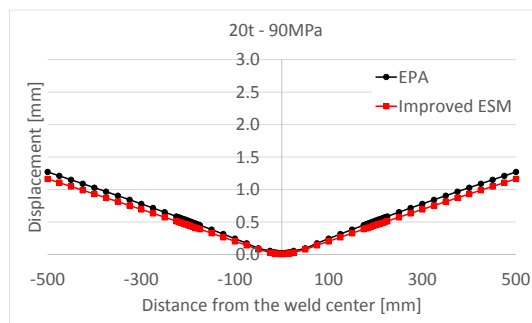


Fig. 124 Displacement in z direction (90 MPa)

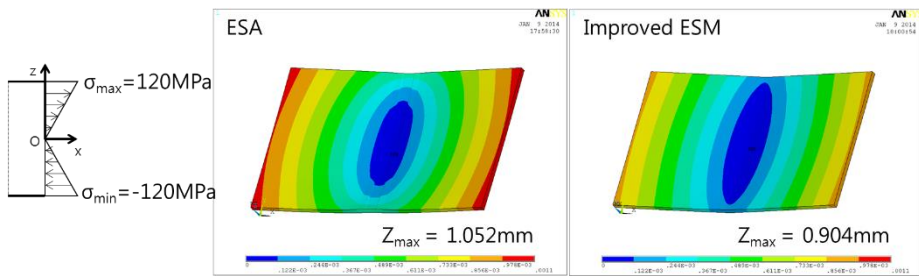


Fig. 125 Displacement in z direction (120 MPa)

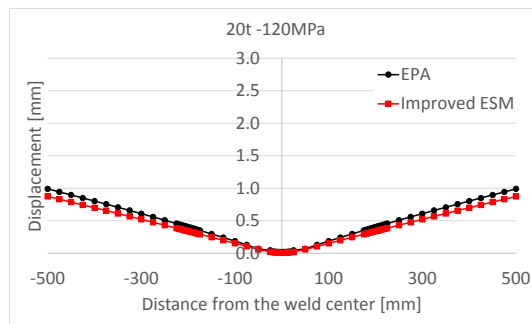


Fig. 126 Displacement in z direction (120 MPa)

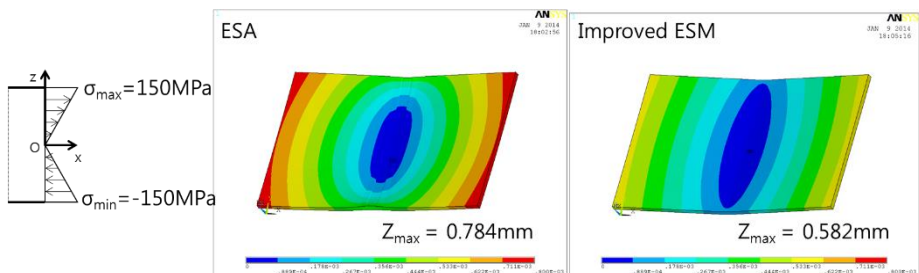


Fig. 127 Displacement in z direction (150 MPa)

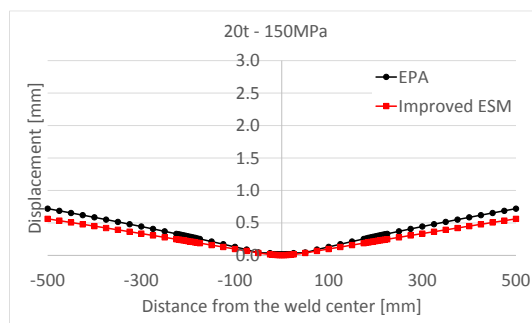


Fig. 128 Displacement in z direction (150 MPa)

Table 42 Maximum displacement in z direction (0 to 150 MPa)

Max. stress (MPa)	EPA	Improved ESM	Ratio
0	2.247	1.927	0.86
30	1.928	1.717	0.89
60	1.623	1.474	0.91
90	1.331	1.202	0.90
120	1.052	0.904	0.86
150	0.784	0.582	0.74

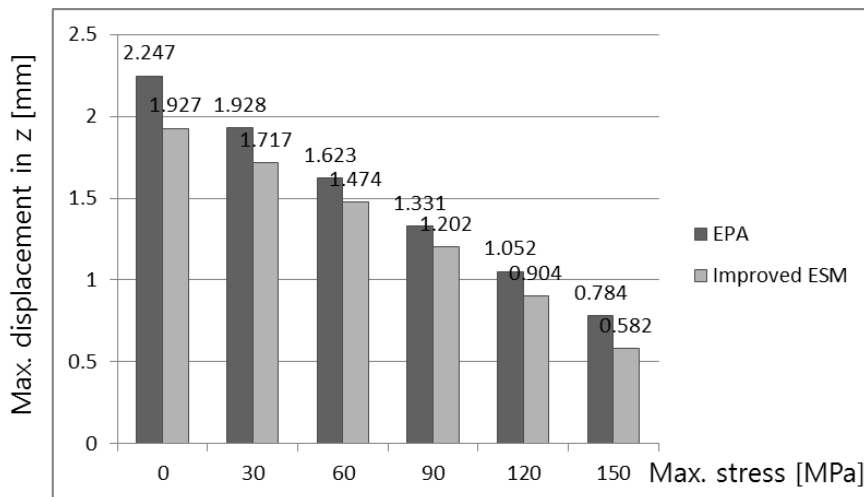


Fig. 129 Maximum displacement in z direction (0 to 150 MPa)

Maximum displacements in z direction are shown in Table 42 and Fig. 129. It can be confirmed that the deformation is reduced as the external constraint force during cooling

increases. The results of EPA and Improved ESM show a difference of 14% on the average.

## 7.2. Analysis of model related to external force inducing equal bending moment

Three analyses are compared in this section. One is improved equivalent strain analysis considering external constraint during cooling stage. The others are thermal elasto-plastic analyses about two loading conditions induced the stress in the range from  $-30$  to  $30$  MPa during cooling.

Latter two loading conditions are divided by magnitude and location of external force as shown in Fig. 130. Dimension for analysis model is listed in Table 43. Corresponding Improved ESM model can be defined as illustrated in Fig. 131. Analysis results are shown in Fig. 132–137. They show the distribution shapes of the model and graphs of values in the  $x$  direction which are measured at  $y=L/2$  in top of plate.

**Table 43 Dimension of analysis model**

Length	600 mm
Width	800 mm
Thickness	15 mm

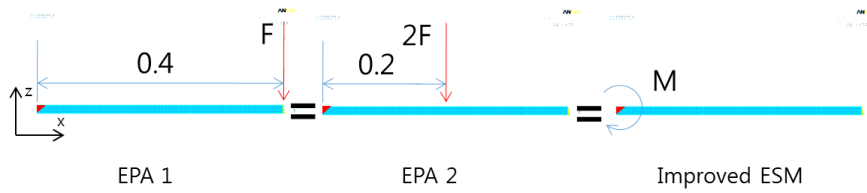


Fig. 130 Three analysis cases that the external force is applied

Where

$$F = 1.69 \text{ kN}$$

$$M = 0.4 \times F = 0.2 \times 2F = 674.68 \text{ Nm}$$

$$\sigma_{max} = \frac{Mh}{2I} = 30 \text{ MPa}$$

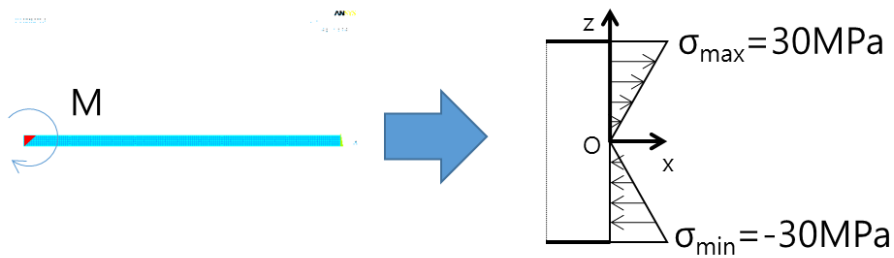


Fig. 131 Improved equivalent strain method model that the external force is applied

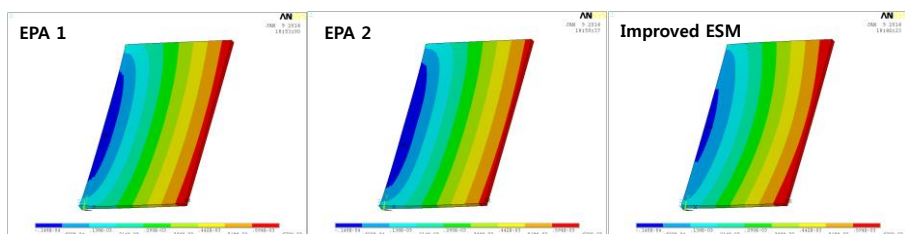


Fig. 132 Displacement in z direction (M)

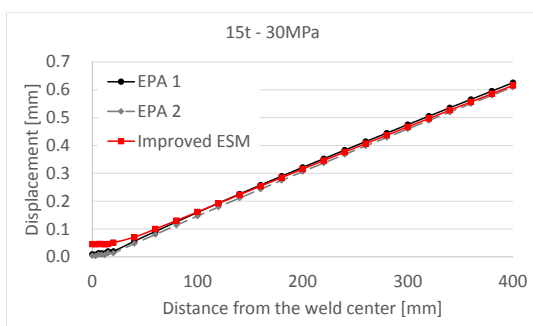


Fig. 133 Displacement in z direction (M)

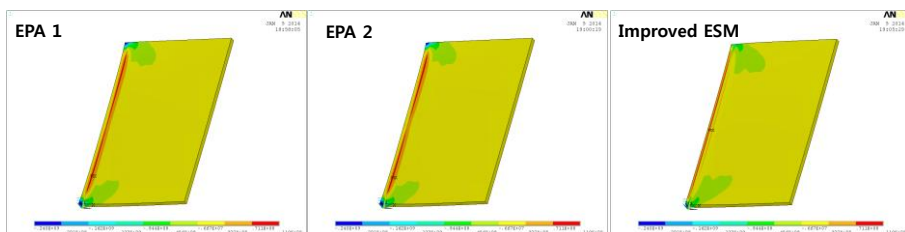


Fig. 134 Residual stress in x direction (M)

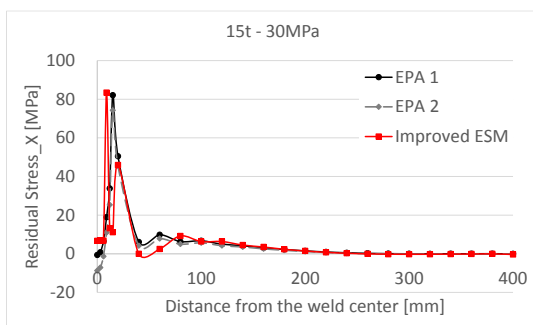


Fig. 135 Residual stress in x direction (M)

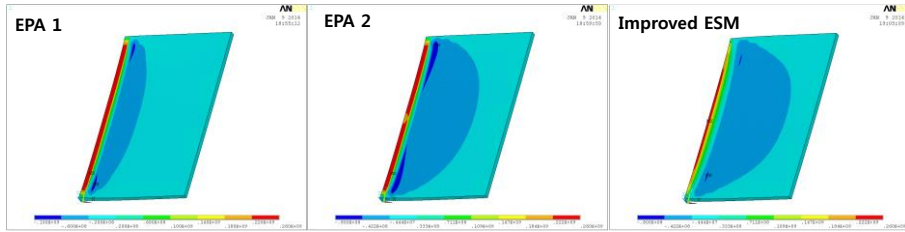


Fig. 136 Residual stress in y direction (M)

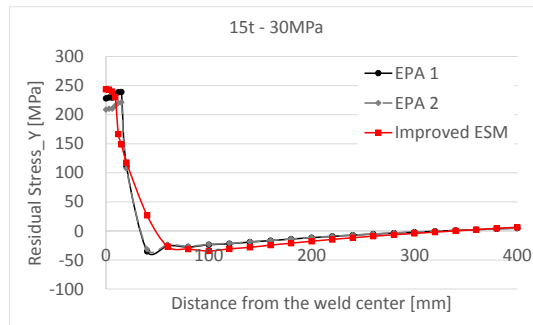


Fig. 137 Residual stress in y direction (M)

The cases of stress in the range from  $-60$  to  $60$  MPa are also compared as illustrated in Fig. 138. Improved ESM model can be regarded as shown in Fig. 139. Analysis results are shown in Fig. 140–145.

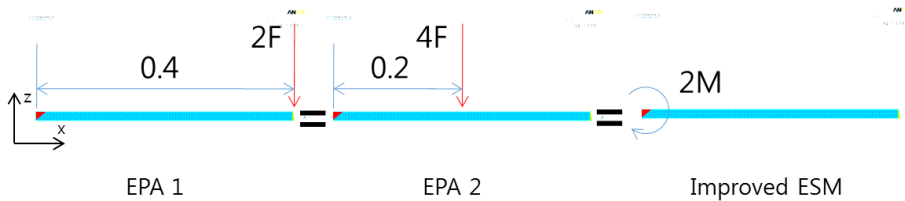


Fig. 138 Three analysis cases that the external force is applied

Where

$$F = 1.69 \text{ kN}$$

$$2M = 0.4 \times 2F = 0.2 \times 4F = 1349.36 \text{ Nm}$$

$$\sigma_{max} = \frac{Mh}{2I} = 60 \text{ MPa}$$



Fig. 139 Improved equivalent strain method model that the external force is applied

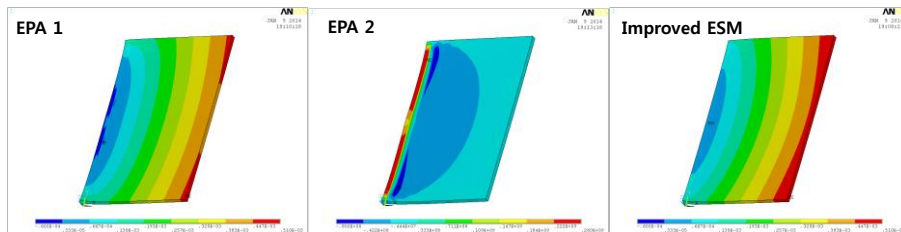


Fig. 140 Displacement in z direction (2M)

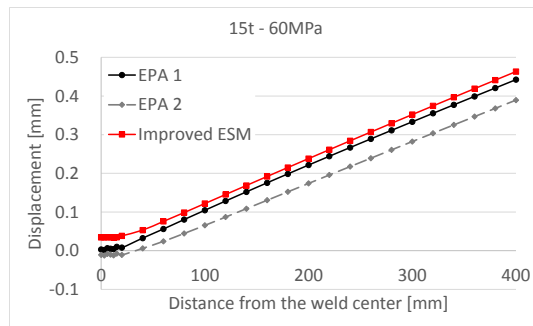


Fig. 141 Displacement in z direction (2M)

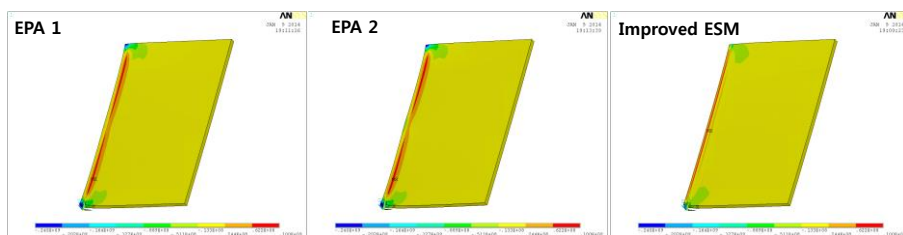


Fig. 142 Residual stress in x direction (2M)

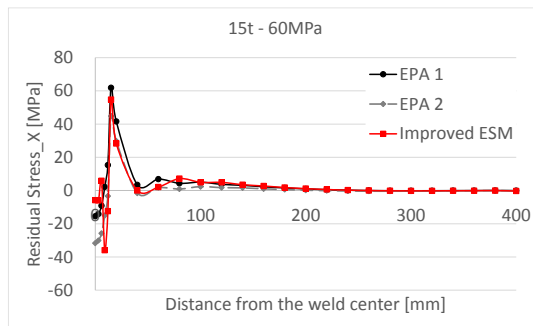


Fig. 143 Residual stress in x direction (2M)

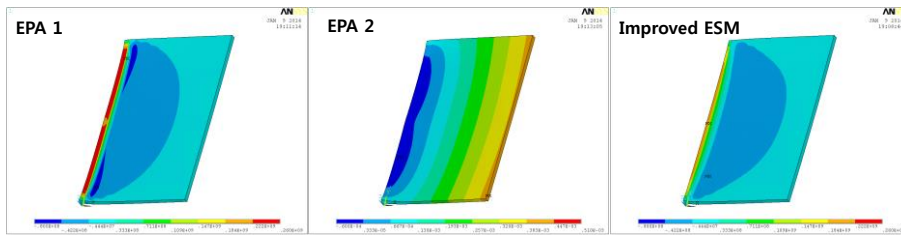


Fig. 144 Residual stress in y direction (2M)

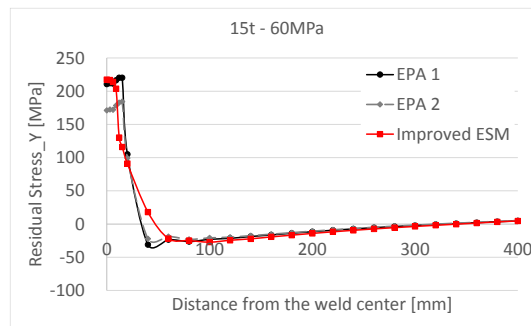


Fig. 145 Residual stress in y direction (2M)

Analysis results are shown in Fig. 146 and Table 44. The numbers in parentheses of Table 44 are the ratio obtained by dividing EPA result by Improved ESM result. It can be confirmed that the deformation is reduced as the external constraint force during cooling increases. The results of EPA and Improved ESM show a difference of 7% on the average. It can be also confirmed that it is possible to apply the simplified method to various loading conditions.

Table 44 Analysis results of external constraint model

Analysis condition and method		Max. Disp. (z) (mm)	Max. Stress (x) (MPa)	Max. Stress (y) (MPa)
No external constraint	EPA	0.824 (1.04)	107 (1.18)	259 (1.05)
	Improved ESM	0.793	91	247
-30-30MPa during cooling	EPA 1	0.646 (0.98)	98 (1.17)	258 (1.06)
	EPA 2	0.629 (0.95)	102 (1.21)	258 (1.06)
	Improved ESM	0.661	84	244
-60-60MPa during cooling	EPA 1	0.468 (0.93)	89 (1.24)	257 (1.18)
	EPA 2	0.408 (0.81)	96 (1.33)	258 (1.18)
	Improved ESM	0.503	72	218

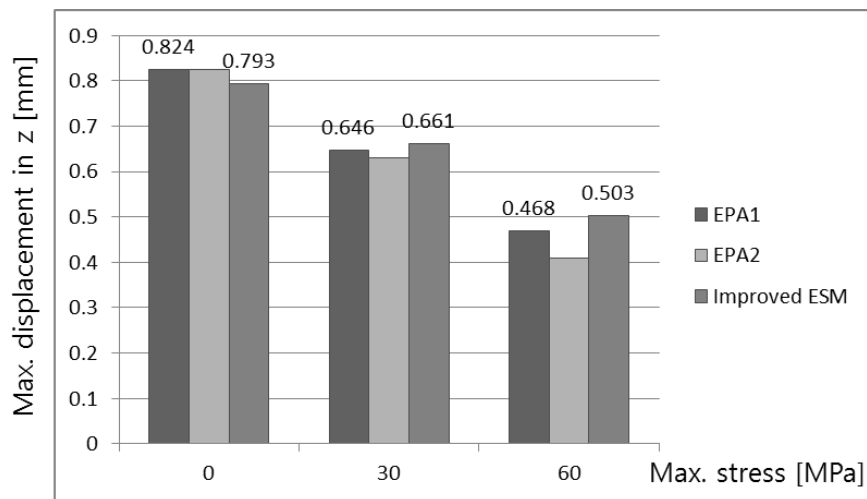


Fig. 146 Maximum displacement in z direction

## 8. Comparison of analysis time

Analysis time of two different methods (EPA, Improved ESM) is compared. Comparison was made to the three dimensional solid element model consisting of 174,870 nodes as shown in Fig. 147.

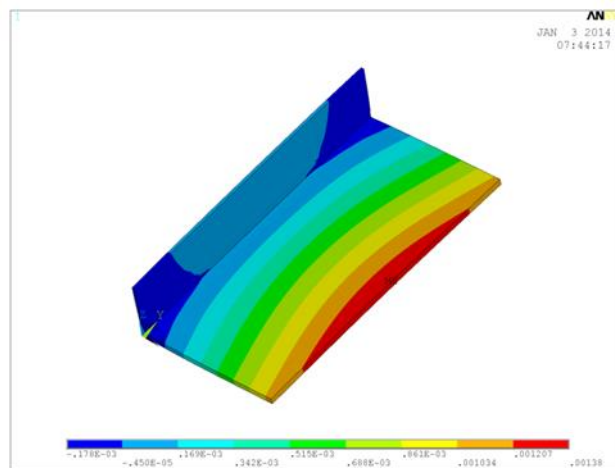


Fig. 147 Analysis model of 1000x1000x10

In the case of the elasto-plastic method (Table 45), the analysis time is 11.2 times more compared to the improved equivalent strain method. Even though there is a stark contrast of analysis time between two methods, it can be considered as negligible because the absolute analysis time is short. But the analysis time of elasto-plastic method grows exponentially as the number of elements increases. Elasto-plastic method has

been limited on large structure analysis due to time-consuming analysis. The Improved ESM, on the other hand, suggested possibility of analysis for large scaled structure.

**Table 45 Comparison of analysis time**

	EPA	Improved ESM	Ratio
Heat transfer analysis time (min.)	12 (25 steps)	10 (20 steps)	1.2
Structural analysis time (min.)	145 (25 steps)	4 (1 step)	36.3
Total (min.)	157	14	11.2
I-7 3.4 GHz 8 Core CPU, 12G RAM, Microsoft Windows 7			

## 9. Conclusion

In the present study, the existing equivalent strain method is improved to make up for its weaknesses. The improved inherent strain model is built considering more sophisticated three dimensional constraints which are embodied by six cubic elements attached on three sides of a core cubic element. The effect of temperature gradients over plate thickness and plate transverse direction normal to welding is reflected in the calculation of the inherent strain chart.

The proposed method is verified by comparing the calculated welding deformation analysis results with the existing method, thermal elasto-plastic FE analysis, and experimental results.

External restraints imposed normal to plate during cooling stage is identified to be effective to the reduction of angular distortion of butt-welded or fillet-welded plate.

The main conclusions of present study are summarized as follows:

1. Two important factors to determine inherent strain are the highest temperature and degree of restraint. However it is difficult to evaluate residual deformation and stress of weld model accurately by these two factors. To make up for its weaknesses, the additional factor that determines inherent

strain, temperature gradient is suggested.

2. A value of 0.57 is to be used as degree of restraint value in all axial directions at room temperature regardless of the shape of the analysis model and analysis position for a calculation of inherent stain. Repetitive calculation to find the degree of restraint is no longer required.

3. Improved inherent strain charts obtained by applying the new solid–spring model and considering the effect of the temperature gradient are suggested. The proposed restraint model is closer to the actual phenomenon and more intuitive by placing proper elements matching with actual restraint than the previous model.

4. The inherent strain is inputted in form of temperature and a simple one step heat transfer analysis is performed to spread the temperature out to the surroundings. In this research, strains are imposed on the top and bottom surfaces. It can make the distributed inherent strain obtained from the simple heat transfer analysis close to the actual strain distribution.

5. External restraints imposed normal to plate during cooling stage is identified to be effective to the reduction of angular distortion of butt–welded or fillet–welded plate.

6. Welding analysis model under external force during cooling stage is idealized as a prismatic member subjected to pure bending. The external restraint is represented by vertical force on work piece at both sides and bending stress forms in transverse direction. The additional bending stress distribution across plate thickness is reflected into the improved inherent strain model.

7. Improved equivalent strain method in present study can be adaptable to analysis of welding model under external constraint during cooling stage. Welding deformation can be calculated from an elastic linear FE analysis using the inherent strain values taken from the chart and compared with those from a 3D thermal elastoplastic FE analysis.

7. A quick and accurate method for welding analysis is developed in the present study. This result suggested possibility of analysis for large scaled structure.

# REFERENCES

- [1] C. D. Jang. Welding Distortion Analysis of Hull Blocks using Equivalent Load Method based on Inherent Strain. 2008. SSC-453.
  
- [2] Watanabe M and Satoh K. Effect of Welding Conditions on the Shrinkage Distortion in Welded Structures. 1961. Welding Journal 40:377-384.
  
- [3] Satoh K and Terasaki T. Effect of Welding Conditions on Welding Deformations in Welded Structural Materials. 1976. Journal of the Japanese Welding Society 45(4).
  
- [4] Tall L. Residual Stresses in Welded Plates-A Theoretical Study. 1964. Welding Journal 43.
  
- [5] Masubuchi K et al. Analysis of Thermal Stresses and Metal Movements of Weldments: A Basic Study toward Computer-Aided Analysis and Control of Welded Structures. 1974. SNAME Trans. 82:143-167.
  
- [6] Fujita Y and Nomoto T. Studies on Thermal Elasto-Plastic Problems(1st Report). 1972. Journal of the Society of Naval Architects of Japan 130. (in Japanese)

- [7] Ueda Y and Yamakawa T. Analysis of Thermal Elasto-Plastic Behavior of Metals during Welding by Finite Element Method. 1973. Journal of the Japanese Welding Society 42(6).
- [8] Masubuchi K and Papazoglou VJ. Analysis and Control of Distortion in Welding Aluminum Structures. 1978. SNAME Trans. 86.
- [9] Papazoglou VJ, Masubuchi K, Goncalves E and Imakita A. Residual Stresses Due to Welding : Computer-Aided Analysis of Their Formation and Consequences. 1982. SNAME Trans. 90.
- [10] Yasuhisa O. Simulation of Welding Deformation by FEM. 1996. TEAM '96 PUSAN 593-605.
- [11] Ueda Y, Kim YC, Yamakita T and Bang HS. Applicability of Substituting Plane-deformation problems. 1998. Trans of the Japanese Welding Society 6(1).
- [12] Nomoto T, Ohmori T, Sutoh T, Enosawa M, Aoyama K and Saitoh M. Development of Simulator for Plate Bending by Line Heating. 1990. SNAV 168:527-535. (in Japanese)
- [13] Nomoto T, Ohmori T, Sutoh T, Enosawa M, Aoyama K and

Saitoh M. Development of Simulator for Plate Bending by Line Heating Considering In-plane Shrinkage. 1991. SNAV 170:599–607. (in Japanese)

[14] Kim SI and Lee JS. Development of Simple Prediction method for Welding Distortion In Fillet Joints. 1996. Proceedings of the Annual Spring Meeting, The Society of Naval Architects of Korea 265–270. (In Korean)

[15] Murakawa H, Luo Y, Ueda Y. Prediction of Welding Deformation and Residual Stress by Elastic FEM Based on Inherent Strain (1st Report). 1996. Journal of the Society of Naval Architects of Japan 180:739–751. (In Japanese)

[16] Seo SI and Jang CD. A Study on the Prediction of Deformation of Welded Ship Structures. 1997. Journal of Korean Welding Society 15(4):438–447. (In Korean)

[17] Jang CD, Seo SI and Ko DE. A Study on the Prediction of Deformations of Plates Due to Line Heating Using a Simplified Thermal Elasto-Plastic Analysis. 1997. Journal of Ship Production 13(1):22–27.

[18] Lee CH. Prediction of Welding Deformation of Ship Hull Panel Blocks using Equivalent Loading Method based on

Inherent Strain. 2002. Ph. D. Thesis of Seoul National University. (In Korean)

[19] Kim JT. Analysis of Post Weld Deformation at HAZ by External Forces based on Inherent Strain. 2006. MS Thesis of Seoul National University. (In Korean)

[20] Ha YS. Development of Thermal Distortion Analysis Method on Large Shell Structure using Inherent Strain as Boundary Condition. 2008. Journal of the Society of Naval Architects of Korea. 45(1):93–100. (In Korean)

[21] Lee JH. Relations between Input Parameters and Residual Deformations in Line Heating Process using Finite Element Method and Multi-variate Analysis. 1999. Ph. D. Thesis of Seoul National University. (In Korean)

[22] Tekriwal P, and Mazumder J. Transient and Residual Thermal Strain–Stress Analysis of GMAW. 1991. ASME Journal of Engineering Material Technology 336–343.

[23] Kim YT. Structural Analysis of Ship Hull Block considering Welding Residual Stress using Equivalent Strain Method based on Inherent Strain. 2010. Ph. D. Thesis of Seoul National University. (In Korean)

[24] Moon HS. Prediction of Angular Distortion of Welded Structures by Improved inherent Strain Analysis based on Laminated Beam Modeling for the Inherent Region and Heat Equilibrium Zone. 2008. Ph. D. Thesis of Seoul National University. (In Korean)

[25] Adams CM Jr. Cooling Rates and Peak Temperatures in Fusion Welding. 1958. Welding Journal37:201–215. .

[26] Aoyama K, Nomoto T, and Takechi S. Basic Studies on Accuracy Management System for Shipbuilding. 1997. International Conference on Computer Applications in Shipbuilding323–338.

[27] Chris C and Randy D, Control of Distortion in Thin Ship Panels. Journal of Ship Production. 1997. 13(2):83–92.

[28] Jang CD and Lee CH. A Study on the Prediction and Control of Welding Deformations of Ship Hull Blocks. 2000. Journal of the Society of Naval Architects of Korea 37(2):127–136. (in Korean)

[29] Jang CD and Seo SI. A Simplified Method to Estimate Longitudinal Deformations of Built-up Beams Due to Welding

and Heating. 1995a. Journal of Ship Research 39(2):176–183.

[30] Jang CD, Ha Y, Ko DE, and Moon SC. Determination of Inherent Strain Regions to Estimate Plate Deformation by Line Heating. 2002. Journal of the Society of Naval Architects of Korea 39(1): 82–89. (in Korean)

[31] Jang CD, Seo SI and Ko DE. A Study on the Simulation of Line Heating Process using a Simplified Thermal Elasto–plastic Analysis Method. 1995b. Proceedings of Practical Design of Ships and Mobile Units95,Seoul (2):1421–1432.

[32] Lee JH. Relationships between Input Parameters and Residual Deformations in Line Heating Process Using Finite Element Method and Multi–Variable Analysis. 1999. Ph. D. Thesis Dept. of Naval Architecture and Ocean Engineering, Seoul National University, Seoul, Korea.

[33] Kim SI, Cho YK, Lee HW, and Lee JS. Prediction of Welding Deformation of Panel Block using Simplified Analysis Method. 1996. Proceedings of the Annual Spring Meeting, The Society of Naval Architects of Korea271–276. (in Korean)

[34] Luo Y, Murakawa H, and Ueda Y. Prediction of Welding Deformation and Residual Stress by Elastic FEM Based on

Inherent Strain(3rd Report). 1998. Journal of the Society of Naval Architects of Japan 183:323–333. (in Japanese)

[35] Matsuoka K. An Analytical Method on Residual Stresses in Welded Built-Up Shell Structures. 1983. Journal of the Society of Naval Architects of Japan 153:210–217. (in Japanese)

[36] Nomoto T, Takechi S, and Aoyama K. Basic Studies on Accuracy Management System Based on Estimation of Weld Deformations. 1997. Journal of the Society of Naval Architects of Japan 181:249–260. (in Japanese)

[37] Seo SI, and Jang CD. A Study on the Prediction of Deformation of Welded Ship Structures. 1999. Journal of Ship Production 15(2): 73–81.

[38] Ueda Y, Fukuda K, and Tanigawa M. New Measuring Method of Three Dimensional Residual Stresses Based on Theory of Inherent Strain. 1979. Transactions of Japanese Welding Research Institute 8(2): 249–256.

[39] Ueda Y, Murakawa H, and Ma NX. Measuring Method for Residual Stresses in Explosively Clad Plates and a Method of Residual Stress Reduction. 1996a. Journal of Engineering Materials and Technology 118(4):576–582.

[40] Ueda Y and Ma NX. Measuring Method of Three-Dimensional Residual Stresses with Aid of Distribution Function of Inherent Strain(Report 1). 1994. Transactions 01 Japanese Welding Research Institute23(1): 71–78.

[41] Ueda Y and Ma NX. Measuring Method of Three-Dimensional Residual Stresses with Aid of Distribution Function of Inherent Strain(Report III). 1995. Transactions 01 Japanese Welding Research Institute24(2):123–130.

[42] Ueda Y, Nakacho K, and Moriyama S. Compressive Ultimate Strength of Rectangular Plate with Initial Imperfections due to Welding (4<sup>th</sup>Report). 1986. Journal of the Society of Naval Architects of Japan159:282–294. (in Japanese)

[43] Ueda Y, You CK and Yuan MG.A Predicting Method of Welding Residual Stress Using Source of Residual Stress. 1988. Quarterly Journal of the Japan Welding Society 6(1):59–64. (in Japanese)

[44] Ueda Y and Yuan MG. Theoretical Determination of the Sizes of Standard Model and Effect of Changes in Heat Input and Kind of Steel on Inherent Strain – A Predicting Method of Welding Residual Stress Using Source of Residual Stress

(Report 2). 1988. Quarterly Journal of the Japan Welding Society 6(3): 349–353. (in Japanese)

[45] Ueda Y and Yuan MG. Prediction of Welding Residual Stress Using Source of Residual Stress (Report 3). 1991. Quarterly Journal of the Japan Welding Society 9(3):337–343. (in Japanese)

[46] Ko DE. A Study on the Prediction of Deformations of Plates due to Line Geating using a Thermal Elasto–plastic Analysis Model. 1998. Ph. D. Thesis of Seoul National University. (In Korean)

[47] Luo Y, Murakawa H and Ueda Y. Prediction of Welding Deformation and Residual Stress by Elastic FEM Based on Inherent Strain(3rd Report). 1994. Journal of the Society of Naval Architects of Japan 23(2): 239–247.

[48] K HC. Analysis of Multi-layered Butt Welding using Equivalent Load Method based on Inherent Strain Method. 2007. MS Thesis of Seoul National University. (In Korean)

[49] Jang CD, Ha YS and Kim YT. Determination of optimal heating conditions in line heating process with weaving motions. 2006. Proc. of ISOPE182–186.

[50] Jo YC, Kim YT, Ryu HS, Han MS, Ha JH and Jang CD. Analysis of Redistribution of the Welding Deformation Due to External Loads using Layered Shell Approach. 2007. Proc. Of TEAM.

[51] Jang CD, Kim YT, Jo YC and Ryu HS. Welding Distortion Analysis of Hull Blocks using Equivalent Load Method Based on Inherent Strain. 2007. PRADS.

[52] Kim YT, Jang CD, Kim TJ, Kim JW. Structural Analysis of Ship Hull Block using Equivalent Load Method based on Inherent Strain. 2008. Proceedings of the Annual Autumn Meeting, SNAK.

[53] Beer FP, Johnston ER Jr., Dewolf JT, Mazurek D. Mechanics of Materials 5th Edition in SI Units. 2009. McGraw-Hill, New York, NY.

[54] James M. Gere. Mechanics of Materials 5th Edition. 2001. Brooks/Cole